



# Preparation and properties of polymer networks from photoperoxidation of 1,2-dicarbonyl compounds

Branislav Husar

► **To cite this version:**

Branislav Husar. Preparation and properties of polymer networks from photoperoxidation of 1,2-dicarbonyl compounds. Chimie organique. Université Blaise Pascal - Clermont-Ferrand II, 2008. Français. <NNT : 2008CLF21818>. <tel-00728255>

**HAL Id: tel-00728255**

**<https://tel.archives-ouvertes.fr/tel-00728255>**

Submitted on 5 Sep 2012

**HAL** is a multi-disciplinary open access archive for the deposit and dissemination of scientific research documents, whether they are published or not. The documents may come from teaching and research institutions in France or abroad, or from public or private research centers.

L'archive ouverte pluridisciplinaire **HAL**, est destinée au dépôt et à la diffusion de documents scientifiques de niveau recherche, publiés ou non, émanant des établissements d'enseignement et de recherche français ou étrangers, des laboratoires publics ou privés.

N° d'Ordre : D. U. 1818

**UNIVERSITE BLAISE PASCAL**

(U.F.R. de recherche scientifique et technique)

**ECOLE DOCTORALE DES SCIENCES FONDAMENTALES**

N° 560

**THESE**

présentée pour obtenir le grade de

**DOCTEUR D'UNIVERSITE**

*Spécialité : Chimie physique*

Par

**HUSÁR Branislav**

Master en chimie organique

**PREPARATION AND PROPERTIES OF POLYMER NETWORKS  
FROM PHOTOPEROXIDATION OF 1,2-DICARBONYL COMPOUNDS**

Soutenue publiquement le 17 janvier 2008 devant la commission d'examen.

Président : M. Alain MICHEL (rapporteur)

Examineurs : Mme. Sophie COMMEREUC  
M. Mohamed BABA  
M. Dušan BAKOŠ  
M. Štefan CHMELA  
M. Bruno FAYOLLE  
M. Ivan LUKÁČ  
M. Josef RYCHLÝ (rapporteur)

Invité : M. Jacques LACOSTE

## ACKNOWLEDGEMENT

First of all, I would like to sincerely thank Prof. Sophie COMMEREUC, Prof. Mohamed BABA and Dr. Štefan CHMELA for being a patient supervisors and for supporting this work with their knowledge, ideas and criticism.

I would like to thank Dr. Josef RYCHLÝ, Prof. Alain MICHEL, Dr. Bruno FAYOLLE for being jury members and for their valuable comments which helped in improving the manuscript.

I would like to acknowledge the financial support of French government (BGF) for the thesis. I would like to thank Prof. Jacques LACOSTE for helping me with obtaining the scholarship.

I would like to thank Dr. Ivan LUKÁČ for numerous discussions concerning synthesis and photochemistry, Dr. Vincent VERNEY for the help with rheology, Dr. Jiří PAVLINEC for helpful suggestions about characterisation of network, Prof. Pavol HRDLOVIČ for answering me questions about photochemistry and Dr. Jaroslav MOSNÁČEK for reading the manuscript. Many thanks to all members of the laboratory particularly Lawrence FREZET. I would like to thank my friends from both laboratories for caring they provided.

Last but not the least I would like to thank my parents and wife Slávka for the enormous support, patience and love they gave me.

## RÉSUMÉ

Ce travail de thèse traite de l'étude de la réactivité photochimique de copolymères de styrène comportant des groupes pendants benzile (BZ) et en particulier de la caractérisation du réseau final de réticulation. La distribution de BZ dans le copolymère est statistique. Ces groupes photoactifs sont convertis pratiquement quantitativement en fonctions peroxyde de dibenzoyl (BP) par irradiation directement à l'état solide des films polymères à  $\lambda > 400$  nm. La photoperoxydation a été principalement suivie par spectroscopie IRTF. La décomposition par voie thermique ou photochimique des BP est une voie efficace d'obtention d'un réseau tridimensionnel de réticulation.

Le réseau a été suivi au cours de la réticulation par deux méthodes complémentaires : la thermoporosimétrie et la densimétrie. La thermoporosimétrie permet de caractériser le gel par mesure de la taille de maille. La densimétrie caractérise le sol par mesure de la densité de solution d'extrait. Les réseaux finals obtenus par photo-réticulation et thermo-réticulation sont similaires.

Les réseaux finals de copolymères synthétisés pour différents taux d'incorporation du BZ ont été caractérisés par rhéologie, gonflement, thermoporosimétrie et densimétrie. Les méthodes basées sur les évolutions des pentes basses-fréquences des modules  $G'$  et  $G''$  ont été appliquées pour déterminer le point de gel et pour caractériser la densité du réseau. L'utilisation de la représentation de Cole-Cole apporte des informations, tant sur la caractérisation à l'état initial des copolymères que sur le comportement du réseau final. Un modèle rhéologique permet de calculer la concentration des ponts de réticulation chimiques. La partie soluble a été caractérisée par densimétrie. Le gonflement permet de calculer la masse molaire entre deux noeuds de réticulation. Les résultats de gonflement sont en accord avec ceux de thermoporosimétrie. Une corrélation a été établie entre les résultats des différentes techniques et le nombre des groupes BP par chaîne. Les facteurs favorisant une construction du réseau dense sont : des masses molaire élevées et une faible polydispersité du copolymère initial et une concentration élevée du BP.

Le copolymère portant des groupes pendants camphrequinone a été synthétisé pour comparer sa réticulation avec le copolymère précédent. Après irradiation, aucun peroxyde n'a été détecté. L'efficacité de la réticulation de ce copolymère est nettement inférieure.

**Mots clés :** benzile, polystyrène, copolymérisation, photochimie, réseau, rhéologie, thermoporosimétrie

## ABSTRAKT

Táto dizertačná práca sa venuje štúdiu fotoreaktivity styrénových kopolymérov obsahujúcich benzilovú (BZ) štruktúru naviazanú na polymérny reťazec a najmä charakterizácii polymérnej siete. BZ je štatisticky distribuovaný v kopolyméri. Ožarovaním polymérneho filmu pri  $\lambda > 400$  nm sa tieto fotoaktívne skupiny transformujú kvantitatívne na benzoyl peroxid (BP). Fotoperoxidácia sa sledovala FTIR spektroskopiou. Termický alebo fotochemický rozklad BP skupín vedie k vzniku trojrozmiernej polymérnej siete.

Počas sieťovania sa sieť sledovala dvoma komplementárnymi metódami: termopozimetriou a denzimetriou. Termopozimetria umožňuje charakterizáciu gélu meraním veľkosti oka siete. Denzimetria charakterizuje sôl meraním hustoty roztoku extraktu. Siete pripravené fotochemickou a termickou cestou sú podobné.

Siete kopolymérov s rôznymi obsahmi BZ boli charakterizované reologicky, napučívaním, termopozimetriou a denzimetriou. Metódy založené na zmene smernice modulov  $G'$  a  $G''$  pri nízkych frekvenciách boli úspešne aplikované na stanovenie bodu gélovania a na charakterizáciu sieťovej hustoty. Cole-Coleova reprezentácia prináša informácie o východiskovom kopolyméri, ako aj o sieti. Reologický model umožňuje vypočítať koncentráciu chemických priečných väzieb. Rozpustná časť sa charakterizovala denzimetriou. Napučívanie umožňuje vypočítať mólovú hmotnosť polymérneho reťazca medzi dvoma uzlami. Výsledky z napučievania sú v súhlase s termopozimetriou. Zostrojila sa korelácia medzi výsledkami viacerých metód a počtom BP skupín na polymérny reťazec. Faktory podporujúce vznik hustejšej siete sú: zvýšená mólová hmotnosť a nízka polydisperzita východiskového kopolyméru a väčšia koncentrácia BP.

Kopolymér obsahujúci gáforchinónovú štruktúru naviazanú na polymérny reťazec bol pripravený, aby sa porovnávalo jeho sieťovanie s predošlým kopolymérom. Po ožarovaní nebol detegovaný žiadny stabilný peroxid. Účinnosť sieťovania tohto kopolyméru je výrazne nižšia.

**Kľúčové slová:** benzil, polystyrén, kopolymerizácia, fotochémia, sieť, reológia, termopozimetria

# TABLE OF CONTENTS

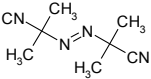
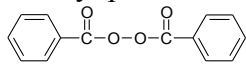
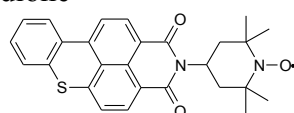
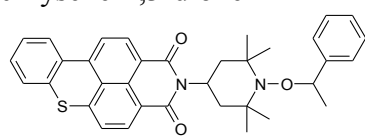
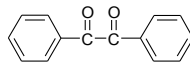
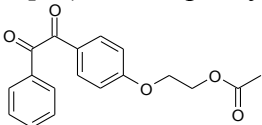
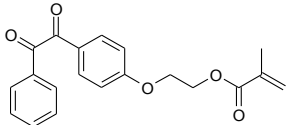
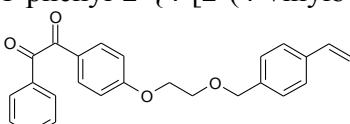
<b>ACKNOWLEDGEMENT.....</b>	<b>2</b>
<b>RÉSUMÉ.....</b>	<b>3</b>
<b>ABSTRAKT.....</b>	<b>4</b>
<b>TABLE OF CONTENTS.....</b>	<b>5</b>
<b>LIST OF ABBREVIATIONS.....</b>	<b>8</b>
<b>LIST OF FIGURES.....</b>	<b>11</b>
<b>LIST OF SCHEMES.....</b>	<b>13</b>
<b>LIST OF TABLES.....</b>	<b>14</b>
<b>1 INTRODUCTION.....</b>	<b>15</b>
<b>2 BIBLIOGRAPHIC STUDY.....</b>	<b>17</b>
2.1 PHOTOCHEMISTRY OF BENZIL.....	17
2.1.1 Photochemistry of benzil in solution in inert atmosphere.....	17
2.1.2 Photochemistry of benzil in solution in presence of oxygen.....	19
2.1.3 Photochemistry of benzil in polymer film.....	20
2.1.4 Photochemistry of polymers bearing benzil units.....	21
2.2 PHOTOCHEMISTRY OF CAMPHORQUINONE.....	25
2.3 CHARACTERISATION OF POLYMER NETWORK.....	26
2.3.1 Swelling.....	26
2.3.2 Thermoporometry.....	29
2.3.3 Sol fraction.....	32
2.3.4 Densitometry.....	32
2.3.5 Rheology.....	33
<b>3 MATERIALS AND EXPERIMENTAL TECHNIQUES.....</b>	<b>38</b>
3.1 CHEMICAL PRODUCTS.....	38
3.1.1 Chemical products for the synthesis of BZS.....	38
3.1.2 Chemical products for the synthesis of StNOR.....	38
3.1.3 Chemical products for the synthesis of CQMA.....	38
3.1.4 Chemical products for the polymerizations.....	39
3.1.5 Chemical products for the other experiments.....	39
3.2 USED TECHNIQUES.....	39
3.2.1 Synthetic techniques and spectral characterisation.....	39
3.2.2 GPC measurements.....	40
3.2.3 Preparation of films.....	40
3.2.4 Irradiation devices.....	41
3.2.5 Thermal decomposition of peroxides.....	42
3.2.6 Melt rheology measurements.....	42
3.2.7 DSC measurements.....	42
3.2.8 Swelling measurements.....	43
3.2.9 Densitometry measurements.....	43
<b>4 STUDY OF PHOTOPEROXIDATION.....</b>	<b>45</b>
4.1 INTRODUCTION.....	45

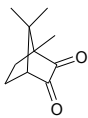
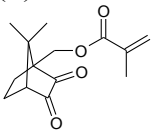
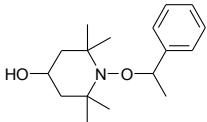
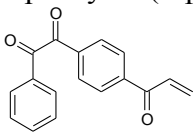
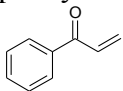
4.2 SYNTHESIS OF THE MONOMER BZS.....	45
4.2.1 Synthesis of 2-(4-phenylacetylphenoxy)ethyl acetate (I).....	46
4.2.2 Synthesis of 1-[4-(2-hydroxyethoxy)phenyl]-2-phenylethanone (II).....	47
4.2.3 Synthesis of 1-[4-(2-hydroxyethoxy)phenyl]-2-phenylethan-1,2-dione (III).....	47
4.2.4 Synthesis of 1-phenyl-2-{4-[2-(4-vinylbenzyloxy)ethoxy]phenyl}-ethane-1,2-dione (BZS).....	48
4.3 SYNTHESIS, PHOTOPEROXIDATION AND CROSSLINKING OF STYRENE COPOLYMER WITH PENDANT BZ MOIETIES.....	48
4.4 CONCLUSION.....	56
<b>5 STUDY OF CROSSLINKING.....</b>	<b>57</b>
5.1 INTRODUCTION.....	57
5.2 CARBON TETRACHLORIDE AS THERMOPOROMETRY LIQUID PROBE TO STUDY THE CROSS-LINKING OF STYRENE COPOLYMER NETWORKS.....	57
5.3 CORRELATION OF THERMOPOROMETRY WITH DENSITOMETRY RESULTS.....	64
5.4 CONCLUSION.....	65
<b>6 STUDY OF FINAL POLYMER NETWORK.....</b>	<b>66</b>
6.1 INTRODUCTION.....	66
6.2 SYNTHESIS OF COPOLYMERS.....	66
6.3 CHARACTERISATION OF MOLECULAR PARAMETERS OF INITIAL BZS/S.....	69
6.3.1 Gel permeation chromatography.....	69
6.3.2 Rheological master curves.....	71
6.3.3 Cole-Cole representation.....	73
6.3.4 Number of BZ units per polymer chain.....	74
6.4 CHARACTERISATION OF MOLECULAR PARAMETERS OF PHOTOPEROXIDISED BZS/S.....	75
6.4.1 Content of BP in photoperoxidised copolymers.....	76
6.5 CHARACTERISATION OF THE FINAL NETWORK OF CROSSLINKED BZS/S.....	77
6.5.1 Analysis of the global network.....	77
6.5.1.1 Rheological master curves.....	78
6.5.1.2 Winter-Chambon criterion.....	80
6.5.1.3 Cole-Cole representation.....	81
6.5.1.4 Theoretical rheological model.....	83
6.5.2 Analysis of the global network of additional series of NMP copolymers.....	84
6.5.2.1 Synthesis of mediator StNOR.....	84
6.5.2.2 Synthesis and characterisation of NMP copolymers.....	85
6.5.2.3 Characterisation of molecular parameters of photoperoxidised samples.....	87
6.5.2.4 Characterisation of final network by rheology.....	88
6.5.3 Analysis of the soluble part.....	90
6.5.3.1 Densitometry.....	90
6.5.3.2 Sol fraction.....	91
6.5.4 Analysis of the insoluble part.....	92
6.5.4.1 Swelling.....	92
6.5.4.2 Thermoporometry.....	94
6.6 DISCUSSION.....	96
6.7 CONCLUSION.....	100
<b>7 STUDY OF PHOTOCHEMISTRY OF CAMPHORQUINONE-BEARING POLYMER. .101</b>	
7.1 INTRODUCTION.....	101

---

7.2 SYNTHESIS OF CQMA.....	101
7.2.1 Synthesis of Potassium ( $\pm$ )-10-Camphorsulphonate (IV).....	103
7.2.2 Synthesis of ( $\pm$ )-10-Camphorsulphonic Acid Bromide (V).....	104
7.2.3 Synthesis of ( $\pm$ )-10-Bromocamphor (VI).....	104
7.2.4 Synthesis of ( $\pm$ )-10-Acetoxyamphor (VII).....	105
7.2.5 Synthesis of ( $\pm$ )-10-Acetoxyamphorquinone (VIII).....	105
7.2.6 Synthesis of ( $\pm$ )-10-Hydroxyamphorquinone (IX).....	106
7.2.7 Synthesis of ( $\pm$ )-10-Methacryloyloxyamphorquinone (CQMA).....	106
7.3 SYNTHESIS OF THE COPOLYMER CQMA/S.....	107
7.4 CHARACTERISATION OF MOLECULAR PARAMETERS OF INITIAL AND IRRADIATED CQMA/S.....	108
7.4.1 Rheological curves.....	108
7.4.2 Gel permeation chromatography and Cole-Cole representation.....	109
7.5 IRRADIATION OF CQMA/S.....	109
7.6 CONCLUSION.....	111
<b>8 CONCLUSION AND PERSPECTIVES.....</b>	<b>112</b>
<b>REFERENCES.....</b>	<b>115</b>

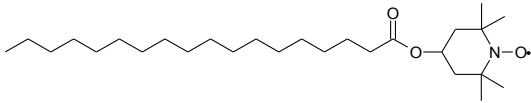
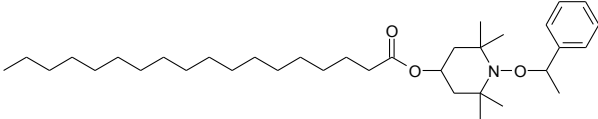
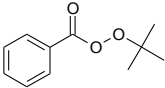
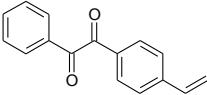
## LIST OF ABBREVIATIONS

Ac	acetyl
AIBN	2,2'-azobisisobutyronitril; 2,2'-azobis(2-methylpropionitrile) 
Ar	aryl
BP	benzoyl peroxide 
br.s	broad singlet
BTXNO	2-(1-oxy-2,2,6,6-tetramethyl-piperidin-4-yl)-6-thia-2-aza-benzo[def]-chrysene-1,3-dione 
BTXNOR	2-(2,2,6,6-tetramethyl-1-phenylethoxy-piperidin-4-yl)-6-thia-2-aza-benzo[def]-chrysene-1,3-dione 
Bu	butyl
BZ	benzil 
BZAc	2-[4-(2-oxo-2-phenylacetyl)phenoxy]ethyl acetate 
BZMA	1-{4-(2-methacroyloxyethoxyphenyl)}-2-phenylethane-1,2-dione 
BZMA/S	poly[1-{4-(2-methacroyloxyethoxyphenyl)}-2-phenylethane-1,2-dione-co-styrene]
BZS	1-phenyl-2-{4-[2-(4-vinylbenzyloxy)ethoxy]phenyl}ethane-1,2-dione 

BZS/S	poly[1-phenyl-2-{4-[2-(4-vinylbenzyloxy)ethoxy]phenyl}ethane-1,2-dione- <i>co</i> -styrene]
CQ	camphorquinone 
CQMA	(±)-10-methacryloyloxycamphorquinone 
DSC	differential scanning calorimetry
DS <sub>E</sub>	equilibrium degree of swelling
Et	ethyl
FTIR	Fourier transform infrared spectroscopy
GPC	gel permeation chromatography
HONOR	2,2,6,6-tetramethyl-1-(1-phenylethoxy)piperidin-4-ol 
MALS	multi-angle light scattering
mp	melting point
NMP	nitroxide mediated polymerization
NMR	nuclear magnetic resonance
PCOCO	1-phenyl-2-(4-propenoylphenyl)ethane-1,2-dione 
PCOCO/S	poly[1-phenyl-2-(4-propenoylphenyl)ethane-1,2-dione- <i>co</i> -styrene]
PDI	polydispersity index
Ph	phenyl
PMMA	poly(methyl methacrylate)
PS	polystyrene
PVK	phenylvinylketone 
PVK/VBz	poly(phenylvinylketone- <i>co</i> -4-vinylbenzil)
R <sub>f</sub>	retention factor

## LIST OF ABBREVIATIONS

---

RI	refractive index
SEPAP	Service d'Etude du Photovieillissement Accéléré des Polymères
StNO	1-oxy-2,2,6,6-tetramethyl-piperidin-4-yl octadecanoate
	
StNOR	2,2,6,6-tetramethyl-1-(1-phenyl-ethoxy)-piperidin-4-yl octadecanoate
	
TBPB	<i>tert</i> -butyl peroxybenzoate
	
THF	tetrahydrofuran
UV	ultraviolet light
VBz	4-vinylbenzil; 1-phenyl-2-(4-vinylphenyl)ethane-1,2-dione
	
VBz/S	poly[1-phenyl-2-(4-vinylphenyl)ethane-1,2-dione- <i>co</i> -styrene]
VIS	visible light
wt	weight

## LIST OF FIGURES

<b>Figure 1:</b> DSC thermal curve of swelling solvent in a divided medium, recorded with 0.7 °C/min as cooling temperature rate.....	30
<b>Figure 2:</b> Relationship between imposed strain $\gamma$ and resultant stress $\tau_{12}$ , showing the phase $\log \delta$ between the two. The stress is deconvoluted in the in-phase $\tau'$ and out-of-phase $\tau''$ components of stress.....	34
<b>Figure 3:</b> Cole-Cole plot.....	36
<b>Figure 4:</b> NMR spectrum of BZS/S copolymer with labelled peaks.....	40
<b>Figure 5:</b> Transmittance spectra of the liquid filter (solid), “416” Schott filter (dot) and Hg Mon 436 filter (dash).....	41
<b>Figure 6:</b> Correlation of thermoporometry with densitometry. Density of the extract ( $\square$ , $\blacksquare$ ) and average mesh size $\zeta$ of crosslinked sample ( $\circ$ , $\bullet$ ) as a function of time. Interval 0-4 h is a photoperoxidation step ( $\lambda > 390$ nm), initial copolymer BZS/S is labelled as ( $\star$ ). Interval 4-8 h is a thermo-crosslinking (110 °C, hollow) or photo-crosslinking step ( $\lambda > 300$ nm, solid).....	64
<b>Figure 7:</b> Chromatograms of a series of BZS/S copolymers (MALS + RI detector).....	70
<b>Figure 8:</b> Storage ( $G'$ , $\blacksquare$ ) and loss ( $G''$ , $\circ$ ) moduli as a function of frequency pulsation $\omega$ for PS. The reference temperature was 170 °C.....	71
<b>Figure 9:</b> Storage ( $G'$ , $\blacksquare$ ) and loss ( $G''$ , $\circ$ ) moduli as a function of frequency pulsation $\omega$ for initial BZS/S 0.5%. The reference temperature was 170 °C.....	71
<b>Figure 10:</b> Storage ( $G'$ , $\blacksquare$ ) and loss ( $G''$ , $\circ$ ) moduli as a function of frequency pulsation $\omega$ for initial BZS/S 1%. The reference temperature was 170 °C.....	72
<b>Figure 11:</b> Storage ( $G'$ , $\blacksquare$ ) and loss ( $G''$ , $\circ$ ) moduli as a function of frequency pulsation $\omega$ for initial BZS/S 2%. The reference temperature was 170 °C.....	72
<b>Figure 12:</b> Storage ( $G'$ , $\blacksquare$ ) and loss ( $G''$ , $\circ$ ) moduli as a function of frequency pulsation $\omega$ for initial BZS/S 4%. The reference temperature was 170 °C.....	72
<b>Figure 13:</b> Storage ( $G'$ , $\blacksquare$ ) and loss ( $G''$ , $\circ$ ) moduli as a function of frequency pulsation $\omega$ for initial BZS/S 8%. The reference temperature was 170 °C.....	72
<b>Figure 14:</b> Storage ( $G'$ , $\blacksquare$ ) and loss ( $G''$ , $\circ$ ) moduli as a function of frequency pulsation $\omega$ for initial BZS/S 4% BTXNOR. The reference temperature was 170 °C.....	72
<b>Figure 15:</b> Storage ( $G'$ , $\blacksquare$ ) and loss ( $G''$ , $\circ$ ) moduli as a function of frequency pulsation $\omega$ for initial BZS/S 4% StNO. The reference temperature was 170 °C.....	72
<b>Figure 16:</b> Cole-Cole plot of the initial copolymers BZS/S: Imaginary component of dynamic viscosity ( $\eta''$ ) as a function of real component of dynamic viscosity ( $\eta'$ ).....	73
<b>Figure 17:</b> Logarithmic plot of zero shear viscosity ( $\eta_0$ ) against weight-average molar mass ( $M_w$ ) for initial BZS/S copolymers.....	74
<b>Figure 18:</b> FTIR spectra used to calculate the conversion of BZ group. Band corresponding to BZ group is situated in the rectangle.....	76
<b>Figure 19:</b> Logarithmic plot of the storage ( $G'$ ) and loss ( $G''$ ) moduli as a function of frequency pulsation $\omega$ showing the changes in the terminal zone of a crosslinked polymer.....	78
<b>Figure 20:</b> Storage ( $G'$ , $\blacksquare$ ) and loss ( $G''$ , $\circ$ ) moduli as a function of frequency pulsation $\omega$ for photoperoxidised and thermally treated BZS/S 0.5%. The reference temperature was 170 °C.....	79
<b>Figure 21:</b> Storage ( $G'$ , $\blacksquare$ ) and loss ( $G''$ , $\circ$ ) moduli as a function of frequency pulsation $\omega$ for photoperoxidised and thermally treated BZS/S 1%. The reference temperature was 170 °C.....	79
<b>Figure 22:</b> Storage ( $G'$ , $\blacksquare$ ) and loss ( $G''$ , $\circ$ ) moduli as a function of frequency pulsation $\omega$ for	

crosslinked BZS/S 2%. The reference temperature was 170 °C.....	79
<b>Figure 23:</b> Storage ( $G'$ , ■) and loss ( $G''$ , ○) moduli as a function of frequency pulsation $\omega$ for crosslinked BZS/S 4%. The reference temperature was 170 °C.....	79
<b>Figure 24:</b> Storage ( $G'$ , ■) and loss ( $G''$ , ○) moduli as a function of frequency pulsation $\omega$ for crosslinked BZS/S 8%. The reference temperature was 170 °C.....	79
<b>Figure 25:</b> Storage ( $G'$ , ■) and loss ( $G''$ , ○) moduli as a function of frequency pulsation $\omega$ for crosslinked BZS/S 13%. The reference temperature was 170 °C.....	79
<b>Figure 26:</b> Storage ( $G'$ , ■) and loss ( $G''$ , ○) moduli as a function of frequency pulsation $\omega$ for crosslinked BZS/S 4% BTXNOR. The reference temperature was 170 °C.....	80
<b>Figure 27:</b> Storage ( $G'$ , ■) and loss ( $G''$ , ○) moduli as a function of frequency pulsation $\omega$ for crosslinked BZS/S 4% StNO. The reference temperature was 170 °C.....	80
<b>Figure 28:</b> Calculated slopes at low frequencies ( $n'$ , $n''$ ) as a function of theoretical crosslinking index $\gamma$ . Experimental points for BZS/S 13% are not shown. A minimum value of $\gamma$ to reach the gel point is indicated by an arrow.....	81
<b>Figure 29:</b> Cole-Cole plot of the thermally treated photoperoxidised copolymers BZS/S: Imaginary component of dynamic viscosity ( $\eta''$ ) as a function of the real component of dynamic viscosity ( $\eta'$ ).....	82
<b>Figure 30:</b> Slopes calculated from the Cole-Cole plot as a function of theoretical crosslinking index $\gamma$ .....	82
<b>Figure 31:</b> Cole-Cole plot of the initial copolymers BZS/S prepared by NMP: Imaginary component of dynamic viscosity ( $\eta''$ ) as a function of real component of dynamic viscosity ( $\eta'$ ). Sample VZ4 is overlapped by VZ6.....	87
<b>Figure 32:</b> Logarithmic plot of the zero shear viscosity ( $\eta_0$ ) against the weight-average molar mass ( $M_w$ ) for initial polymers VZ1-VZ9.....	87
<b>Figure 33:</b> Apparent exponents ( $n'$ - ■, $n''$ - □) as a function of theoretical crosslinking index $\gamma$ for copolymers prepared by conventional free radical polymerization and by NMP.....	90
<b>Figure 34:</b> Slope of Cole-Cole representation as a function of theoretical crosslinking index $\gamma$ . First series of copolymers prepared by conventional free radical polymerization and two copolymers by NMP (■). New series of NMP copolymers (□).....	90
<b>Figure 35:</b> Density of CCl <sub>4</sub> extract solutions (10 ml) of crosslinked polymer (100 mg) as a function of theoretical crosslinking index $\gamma$ .....	91
<b>Figure 36:</b> Mesh size distributions of the final networks of crosslinked BZS/S samples swollen in tetrachloromethane.....	95
<b>Figure 37:</b> Correlation between the average mesh size $\xi$ of the CCl <sub>4</sub> swollen final network and the equilibrium degree of swelling $DS_E$ .....	95
<b>Figure 38:</b> Correlations between Winter-Chambon criterion, Cole-Cole representation, densitometry, swelling measurement, thermoporometry as a function of an average number of BP groups per polymer chain of photoperoxidised polymer.....	97
<b>Figure 39:</b> Storage ( $G'$ , ■, □) and loss ( $G''$ , ●, ○) moduli as a function of frequency pulsation $\omega$ for initial (solid) and for irradiated CQMA/S 1 (hollow). The reference temperature was 170 °C..	108
<b>Figure 40:</b> Storage ( $G'$ , ■, □) and loss ( $G''$ , ●, ○) moduli as a function of frequency pulsation $\omega$ for initial (solid) and for irradiated CQMA/S 2 (hollow). The reference temperature was 170 °C..	108
<b>Figure 41:</b> FTIR spectra of CQMA/S 1 film after irradiation in a SEPAP apparatus for the indicated periods. Spectrum of PS film was subtracted.....	110
<b>Figure 42:</b> FTIR spectra of CQMA/S 1 film after irradiation in a SEPAP apparatus for the indicated periods. Spectrum of initial CQMA/S 1 film was subtracted.....	110
<b>Figure 43:</b> UV/VIS spectra of CQMA/S 1 film after irradiation in a SEPAP apparatus for the indicated periods.....	110

## LIST OF SCHEMES

<b>Scheme 1:</b> Interaction of the lowest triplet state of BZ with hydrogen donor.....	17
<b>Scheme 2:</b> Photoreduction of BZ in 2-propanol.....	17
<b>Scheme 3:</b> Irradiation of a mixture BZ - benzhydrylamine (1:2) by UV light.....	18
<b>Scheme 4:</b> Photoreduction of BZ in ethyleneglycol.....	19
<b>Scheme 5:</b> Mechanism of photooxidation of BZ in the presence of oxygen.....	19
<b>Scheme 6:</b> Mechanism of photooxidation of 2,2'-thenil in the presence of oxygen.....	19
<b>Scheme 7:</b> Photooxidation of BZ in a benzene solution and in a polymer film.....	20
<b>Scheme 8:</b> Structures of polymers bearing BZ moiety: poly(oxyhexyleneoxy-4,4'-benzilylene) (a), poly(oxy-4,4'-benzilyleneoxysebacoyl) (b) and poly(phenyl methacrylate)-co-4-methacryloyloxy-4'-methoxybenzil) (c).....	21
<b>Scheme 9:</b> Photoperoxidation of styrene copolymers with pendant BZ group.....	22
<b>Scheme 10:</b> Decomposition of formed peroxides in photoperoxidised styrene copolymers with pendant BZ group.....	23
<b>Scheme 11:</b> Crosslinking of photoperoxidised styrene copolymers with pendant BZ group: addition of an acyloxy macroradical to a phenyl ring of another chain.....	24
<b>Scheme 12:</b> Photoperoxidation, thermal crosslinking and photo-decrosslinking of PVK/VBz.....	25
<b>Scheme 13:</b> Various photoproducts of CQ.....	25
<b>Scheme 14:</b> Mechanism proposed for CQ photooxidation in liquid solutions and in polymer films.....	26
<b>Scheme 15:</b> Synthesis of the monomer BZS.....	46
<b>Scheme 16:</b> Synthesis of the mediator StNOR.....	85
<b>Scheme 17:</b> Synthesis of the monomer CQMA.....	102
<b>Scheme 18:</b> Alternative synthesis of ( $\pm$ )-10-acetoxycamphorquinone ( <b>VIII</b> ).....	103

## LIST OF TABLES

<b>Table 1:</b> Rate constants of BP derivatives decomposition at 91 °C.....	25
<b>Table 2:</b> Values obtained from oscillatory rheometer.....	35
<b>Table 3:</b> Polymerization conditions for a series of copolymers BZS/S.....	68
<b>Table 4:</b> Content of BZS in monomer mixture and in copolymer BZS/S.....	68
<b>Table 5:</b> PS equivalent molar masses and polydispersities of a series of copolymers BZS/S (0-13 wt% of BZS) determined by GPC using MALS + RI detector.....	69
<b>Table 6:</b> Comparison of zero shear viscosity $\eta_0$ with weight average molar mass $M_w$ and comparison of distribution parameter $h$ with polydispersity index of initial copolymers.....	74
<b>Table 7:</b> Number of BZ units per polymer chain.....	75
<b>Table 8:</b> BZ conversion and BP formation (absorbance of BP carbonyl groups at 1763 cm <sup>-1</sup> ) in BZS/S copolymers irradiated for 4 h. Theoretical crosslinking index $\gamma$ recalculated with a regard to the yield of phototransformation of BZ.....	76
<b>Table 9:</b> Apparent exponents $n'$ for storage and $n''$ for loss moduli of the thermally treated photoperoxidised BZS/S.....	81
<b>Table 10:</b> Zero shear viscosity $\eta_0$ and distribution parameter $h$ of initial and thermally treated photoperoxidised BZS/S that did not reach the gel point.....	81
<b>Table 11:</b> Slopes of Cole-Cole representation of the thermally treated photoperoxidised BZS/S.....	82
<b>Table 12:</b> Value of plateau $G_e$ , elastically effective strands density $\nu$ , molecular weight between crosslinks $M_c$ determined from rheology.....	83
<b>Table 13:</b> Value of plateau $G_e$ , crosslink density $\nu_c$ , molecular weight between crosslinks $M_c$ determined from rheology.....	84
<b>Table 14:</b> Polymerization data for a series of NMP copolymers BZS/S.....	86
<b>Table 15:</b> GPC results for polymers VZ1-VZ9 using MALS + RI detector and the comparison with zero shear viscosity $\eta_0$ and distribution parameter $h$ .....	86
<b>Table 16:</b> BZ conversion, BP formation (absorbance of BP carbonyl groups at 1763 cm <sup>-1</sup> ) in BZS/S copolymers irradiated during 4, 6 or 9 h and theoretical crosslinking index $\gamma$ .....	88
<b>Table 17:</b> Apparent exponents $n'$ for storage and $n''$ for loss moduli and slope of Cole-Cole representation of the thermally treated photoperoxidised BZS/S.....	89
<b>Table 18:</b> Thermally treated photoperoxidised BZS/S (100 mg) density of the CCl <sub>4</sub> extracts (10 ml).....	91
<b>Table 19:</b> Crosslink density $\nu_c$ for a series of crosslinked copolymers BZS/S calculated from sol fraction.....	92
<b>Table 20:</b> Characterisation of the network of crosslinked BZS/S copolymers by swelling.....	94
<b>Table 21:</b> Characterisation of the network of crosslinked BZS/S copolymers by swelling regarding to network imperfections resulting from chain ends.....	94
<b>Table 22:</b> Average mesh sizes $\xi$ of the swollen polymer networks of crosslinked BZS/S samples..	95
<b>Table 23:</b> Comparison of theoretical values of crosslink densities $\nu_c$ with crosslink densities $\nu_c$ determined by various techniques and elastically effective strands $\nu$ determined by rheology.....	99
<b>Table 24:</b> Content of CQMA in monomer mixture and in copolymer CQMA/S determined by means of UV/VIS and FTIR spectroscopy and the theoretical crosslinking index $\gamma$ .....	107
<b>Table 25:</b> GPC and Cole-Cole results of initial and irradiated copolymers CQMA/S.....	109

# 1 INTRODUCTION

This thesis (thèse en co-tutelle) was done in the frame of long-lasting cooperation between Polymer Institute, Slovak Academy of Sciences, Bratislava and Ecole Nationale Supérieure de Chimie de Clermont-Ferrand and Laboratoire de Photochimie Moléculaire et Macromoléculaire, Université Blaise Pascal, Clermont-Ferrand. The Ph.D. study was realised during 3 years, in alternation 6 months in France and 6 months in Slovakia. The stay in France was financed by a scholarship granted by French government (Bourse du Gouvernement Français).

Crosslinking of polymers represents a process of great practical importance. The reason is that crosslinking completely changes the physical properties of polymers. This process has been intensively studied from the point of view of basic research as well as applications. Crosslinking of polymeric material can be accomplished by the addition of special additives, which under the action of heat or light connect polymer chains to produce polymer network. Photo-crosslinking of oligomers and polymers constitutes the basis of important commercial process with broad applicability, including photo-imaging, UV-curing of coatings and inks<sup>1,2</sup>. These processes require absorption of the light energy by photoactive agent and consecutive processes lead to the formation of new chemical bonds. Photo-crosslinking may be accomplished by the use of photo initiators, photo-crosslinking agents and photo-crosslinkable polymers, which represent the photoactive agents. Photoactive agents absorb light in the UV-visible spectral region, generally 250-400 nm to yield electronically excited states which may undergo crosslinking directly or convert this light energy into chemical energy in the form of reactive intermediates, such as free radicals, reactive cations, etc. These species subsequently initiate crosslinking reactions. Photo-crosslinkable polymers contain light sensitive groups in the main chain as well as side chains.

Methods of polystyrene (PS) crosslinking using a small amount of copolymerised crosslinker are scarce. According to our knowledge, vinyl benzocyclobutene structure incorporated into PS chains was used for its crosslinking<sup>3,4</sup>. Crosslinking of these materials proceeds at a temperature exceeding 200 °C via a coupling reaction of two benzocyclobutene structures, which was exploited for the preparation of architecturally defined nanoparticles via intramolecular chain collapse<sup>3</sup>. A generalised approach for the applications of these materials to the modification of solid surfaces, such as a wide variety of metal, metal oxide, semiconductors, and polymeric surfaces is described<sup>4</sup>. Also in a chloroform solution the formation of crosslink between PS chains with phenylindene pendant groups via their photo-dimerization was studied<sup>5</sup>. Another possibility to crosslink

polystyrene is the copolymerization of styrene with monomer bearing perester group<sup>6</sup>.

Benzil (BZ) is one of the most important and the most studied 1,2-dicarbonyl compound. Due to its photochemical properties it has found industrial application mainly as a photoinitiator of radical polymerization<sup>7</sup>. It has been utilised in the preparation of photographic materials<sup>8</sup> and polymer resists<sup>9</sup>. Photochemistry of BZ is more than 100 years old. In 1886, Klinger observed photochemical transformation of BZ<sup>10</sup>. BZ photochemistry was widely studied in solutions of various solvents in the presence or absence of oxygen<sup>11</sup>. Irradiation of BZ in polymer matrix affords benzoyl peroxide (BP) almost quantitatively<sup>12</sup>. BP is photoactive too. To increase the yield of BP formation and at the same time to avoid its photochemical reactions, it is necessary to use the region of light where BP does not absorb. These results opened the possibility for a preparation of new types of photosensitive polymers with BZ in the main chain<sup>13</sup> or with BZ as a pendant group<sup>13,14,15,16,17,18,19</sup>. Polymers bearing BZ units in the main chain or as pendant groups have been examined as potential negative<sup>13</sup> or positive<sup>19</sup> resist materials based on photo degradation of their polymer networks. They were exploited as water-soluble polymeric photoinitiators<sup>14</sup>. Using of combination of BZ and other active part (probes, drugs, stabilisers) in one molecule can be used for the process of bonding without modification of commercial polymers. Photoperoxidation of these combined molecules will lead to the addition of these active parts to any polymers through acyloxy radicals. This process of photoinitiated grafting can find even more general applications in the plastic industry.

This Ph.D. thesis concerns copolymers with pendant BZ groups that are able to convert BP under irradiation ( $\lambda > 400$  nm) and crosslink by irradiation ( $\lambda > 300$  nm) or heating. In the previous studies, styrene copolymers were prepared but due to the different copolymerization parameters, distribution of BZ structure was not homogeneous<sup>16-18</sup>. For this study, 1-phenyl-2-{4-[2-(4-vinylbenzyloxy)ethoxy]-phenyl}ethane-1,2-dione (BZS) was chosen as comonomer because a more similar copolymerization parameters are expected. Copolymerization parameters are almost equal to a value of 1 for copolymerization of styrene with styrene derivative with a weak electro-donating group in para position<sup>20</sup>. A copolymer that exhibits a more regular distribution of BZ pendant groups is suitable to characterise a network after its crosslinking. Due to the fact that mechanism of photoperoxidation has not been fully elucidated, it is necessary to study the details of this process. The network of copolymers bearing BZ units was not studied up till now. The aim is to follow the process of crosslinking by various methods and their comparison.

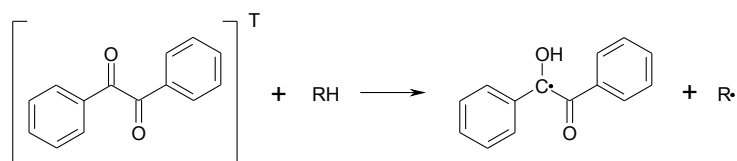
## 2 BIBLIOGRAPHIC STUDY

### 2.1 Photochemistry of benzil

#### 2.1.1 Photochemistry of benzil in solution in inert atmosphere

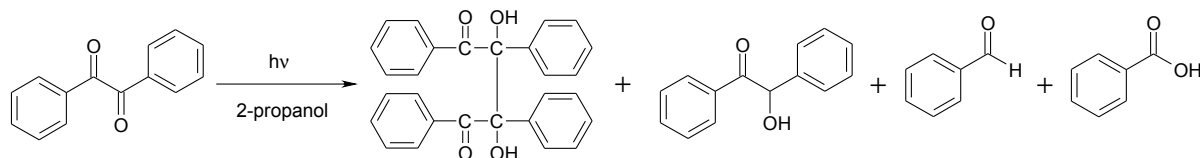
Majority of photochemical reactions of benzil (BZ) in inert atmosphere could be characterised as reaction of lowest excited triplet state with solvent. These reactions are very dependent on solvent or additives. Reactivity of BZ decreases in order: THF > dimethylformamide > methanol > ether >> toluene > *n*-hexane > benzene<sup>21</sup>.

Interaction of the lowest excited triplet state of BZ with solvent or additive causes removing of hydrogen atom from hydrogen donor molecule (RH) and formation of ketyl radical<sup>21,22,23</sup> (Scheme 1)



**Scheme 1:** Interaction of the lowest triplet state of BZ with hydrogen donor.

Then, different products are formed by combination or disproportionation of ketyl radical and radical from hydrogen donor. Usually, the photolysis products of BZ in different solvents are benzoine, benzil pinacol, benzaldehyde, benzoine benzoate, benzoic acid<sup>21-28</sup>. Composition of products is influenced by hydrogen donor, concentration of reagents and light intensity.



**Scheme 2:** Photoreduction of BZ in 2-propanol.

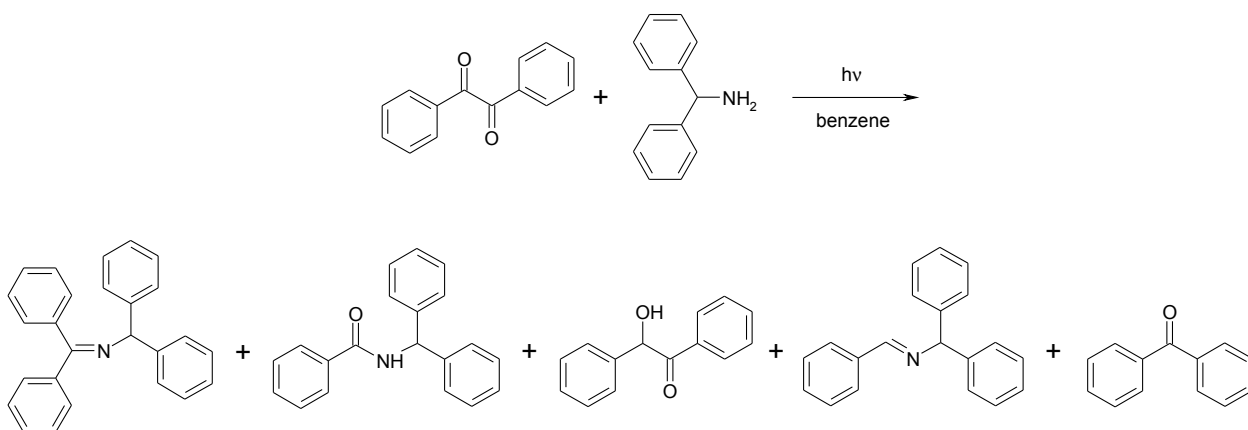
Main products of photoreduction of BZ in 2-propanol and cumene are benzoine and benzil pinacol (Scheme 2). Minor products are benzaldehyde, benzoic acid and some unidentified products

with higher molar mass<sup>22,23</sup>.

The main product of irradiation of BZ in THF, dodecane and cyclohexane is benzaldehyde<sup>21, 22,24</sup>. A small amount of benzoine is observed in THF and cyclohexane. In dodecane, if diethylhydroxylamine is added, the yield of benzaldehyde increases till concentration of additive reaches  $10^{-3}$  mol.dm<sup>-3</sup>. Another increase of concentration causes rapid decrease of yield<sup>24</sup>.

When BZ is irradiated in methanol solution with triethylamine added, the formation of benzoine is increased to 80 %<sup>25</sup>. 85 % yield of benzoine can be reached by an irradiation of BZ at 50 % conversion in a mixture of CH<sub>3</sub>CN-CH<sub>3</sub>OH-H<sub>2</sub>O-triethylamine (88:7:2:3) in the presence of TiO<sub>2</sub> as a photocatalyst<sup>26</sup>.

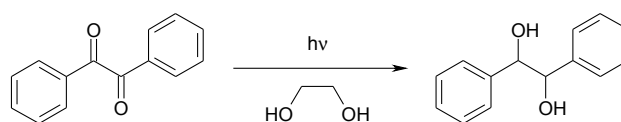
In a contrast to tertiary amines, the main products of BZ photolysis in the presence of primary amine are amine compounds. When a mixture of BZ and benzhydrylamine (1:2) is irradiated by UV light, N-benzhydrylidene-benzhydrylamine, N-benzhydrylbenzamide, benzoine, benzylidene- benzhydrylamine and benzophenone are formed (Scheme 3)<sup>27</sup>. Primary product is benzoine that decomposes into radical intermediates; then, they are transformed to benzaldehyde and benzophenone. Final products are formed by their reaction with benzhydrylamine.



**Scheme 3:** Irradiation of a mixture BZ - benzhydrylamine (1:2) by UV light.

The products of BZ irradiation with N-butylamine in inert atmosphere are N-butylbenzamide (19 %), deoxybenzoine (5 %) and diastereomers of pinacol. N,N-diethylbenzamide (42 %) is formed if diethylamine is used<sup>28</sup>.

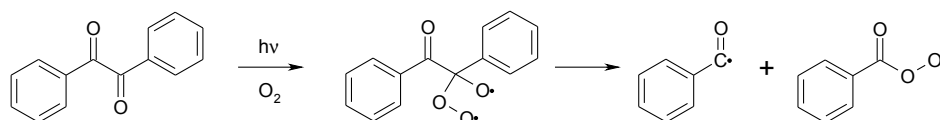
In ethyleneglycol, a hydrogen bond is formed between OH groups of solvent and CO groups of BZ (Scheme 4). This interaction between BZ and solvent cause 1,2-phenylethane-1,2-diol to be formed by photolysis<sup>29</sup>. This unstable product is identical to product created by electrolysis of BZ.



**Scheme 4:** Photoreduction of BZ in ethyleneglycol.

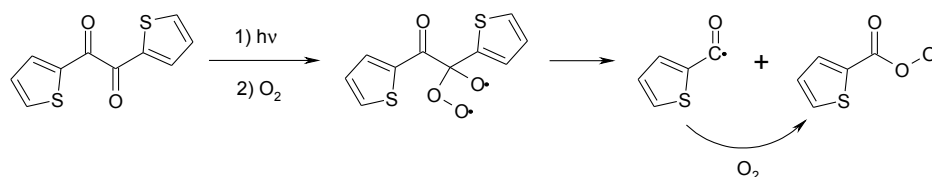
### 2.1.2 Photochemistry of benzil in solution in presence of oxygen

BZ is stable upon irradiation in inert atmosphere in solutions that does not contain hydrogen donor (benzene) but BZ is highly reactive in presence of oxygen<sup>30</sup>. Mechanism was studied on epoxidation of olefins. It was recognised that there are two concurrent reactions: (1) formation of singlet oxygen ( $^1\text{O}_2$ ) by transfer of energy from triplet state BZ to triplet oxygen, (2) addition of basic state oxygen ( $^3\text{O}_2$ ) to diketone triplet yielding acylperoxy radical after decomposition of supposed 1,4-biradical<sup>31</sup> (Scheme 5). Acylperoxy radicals cause epoxidation of olefins.



**Scheme 5:** Mechanism of photooxidation of BZ in the presence of oxygen.

Triplet state oxygen adduct was observed for 2,2'-thenil in acetonitrile using laser flash photolysis<sup>32</sup> (Scheme 6). Attempts to observe triplet-oxygen adduct for BZ failed maybe due to weak absorbances or due to short lifetimes.

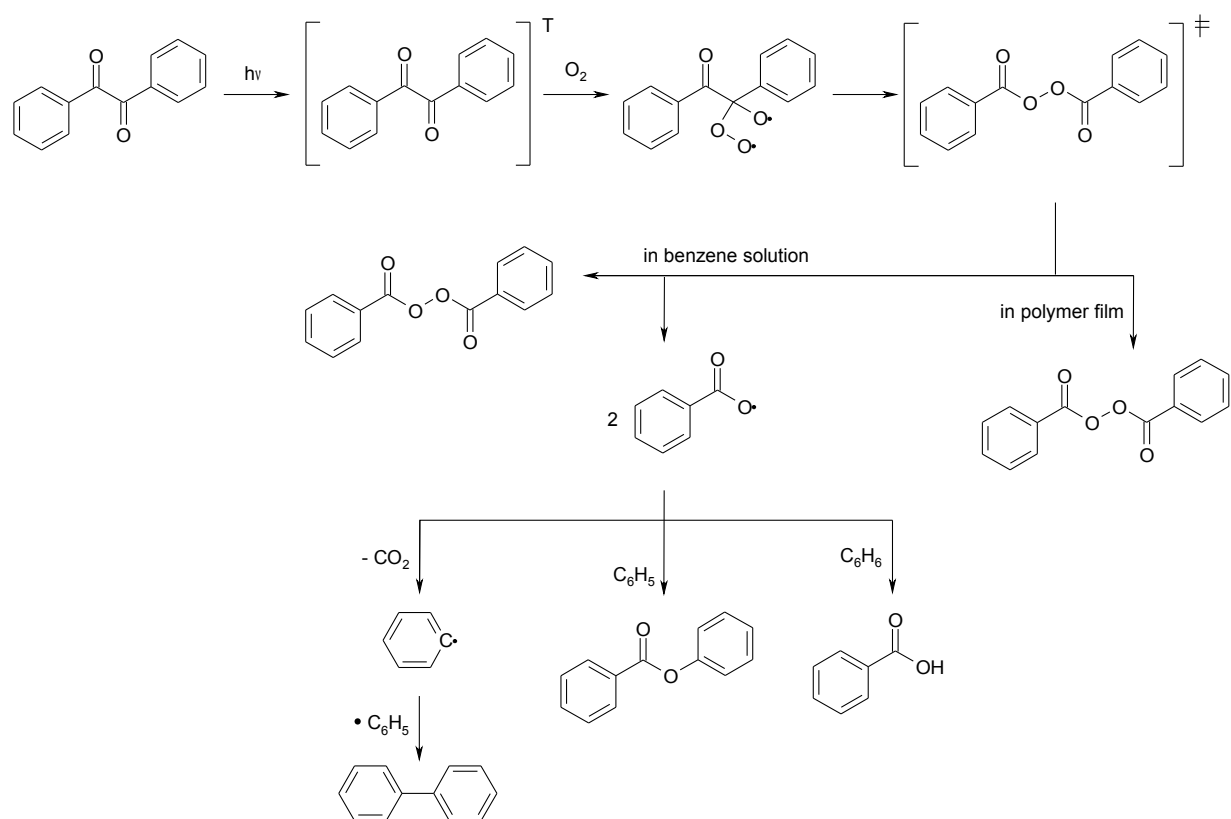


**Scheme 6:** Mechanism of photooxidation of 2,2'-thenil in the presence of oxygen.

Photooxidation products of BZ in benzene are benzoic acid, phenyl benzoate, biphenyl, BP, phenol and perbenzoic acid<sup>33</sup>. Similar products were obtained by photooxidation of poly[1-phenyl-2-(4-propenoylphenyl)ethanedione-*co*-styrene] (PCOCO/S) in benzene in the presence and absence of molecular oxygen<sup>34</sup>.

### 2.1.3 Photochemistry of benzil in polymer film

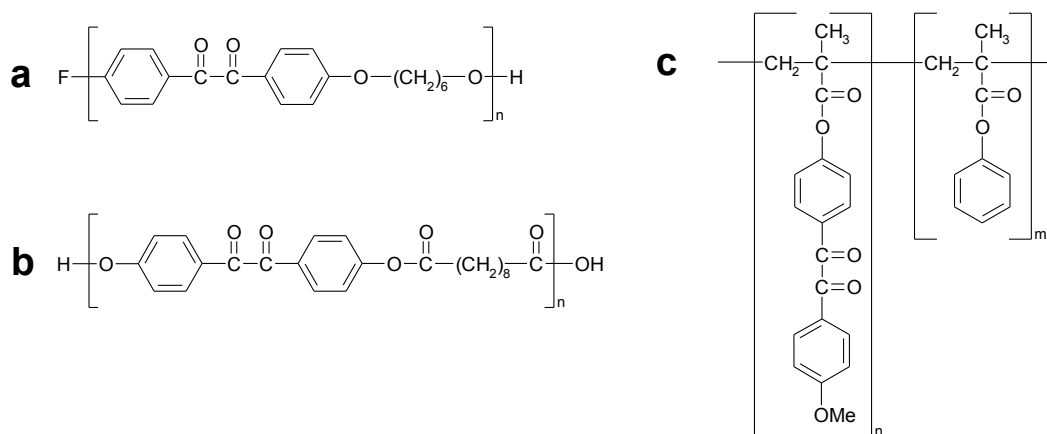
BZ can be converted almost quantitatively to BP in aerated PS or poly(methyl methacrylate) film by irradiation at  $\lambda > 400$  nm (the long wavelength edge of the  $n \rightarrow \pi^*$  absorption band)<sup>12</sup>. The small amount of BP is formed by photooxidation of BZ in solution as well. In a contrast to the irradiation in solution, in polymer film the separation of radicals formed by photooxidation of BZ is less probable and there are less of deactivated excited states. These conditions are favourable for formation of BP. The yield of BP formation is increased by irradiation of light from a region that BP does not absorb. 1,4-biradical was proposed as an intermediate for photooxidation of BZ in film and in benzene solution<sup>12,31</sup>. Formation of 1,4-biradical by addition of oxygen to excited triplet state of BZ followed by its rearrangement, yields to BP with excess of vibrational energy. Common Scheme 7 describes the reactions in benzene solution and in polymer film. The rate of reaction is sensitive to the nature of the glassy polymer matrix and decreases in the order: PS > bisphenol A polycarbonate > poly(vinyl chloride) > bisphenol A polysulfone > PMMA<sup>35</sup>.



**Scheme 7:** Photooxidation of BZ in a benzene solution and in a polymer film.

### 2.1.4 Photochemistry of polymers bearing benzil units

Simbürger et al.<sup>13</sup> prepared polymers bearing BZ units in the main chain poly(oxyhexyleneoxy-4,4'-benzilylene) (a), poly(oxy-4,4'-benzilyleneoxysebacoyl) (b) and copolymer with BZ moiety as pendant side groups poly(phenyl methacrylate)-*co*-4-methacryloyloxy-4'-methoxybenzil) (c) by polycondensation and free radical polymerization (Scheme 8). The polymers became crosslinked during UV irradiation and were assessed as potential negative resist materials. The lithographic sensitivity of these polymers depended on the irradiation source (Hg-lamp, 311 nm; excimer laser, 308 nm) and on the pulse energy of the excimer laser (50-400 J.m<sup>-2</sup>).



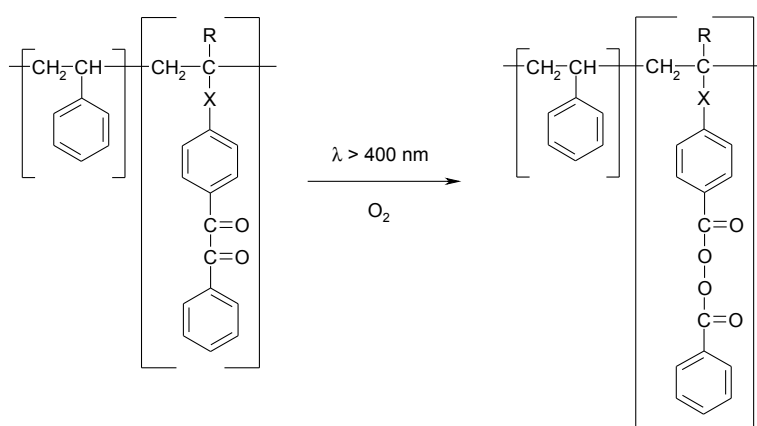
**Scheme 8:** Structures of polymers bearing BZ moiety: poly(oxyhexyleneoxy-4,4'-benzilylene) (a), poly(oxy-4,4'-benzilyleneoxysebacoyl) (b) and poly(phenyl methacrylate)-*co*-4-methacryloyloxy-4'-methoxybenzil) (c).

When the pulse energy of the laser was raised, an increase of the lithographic sensitivity by a factor of up to 4-6 was observed, so that the lithographic sensitivity of these polymers can be tuned by adjusting the laser pulse energy. Both quantum efficiency of crosslinking and chain scission increased as the laser energy was raised. The transformation of the BZ units occurs with higher efficiency when intense laser UV light is employed.

Water soluble copolymers with pendant BZ moieties were prepared by copolymerization of 1-{4-(2-methacroyloxyethoxyphenyl)}-2-phenylethane-1,2-dione (BZMA) with three water soluble comonomers<sup>14</sup>. These macromolecular photoinitiators are as efficient and effective as their low molecular weight counterparts but with the associated advantages derived from their macromolecular nature. In the presence of an amine cosynergist, 2-(*N,N*-diethylamino)ethanol, electron transfer via triplet exciplex with BZ chromophore appears to be the primary mode of action of the initiator. The attachment of BZ moieties to macromolecular chains prevents secondary

reaction (primary radical termination, initiator chain transfer reactions) with respect to those of a low molecular weight model BZ derivative<sup>15</sup>.

Poly[1-{4-(2-methacroyloxyethoxyphenyl)}-2-phenylethane-1,2-dione-*co*-styrene] (BZMA/S) was prepared and irradiated ( $\lambda > 400$  nm) in the presence of molecular oxygen at ambient temperature while BP attached to polymer chain was created<sup>16</sup> (Scheme 9). The rate of BZ group consumption and peroxide formation matched the low molecular analogues BZMA and BZAc in polymer film (Table 1). Higher concentrations of oxygen increased the rate of consumption of BZMA. The first-order rate constants for thermal decomposition at 91 °C of photoperoxidised BZMA and photoperoxidised BZAc in PS are equal and are larger than in the photoperoxidised BZMA/S copolymer (Table 1). A very large portion (91 wt%) of photoperoxidised BZMA/S is insoluble in THF because of partial crosslinking. The insoluble part increases to about 99 wt% after the film is treated at 91 °C for 6 h. Both of the corresponding doped polymers remain completely soluble in THF after irradiation and thermolysis. Crosslinking during the irradiation and heating is ascribed to formation of ester linkages (through abstraction of H atoms from -O-CH<sub>2</sub>-CH<sub>2</sub>-O-groups by acyloxy radicals) and combination of pendant acyloxy radicals with radical sites on neighbouring chains; abstraction of hydrogen from benzylic carbon atoms along PS chains leads to scission. By contrast, irradiation and subsequent heating of BZMA-PS or BZAc-PS films results in more chain scissions than crosslinking since the average molecular weights are decreased. A major conclusion arising from this work is that BZ type groups can crosslink or degrade polymeric chains. The process that dominates is dependent upon the kind of polymer and how the BZ groups are placed within a polymer matrix.



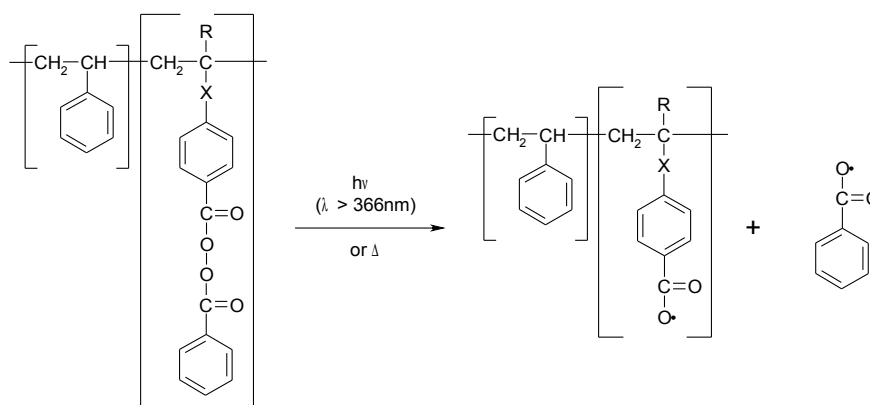
**Scheme 9:** Photoperoxidation of styrene copolymers with pendant BZ group.

X = CO-O-CH<sub>2</sub>-CH<sub>2</sub>-O, R = CH<sub>3</sub><sup>16</sup>

X = CO, R = H<sup>17</sup>

X = chemical bond; R = H<sup>18</sup>.

The photochemistry (366 nm) of PCOCO/S was investigated in benzene. No BP groups were detected in the presence and absence of molecular oxygen<sup>34</sup>. When PCOCO/S films are irradiated at  $\lambda > 400$  nm in air, the BZ carbonyl groups are transformed almost quantitatively to BP carbonyl groups<sup>17</sup> (Scheme 9). Subsequent additional irradiation at 366 nm or heating at 91 °C of the BP carbonyl groups containing copolymer films generates ester moieties. Significantly more crosslinking than main-chain scission is manifested in the copolymer. The rate of the thermal decomposition of the pendant BP carbonyl groups at 91 °C is 3 times slower than that of noncovalently attached BP molecules in polystyrene films (Table 1). Proposed possible mechanism involves conversion of potential energy of the excited states to kinetic energy for homolytic cleavage of peroxide bond (Scheme 10).



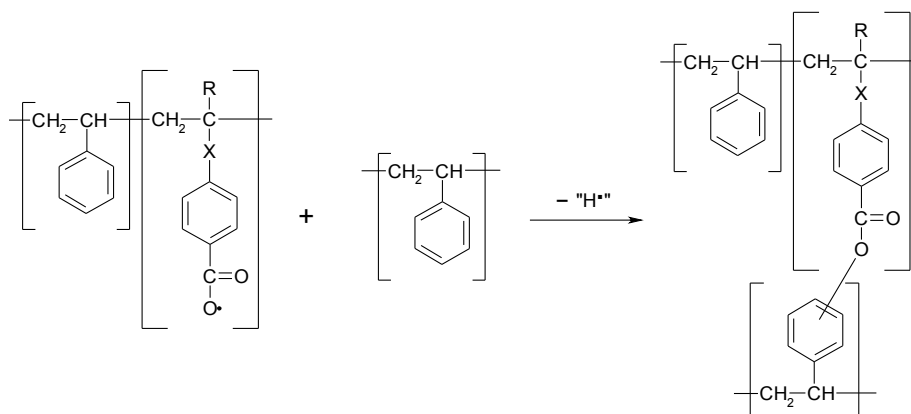
**Scheme 10:** Decomposition of formed peroxides in photoperoxidised styrene copolymers with pendant BZ group.

$X = CO-O-CH_2-CH_2-O$ ,  $R = CH_3$ <sup>16</sup>

$X = CO$ ,  $R = H$ <sup>17</sup>

$X = \text{chemical bond}$ ;  $R = H$ <sup>18</sup>.

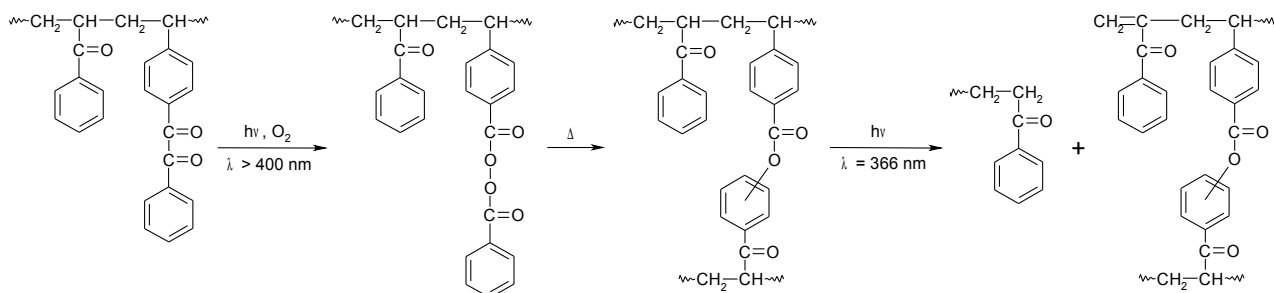
Crosslinking may occur by more than one pathway: (1) addition of one acyloxy macroradical to a phenyl ring on another chain leading to ester formation as shown in Scheme 11; (2) random combination of two macroradicals whose centres are localised at pendant groups or main-chain benzylic sites. Due to entropic factors it is believed that combination between primary pendant acyloxy radical and secondary aryl or alkyl radical are less probable.



**Scheme 11:** Crosslinking of photoperoxidised styrene copolymers with pendant BZ group: addition of an acyloxy macroradical to a phenyl ring of another chain.  
 $X = \text{CO-O-CH}_2\text{-CH}_2\text{-O}$ ,  $R = \text{CH}_3$ <sup>16</sup>;  $X = \text{CO}$ ,  $R = \text{H}$ <sup>17</sup>;  $X = \text{chemical bond}$ ;  $R = \text{H}$ <sup>18</sup>.

Another analogous copolymer poly[1-phenyl-2-(4-vinylphenyl)ethane-1,2-dione-*co*-styrene] (VBz/S) was prepared and studied<sup>18</sup>. The distribution of VBz units in this styrene copolymer is less regular than in previously prepared copolymers. Irradiation at  $\lambda > 400$  nm in air causes almost quantitative transformation of pendant BZ groups into BP groups (Scheme 9). Subsequent heating at 91 °C converts the pendant BP groups to esters and benzoic acid moieties, and there is significantly more crosslinking than main-chain scission. Irradiation of the VBz/S copolymer films at 366, 313 and 254 nm also results in formation of BP groups, but they are transformed in situ upon absorption of a second photon by the matrix. The ratios of the relative rate constants for BP formation and subsequent transformation upon absorption by a second photon decrease with decreasing wavelengths of radiation. The ability of this polymer to form a negative image when irradiated at 254 nm through a mask was demonstrated. Photooxidation of pendant BZ groups of the VBz homopolymer was examined too. Irradiation of a film composed of a nonmiscible intimate mixture of VBz homopolymer and PS at  $\lambda > 400$  nm in air does not lead to discernible BP concentrations as well. Instead, the unreacted pendant BZ groups act as photosensitisers to transform the peroxy moieties almost immediately.

VBz was copolymerised with phenyl vinyl ketone (PVK) to prepare a new photosensitive material PVK/VBz<sup>19</sup>. Its irradiation ( $\lambda > 400$  nm) in air, followed by thermal decomposition of the resulting pendant BP groups leads to crosslinking. The subsequent irradiation of the crosslinked polymer at 366 nm results in the cleavage of the PVK chain between the junction points of the polymer network through a Norrish type II reaction<sup>36,37</sup>. PVK/VBz represents a novel type of photoresist based on polymer network decrosslinking. The process involves three steps: photo-generation of peroxides, crosslinking by its thermal decomposition, and subsequent photo-decrosslinking of the polymer network (Scheme 12).



**Scheme 12:** Photoperoxidation, thermal crosslinking and photo-decrosslinking of PVK/VBz.

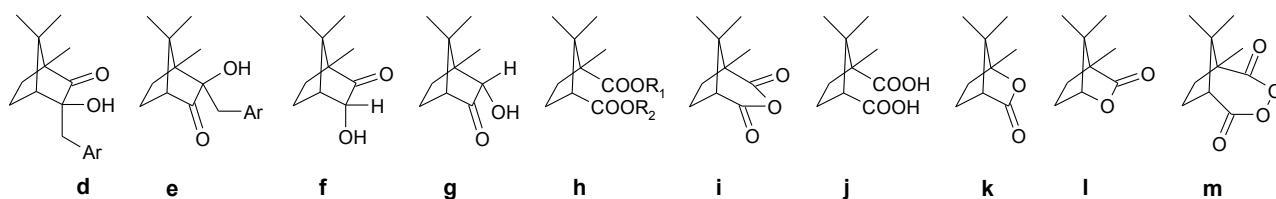
Rate constants of BP group decomposition at 91 °C in the air are summarised in Table 1. Different rate constants for model compounds and copolymer<sup>16</sup> and influence of structure and matrix<sup>17-19</sup> were discussed.

**Table 1:** Rate constants of BP derivatives decomposition at 91 °C.

<i>Photoperoxidised film</i>	<i>Rate constant [h<sup>-1</sup>]</i>
BZ in PS <sup>16</sup>	0.25
BZMA in PS <sup>16</sup>	0.43
BZAc in PS <sup>16</sup>	0.40
BZMA/S <sup>16</sup>	0.26
PCOCO/S <sup>17</sup>	0.08
VBz/S <sup>18</sup>	0.08
PVK/VBz <sup>19</sup>	0.10

## 2.2 Photochemistry of camphorquinone

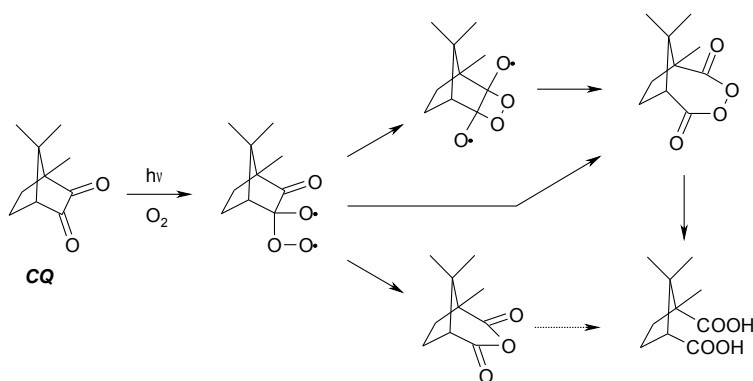
Camphorquinone (CQ) in the presence of H-atom donors is known to be an effective photoinitiator for curing acrylate- and methacrylate-based dental restorative resins<sup>38</sup>. Irradiations in oxygen-free solutions of benzene, CCl<sub>4</sub>, *t*-butylalcohol, methanol, and acetone are reported to produce no discernible loss of CQ while in toluene or *p*-xylene, 1:1 adducts with solvent molecules (**d, e**) are the major photo products<sup>39,40,41</sup>.



**Scheme 13:** Various photoproducts of CQ.

Irradiations of CQ in the presence of molecular oxygen yield products whose structures depend on the specific nature of the solvent. When the solvent has easily abstractable H-atoms, such as methanol or 2-propanol, mixtures of acyloins as *endo*-3-hydroxycamphor (**f**) and *endo*-2-hydroxyepicamphor (**g**), as well as various camphoric acid esters (**h**) are formed<sup>42</sup>. In xylene, the only products obtained were **i** and camphoric diacid **j**<sup>41</sup>. In solvents lacking easily abstractable H-atoms, such as CCl<sub>4</sub> and *t*-butylalcohol, camphoric anhydride (**i**) is the main photoproduct and in benzene, the isomeric camphorolactones (**k**, **l**) are obtained in largest yields<sup>42</sup>.

In benzene, the presumed intermediate predicted to formation of lactones, is camphordiacyl peroxide (**m**), formed by reaction between CQ and molecular oxygen<sup>42</sup>. Preliminary attempts to prepare **m** in solution have not been successful<sup>42</sup>. For the meaning of **d-m**, see Scheme 13.



**Scheme 14:** Mechanism proposed for CQ photooxidation in liquid solutions and in polymer films.

In contrast to BZ, CQ does not yield a stable intramolecular peroxy anhydride (**m**) when irradiated in aerated glassy polymer matrices<sup>43</sup>. Only products of its decomposition or related to triplet-oxygen adduct of CQ were identified. The mechanism proposed for CQ photooxidation is shown in Scheme 14.

## 2.3 Characterisation of polymer network

### 2.3.1 Swelling

A crosslinked polymer, when placed in a good solvent, rather than dissolving completely, will absorb a portion of the solvent and subsequently swell<sup>44,45</sup>. The swollen gel can be characterised as a solution, although it is an elastic one rather than a viscous solution. The extent of swelling

represents a competition between two forces. The free energy of mixing will cause the solvent to penetrate into polymer and try to dilute the polymer solution. This increase of entropy may be enhanced by increasing the temperature. As the polymer chains in the crosslinked polymer network begin to elongate under the swelling action of the solvent, they generate an elastic retractive force in opposition to this deformation. The volumetric swelling reaches steady state when these two forces are in balance.

Given that the steady state swelling ratio is a direct function of extent of crosslinking in the sample, swelling experiments are a simple and low-cost technique to characterise polymer networks. At the simplest level of analysis, swelling measurements can be used for quality control and serve as an indexing tool for polymer systems with different levels of crosslinking. At a higher level of analysis, the crosslink density, molecular weight between crosslinks, and number of crosslinks/chain can be computed if one knows the Flory interaction parameter  $\chi$  for the polymer-solvent system.

The free energy change of mixing when an isotropic polymer sample is placed in a pure solvent can be written in terms of the ordinary free energy of mixing  $\Delta F_m$  and the free energy associated with expansion of the polymer network  $\Delta F_{el}$  as

$$\Delta F = \Delta F_m + \Delta F_{el}$$

The free energy of mixing is described in terms of the number of solvent molecules  $n_1$ , the volume fractions of solvent and polymer,  $v_1$  and  $v_2$ , and the Flory interaction parameter  $\chi$  as

$$\Delta F_m = kT[n_1 \ln v_1 + \chi n_1 v_2]$$

The elastic component of the free energy  $\Delta F_{el}$  is associated with the change in the entropy as the network is deformed, and can therefore be written in terms of the linear deformation factor  $\alpha_s$  as

$$\Delta F_{el} = [kT v_e / 2][3\alpha_s^2 - 3 - \ln \alpha_s^3]$$

where  $v_e$  is the effective number of chains in the network. The chemical potential of the solvent in the gel is defined as

$$\mu_1 - \mu_1^0 = N_A (\partial \Delta F_m / \partial n_1)_{T,P} + N_A (\partial \Delta F_{el} / \partial \alpha_s)_{T,P} (\partial \alpha_s / \partial n_1)$$

where  $N_A$  is Avagadro's number. It is noted that  $\alpha_s^3 = V_\infty / V_0$  where  $V_0$  is the volume of the unswollen network and  $V_\infty$  the volume of the swollen network. Accordingly,  $V_0 / V_\infty = v_2$ . Incorporating the molar volume of the solvent  $V_m$  to compute the solvent contribution to the volume yields the expression:

$$\alpha_s^3 = 1/v_2 = (V_0 + n_1 V_m / N_A) / V_0$$

Therefore, one can evaluate previous equations to yield:

$$\mu_1 - \mu_1^0 = RT [\ln(1 - v_2) + v_2 + \chi v_2^2 + V_m (v_e / V_0) (v_2^{1/3} - v_2 / 2)]$$

At equilibrium, the chemical potential of the solvent in the polymer will equal the pure solvent, so that the left side of equation will be equal to zero. Rearranging the equation yields

$$-\left[\ln(I-v_2)+v_2+\chi v_2^2\right] = V_m(v_e/V_0)(v_2^{1/3}-v_2/2)$$

Rewriting the number of chains/unit volume in terms of the density of the polymer  $\rho_p$  and the molecular weight between crosslinks  $M_c$  such that  $v_e/V_0 = \rho_p/M_c$  and further rearrangement gives the final expression<sup>46</sup> for the crosslink density  $v_c$ .

$$\frac{\rho_p}{M_c} = 2v_c = -\frac{\ln(I-v_2)+v_2+\chi v_2^2}{V_m(v_2^{1/3}-v_2/2)}$$

Experimentally, one measures the equilibrium degree of swelling  $DS_E = V_\infty/V_0 = I/v_2$  and, knowing the Flory interaction parameter  $\chi$ , computes the crosslink density  $v_c$  and molecular weight between crosslinks  $M_c$ .

A hypothetical perfect network may be defined as one having no free chain ends; that is, the primary molecular weight  $M$  for a perfect network would be infinite. Any real network must contain terminal chains bound at one end to a crosslinkage and terminated at the other by the end (free end) of a primary molecule. The factor  $(1 - 2M_c/M_n)$  expresses the correction for network imperfections resulting from chain ends<sup>45</sup>. For a perfect network ( $M = \infty$ ) it reduces to unity:

$$-\ln(1-v_2)+v_2+\chi v_2^2 = \frac{V_m\rho_p}{M_c}\left(1-\frac{2M_c}{M_n}\right)\left(v_2^{1/3}-\frac{v_2}{2}\right)$$

There are several techniques for measuring the swell ratio of crosslinked polymer networks. The first technique uses gravimetric approach<sup>47</sup>. In this method, a sample is carefully weighted ( $M_0$ ), then immersed in a solvent at the required temperature for 24 h. At the end of this period, the sample is again carefully weighted ( $M_\infty$ ), and the swell ratio is computed from this data and the ratio of the density of the solvent ( $\rho_s$ ) and the density of the polymer ( $\rho_p$ ) as:

$$DS_E = 1 + \frac{\rho_p}{\rho_s}\left(\frac{M_\infty}{M_0}\right) - \frac{\rho_p}{\rho_s}$$

This technique is a simple and low-cost approach to measuring the swell ratio  $DS_E$  but it is difficult to obtain exact values when volatile solvents are used, since the solvent evaporates as the sample is being weighted. Additionally, it is difficult to determine when steady state is achieved.

More researchers are turning to techniques that use a probe to measure the change in height of a sample as it swells<sup>48</sup>. Assuming that the sample swells isotropically, the swell ratio is computed from the change in the height:

$$DS_E = \frac{d_\infty - d_0}{d_0}$$

where  $d_\infty$  is height of swollen sample and  $d_0$  is height of unswollen sample. This technique allows

one to measure both the transient and the steady state swell ratio and does not require the removal of the specimen from the solvent to make a measurement.

Degree of swelling can be also obtained by DSC measurements<sup>49</sup> if thermogram peaks of free and confined solvent are not overlapped. Knowing the specific heat of crystallisation of free solvent, it is possible to calculate the amount of the excess solvent from the area under the first peak and, by subtracting it from the total mass of the solvent, to determine the quantity of the confined solvent.

Flory interaction parameters have been measured for a large number of polymer-solvent pairs. The determination of  $\chi$  is a time-consuming task. It was determined by vapour pressure osmometry<sup>50</sup>, viscometry<sup>51</sup>, spectroscopic ellipsometry<sup>52</sup> or by combination of vapour sorption and dynamic laser light scattering methods<sup>53</sup>.

### 2.3.2 Thermoporometry

Thermoporometry, or thermoporosimetry, is a calorimetric method for characterising pore structure from the melting or freezing point depression of a liquid confined in a pore<sup>54</sup> (Figure 1). It is an alternative method to mercury porometry<sup>55</sup> and nitrogen adsorption porometry<sup>56</sup>.

It has been known for a long time<sup>57</sup> that a solvent confined in the pores of a material experiences an important shift of its liquid to a solid transition temperature. In 1920 Tammann described an apparatus for studying melting point depressions for thin films<sup>58</sup>. Using this apparatus, Meissner observed small depressions of melting temperature for crystals about 0.8  $\mu\text{m}$  thick<sup>59</sup>. In 1932 Kubelka<sup>60</sup> reported that iodine absorbed into porous carbon remained liquid at room temperature and proposed an explanation based on the effect of surface energy on the stability of small crystals. The effect of surface energy on melting temperature (known as the Gibbs-Thomson effect) has been discussed in detail by Reiss and Wilson<sup>61</sup> and Still and Skapski<sup>62</sup>. Skapski successfully applied the theory to the formation of ice crystals in clouds at different degrees of undercooling<sup>63</sup>. The first suggestions that melting temperature depression could be used to study pore sizes were made by Kuhn et al in 1955. These authors demonstrated melting temperature depression of about 2 °C for water in poly(vinyl alcohol)-poly(acrylic acid) gels<sup>64</sup> and 5 °C for benzene absorbed in lightly crosslinked rubber<sup>65</sup>. Their limited apparatus prevented quantitative measurements. A detailed theoretical basis for thermoporometry was established by Brun and co-workers<sup>66</sup> in 1977 starting from an application of the Gibbs-Duhem equation to the solid, liquid and vapour interfaces and making some reasonable assumptions concerning bound layers of liquid

which did not undergo phase changes. Scherer reviewed freezing and melting behaviour of liquids confined in small pores in comparison to those in bulk state<sup>67</sup>.

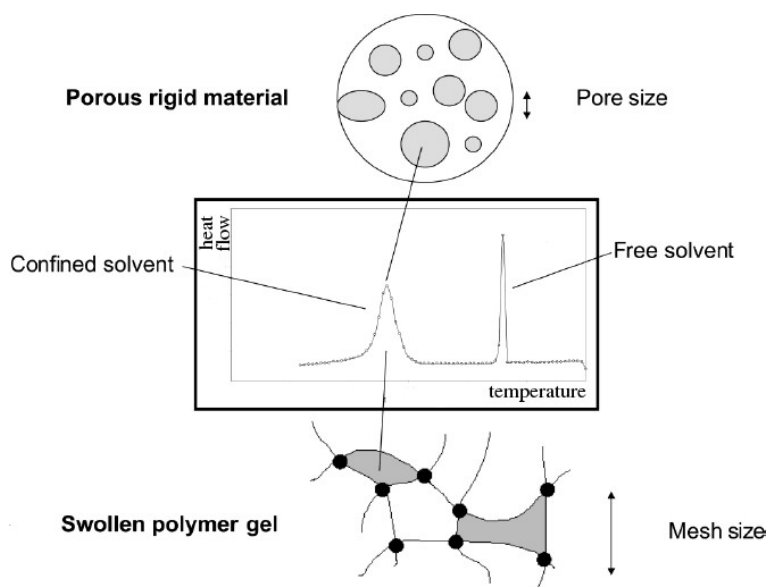


**Figure 1:** DSC thermal curve of swelling solvent in a divided medium, recorded with 0.7 °C/min as cooling temperature rate.

Nucleus must reach a critical radius that allows it to start the growth process. The critical radius is related to temperature: the smaller the size of the nucleus, the lower the temperature. Inside the divided medium the critical nucleus radius cannot be higher than the size of the cavity in which the liquid is trapped. Consequently, to crystallise the confined solvent, it is necessary to decrease the temperature in order to reach that corresponding to the pore size. Thus the freezing point depression undergone by the trapped solvent can be related to the size of the pore and it becomes possible to calculate the pore size distribution of the studied material. The triple point ( $T_0$ ) of the solvent undergoes a depression ( $\Delta T$ ) which is related to the radius of the pore ( $R_p$ ) where the phase transition occurs:

$$R_p = -\frac{A}{\Delta T} + t$$

where  $A$  is a constant depending on the solvent and  $t$  is the thickness of the layer of solvent remaining adsorbed on the surface of the pore which does not take part in the freezing or melting. Differential of previous equation is:

$$dR_p = -\frac{A}{(\Delta T)^2} d(\Delta T)$$

It is possible to calculate the pore-size distribution from the DSC thermal curve obtained from the freezing of the solvent confined inside the pores. The pore volume in which the crystallisation has occurred can be calculated as follows:

$$dV_p = k \frac{y}{W_a} d(\Delta T)$$

where:  $V_p$  is the pore volume,  $y$  is the DSC thermal curve ordinate (this value must be corrected by subtracting the base line of the recording),  $\Delta T$  is the triple point depression,  $k$  is a proportionality coefficient depending on both the rate of cooling and the sensitivity of the DSC instrument and  $W_a$  is the apparent enthalpy of solidification of the confined solvent.

Therefore, the equation for pore size distribution is:

$$\frac{dV_p}{dR_p} = A \frac{y(\Delta T)^2}{W_a}$$

$W_a$  takes into account the decrease of solidification enthalpy with respect to temperature and the proportion of solvent which does not take part in the crystallisation phenomena. One can write

$$W_a = W_{th} \frac{V_p'}{V_p}$$

where  $W_{th}$  represents the solidification enthalpy of the pure solvent and depends on the phase transition temperature,  $V_p'$  is the volume of the solvent really crystallised,  $V_p$  is the pore volume.

Unfortunately  $W_{th}$  is not available at the temperature of crystallisation of the solvent inside the pore. However,  $W_a$  can be calculated from the DSC thermal curve and the pore volume known by gas sorption for each silica gel sample. Then,  $W_a$  can be expressed as follows

$$W_a = \frac{\Delta H}{\rho V_p^*}$$

where  $H$  is the crystallisation enthalpy of the solvent calculated per gram of dry silica gel sample,  $V_p^*$  is the pore volume per gram of sample and  $\rho$  is the density of the solvent in the solid state.

This technique has been essentially applied to calculate pore size distributions in rigid porous substrates mainly using water as a probe liquid. It was used to study water altered glass<sup>68</sup>, texture of silica aerogels<sup>69</sup>, polymer electrolyte membranes<sup>70</sup>, titania gels<sup>71</sup>.

Thermoporometry was successfully used for characterising of polymer gels swollen in water like hydrogel membranes<sup>72</sup> or cellulose films<sup>73</sup>. Water migration was observed during thermoporometry studies<sup>73</sup>.

Different solvents were used as a probe liquid. Nitrobenzene and carbon tetrachloride were used to study controlled pore glass<sup>74</sup>. Thermoporometry technique was calibrated by using well-characterised polystyrene/divinylbenzene samples for acetonitrile<sup>75</sup>. Heptane<sup>76</sup> and cyclohexane<sup>77</sup> were used to swell crosslinked elastomers followed by DSC measurements. Various benzene substituted solvents including *o*-, *m*- and *p*-xylene, *p*-dichlorobenzene, 1,2,4-trichlorobenzene, naphthalene<sup>78</sup> and acetone<sup>79</sup> were used for swelling of polyolefins. Proposed general law can avoid

preliminary calibrations<sup>78</sup>.

### 2.3.3 Sol fraction

Relation between weight fraction of sol  $S$  and degree of crosslinking  $q$  using the polymer with primary molecular weight distribution  $w_y$  is given:

$$S = \sum_{y=1}^{\infty} w_y [1 - q(1 - S)]^y$$

For high-molecular polymer with primary molecular weight distribution  $w(y)dy$ , summation can be replaced by integration. For low values of  $k$  is  $(1 - k)^y$  equal to  $e^{-ky}$ . We obtain the relation for weight fraction of sol:

$$S = \int_0^{\infty} w(y) e^{-q(1-S)y} dy$$

The relation between crosslinking index  $\gamma$  and sol fraction is as follows<sup>80</sup>:

$$\gamma = \frac{2 v_c M_w}{\rho} = \frac{M_w}{M_c} = \frac{1 - S^\varepsilon}{\varepsilon S^\varepsilon (1 - S)}$$

where  $v_c$  is a concentration of crosslinks,  $\rho$  presents polymer density and  $\varepsilon$  is a dispersion parameter defined by

$$\varepsilon = 1 - \frac{M_n}{M_w}$$

$\varepsilon$  is a number between 0 (monodispersed polymer) and 1 (infinite polymer).

### 2.3.4 Densitometry

Instead of measuring the gel fraction by gravimetry in the case of the gel swelling method, this technique concerns the soluble part of the samples, i.e. the uncrosslinked fraction<sup>81,82</sup>. During the crosslinking reactions, the average molecular weight of the chains increases, thus causing the sample to become gradually insoluble in solvents for the linear polymer. By measuring the density of the solution of the soluble part, the branching can be followed particularly before the gel point, that is as long as a soluble part exists. This technique also enables to detect chain scissions or any other phenomenon leading both to a decrease in the average molecular weight of the polymer and an increase in its solubility.

### 2.3.5 Rheology

Rheology is the science of flow and deformation of matter and describes the interrelation between force, deformation and time. Rheology is applicable to all materials, from gases to solids. The science of rheology is only about 70 years of age. It was founded by Reiner<sup>83</sup> and Bingham<sup>84</sup> meeting in the late '20s and finding out having the same need for describing fluid flow properties.

A solid is considered as ideally elastic in which deformation under a specific kind of stress takes place instantaneously on application, and disappears completely and instantaneously on withdrawal of the deforming stress. When the ideal elastic body is subjected to tensile or compressive stress, the proportionality is expressed as

$$\sigma = E \varepsilon$$

where  $\sigma$  is the applied stress (tensile/compressive),  $\varepsilon$  is the axial strain, and  $E$  is the modulus of elasticity. The proportionality law as defined above is known as Hooke's Law. If the ideal solid is subjected to a shear stress  $\tau$ , then the shear strain  $\gamma$  developed as a function of the stress applied is given by the expression

$$\tau = G \gamma$$

where  $G$  is the shear modulus.

A material is considered as ideally viscous when a fixed and constant stress is applied to a liquid or fluid body and it undergoes continuously increasing amount of strain or deformation which is non-recoverable on withdrawal of the stress. Newton developed similar formula to Hooke's Law for ideal viscous fluids. The shear stress  $\tau$  required to shear a Newtonian fluid is linearly and directly proportional to the shear strain rate  $d\gamma/dt$ :

$$\tau = \eta \frac{d\gamma}{dt} = \eta \dot{\gamma}$$

where  $\eta$  is the coefficient of viscosity.

Viscoelastic solids are solids which exhibit combination of properties of elastic solids and truly viscous liquids. Most polymeric materials exhibit a viscoelastic behaviour. Viscoelastic properties are investigated using rheological experiments such as dynamic mechanical testing, which offers a convenient way to assess time dependence of mechanical properties of polymers.<sup>85</sup>

Mathematically, the controlled strain experiment is represented as follows:

$$\gamma = \gamma_0 \sin \omega t$$

$$\tau = \tau_0 \sin(\omega t + \delta)$$

In general, the resultant stress will be delayed in time by a phase angle  $\delta$ . As shown in the plot below, the stress wave can be deconvoluted into two waves of frequency  $\omega$ , with one wave in phase

with the strain wave and one 90° out-of-phase (Figure 2). In other words,

$$\tau = \tau' + \tau'' = \tau_0' \sin \omega t + \tau_0'' \cos \omega t$$

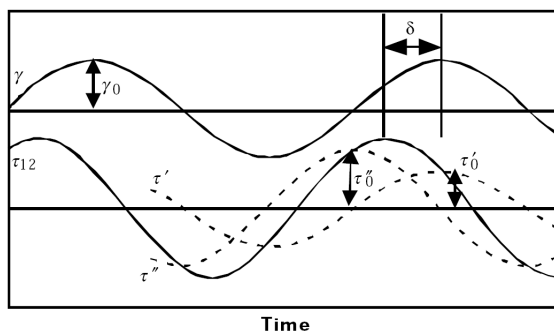


**Figure 2:** Relationship between imposed strain  $\gamma$  and resultant stress  $\tau_{12}$ , showing the phase lag  $\delta$  between the two. The stress is deconvoluted in the in-phase  $\tau'$  and out-of-phase  $\tau''$  components of stress.

Therefore, no single parameter can be used to characterise the stress-strain relationship in viscoelastic material. The complex dynamic modulus ( $G^*$ ) is resolved into two components using complex notation:

$$G^* = \frac{\tau}{\gamma} = G' + iG''$$

The real part of the complex modulus ( $G'$ ) describes stress-strain relationships that are in-phase.  $G'$  is called the storage modulus or elastic modulus. The imaginary component ( $G''$ ) characterises the out-of-phase component and is named the loss modulus or viscous modulus.

Dynamic viscosity ( $\eta^*$ ) is related to the complex modulus by

$$\eta^* = \frac{\tau}{d\gamma/dt} = \frac{G^*}{i\omega} = \eta' - i\eta''$$

where  $\eta' = G''/\omega$  and  $\eta'' = G'/\omega$ . Then, the real component of the complex viscosity ( $\eta'$ ) describes the viscous dissipation in the sample, while the imaginary component ( $\eta''$ ) represents the stored elastic energy.

The tangent of the phase angle ( $\tan \delta$ ) describes the balance between the viscous and elastic behaviours in a polymer melt:

$$\tan \delta = \frac{G''}{G'} = \frac{\eta'}{\eta''}$$

It is well known that the evolution of the rheological material properties directly reflects changes in molecular parameters. The linear viscoelastic properties in dynamic experiments are sensitive both to the chain scission and to the three-dimensional network formation.

**Table 2:** Values obtained from oscillatory rheometer.

<i>Newtonian Liquid</i>	$G' = 0$	$\eta' = \mu$	$\delta = \pi/2$
<i>Hookean Solid</i>	$G' = G$	$\eta' = 0$	$\delta = 0$
<i>Viscoelastic Material</i>	$G'(\omega) > 0$	$G''(\omega) > 0$	$0 < \delta(\omega) = \pi/2$

The evolution of the rheological material properties directly reflects changes in molecular parameters. Hence, rheology can be used to determine a gel point<sup>86</sup>. A crosslinking polymer at its gel point is in a transition state between liquid and solid. The gel point is defined unambiguously as the instant at which the weight average molecular weight diverges to infinity. At this juncture, the molecular weight distribution is infinitely broad ( $M_w/M_n \rightarrow \infty$ )<sup>87</sup>.

Winter and Chambon proposed a general criterion that can be used to identify the gel point. They have shown that at the gel point, both the elastic modulus ( $G'$ ) and the viscous modulus ( $G''$ ) exhibit a power-law dependence on the frequency of oscillation  $\omega$ <sup>88,89,90</sup>. The corresponding expressions describing dynamic moduli at the gel point are as follows:

$$G'(\omega) = S\Gamma(1-n)\cos(n\pi/2)\omega^n$$

$$G''(\omega) = S\Gamma(1-n)\sin(n\pi/2)\omega^n$$

where the  $S$  is the strength of the gel and depends on the flexibility of molecular chains and crosslinks, and on the crosslink density at gel point. The relaxation exponent  $n$  can have values in the range of  $0 < n < 1$ .

At the gel point, the storage and viscous moduli depend on frequency in an identical manner, corresponding to parallel lines in a frequency spectrum:

$$G'(\omega) \propto G''(\omega) \propto \omega^n$$

The loss tangent  $\tan \delta$  becomes independent of frequency ( $\omega$ ), but proportional to the relaxation exponent  $n$ :

$$\tan \delta = \frac{G''}{G'} = \tan(n\pi/2)$$

The frequency independence of the loss tangent in the vicinity of the gel point has been widely used to determine the gel point of crosslinked polymers<sup>91,92,93,94</sup>.

The gel point can be determined using definition of the sol-gel transition implying that  $\tan \delta$  loses its dependency on frequency and converges at the gel point. In a multifrequency plot of  $\tan \delta$  versus time of crosslinking, the values of  $\tan \delta$  converge at a time corresponding to the gel time.

An alternative way to determine gel points is by plotting the apparent viscoelastic exponents  $n'$  and  $n''$  ( $G' \propto \omega^{n'}$ ,  $G'' \propto \omega^{n''}$ ), obtained from the approximate scaling laws of the frequency dependence of  $G'(\omega)$  and  $G''(\omega)$  versus time of crosslinking. Hence, curves become congruent and the crossover at  $n' = n'' = n$  is an indicator of the gel point.

The average molecular weight increases as the crosslinking reaction proceeds, and diverges at the gel point<sup>92</sup>. This property could be used to measure the evolution of an incipient gel near the sol-gel transition. The zero shear viscosity  $\eta_0$  depends on the molecular weight and obeys a power law<sup>95</sup>

$$\eta_0 \propto M_w^a$$

with the widely quoted viscosity exponent  $a = 3.4$ .

At the gel point, the zero shear viscosity becomes infinite and immeasurable. It can be obtained from the complex viscosity  $\eta^*(\omega)$ :

$$\eta^* = G^*(\omega)i\omega = \eta' - i\eta''$$

$$|\eta^*|_{\omega \rightarrow \infty} = |\eta'|_{\omega \rightarrow \infty} = \eta_0$$

An empirical rheological model used to fit dynamic data is the Cole-Cole distribution expressed by<sup>86,96,97</sup>:

$$\eta^*(\omega) = \frac{\eta_0}{1 + (i\omega\lambda_0)^{1-h}}$$

where  $\lambda_0$  is the average relaxation time and  $h$  the parameter of the relaxation-time distribution. In the complex plane this model predicts the variation of the viscosity components ( $\eta''$  versus  $\eta'$ ) to be an arc of circle (Figure 3). From this representation it is easy to determine the parameters of the distribution:  $\eta_0$  is obtained through the extrapolation of the arc of the circle on the real axis and the distribution parameter  $h$  through the measurement of the angle  $\Phi = h\pi/2$  between the real axis and the radius going from the origin of the axis to the centre of the arc of the circle.

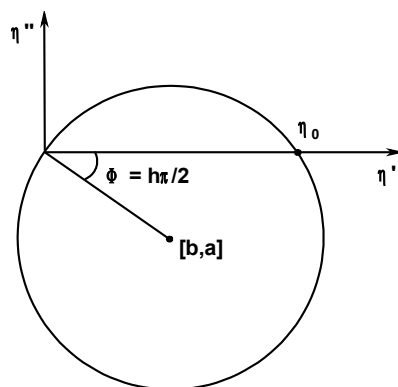


Figure 3: Cole-Cole plot.

Dynamic rheological measurements may be used to characterise a crosslinked polymer<sup>98</sup>. A crosslinked polymer storage modulus reaches a plateau  $G_e$  lower than the rubbery plateau of uncrosslinked material  $G_N^0$ . From the statistical rubber elasticity theory<sup>99</sup> it is possible to determine crosslinking densities. Equilibrium shear modulus should be related to the moles of elastically

effective network strands per ml:

$$G_e = g \nu RT$$

where  $g$  is a numerical factor not far from unity. As an improvement<sup>100</sup>, it can be assumed that all four strands radiating from an entanglement locus must be terminated by chemical crosslinks; this led to the relation:

$$\nu = 2\nu_c \left(1 - \frac{b}{2\nu_c M_n}\right) + a \left(1 - \frac{b}{2\nu_c M_n}\right)^2$$

where  $\nu$  is an amount of elastically effective network strands per ml,  $\nu_c$  is an amount of chemical crosslinks per ml,  $b$  is near  $2\rho^{101}$ ,  $M_n$  is the number-average molar mass before crosslinking,  $a$  is amount of entanglements per ml and can be expressed from the equation:

$$G_N^0 = g a RT$$

## 3 MATERIALS AND EXPERIMENTAL TECHNIQUES

### 3.1 Chemical products

#### *3.1.1 Chemical products for the synthesis of BZS*

Phenylacetyl chloride and 2-phenoxyethylacetate were distilled before using. SeO<sub>2</sub> was resublimed (Reachim, USSR). AlCl<sub>3</sub> (Merck, Germany), 4-vinylbenzyl chloride (90 %, Aldrich, Germany), Bu<sub>4</sub>NBr, NaOH, dichloromethane, ethanol, dioxane and benzene (analytical grade) were used as received.

#### *3.1.2 Chemical products for the synthesis of StNOR*

Stabilised styrene (Aldrich, Germany) was washed with diluted sodium hydroxide solution and water, dried with anhydrous MgSO<sub>4</sub> and distilled. StNO (Polymer Institute, Slovakia), Mn(OAc)<sub>3</sub> (≥ 98 %, Merck, Germany), NaBH<sub>4</sub> (98 +%, Janssen, Belgium), toluene, ethanol, acetic acid (analytical grade) were used as received.

#### *3.1.3 Chemical products for the synthesis of CQMA*

(±)-10-Camphorsulphonic acid (98 %, Aldrich, Germany), PBr<sub>5</sub> (95 %, Aldrich, Germany), triethylamine (p.a., Fluka, Switzerland), methacryloyl chloride (97 %, Aldrich, Germany), iodine (p.a., Lachema, Czech Republic), triphenylphosphine (p.a., Lachema, Czech Republic), dioxane (anhydrous, Aldrich, Germany), bromobenzene (p.a., Riedel-de-Haën, Germany), toluene (analytical grade) were used as received. SeO<sub>2</sub> was resublimed in the presence of HNO<sub>3</sub> (Reachim, USSR). CH<sub>3</sub>COOK (p.a., Lachema, Czech Republic) was freshly molten. Acetic acid (99.8 %, Slavus, Slovakia) was distilled from P<sub>2</sub>O<sub>5</sub>. Diethylether (Centralchem, Slovakia) was dried over anhydrous Na<sub>2</sub>SO<sub>4</sub> for several days, filtered and dried with a sodium wire. Xylene (p.a., Lachema, Czech Republic) was dried with a sodium wire.

### ***3.1.4 Chemical products for the polymerizations***

Stabilised styrene (Aldrich, Germany) was washed with diluted sodium hydroxide solution and water, dried with anhydrous  $\text{MgSO}_4$  and distilled. 2,2'-Azobis(2-methylpropionitrile) AIBN (Fluka, Switzerland) was recrystallised from methanol. *Tert*-butyl peroxybenzoate TBPB (98 %, Merck, Germany), methanol, chloroform, ethanol, tetrahydrofuran (analytical grade) were used as received. StNO, BTXNOR and HONOR were prepared at Polymer Institute, Slovakia.

### ***3.1.5 Chemical products for the other experiments***

Benzoyl peroxide BP (p.a., Merck, Germany) and carbon tetrachloride, 99.8 % (ACROS, Belgium) were used as received.

## **3.2 Used techniques**

### ***3.2.1 Synthetic techniques and spectral characterisation***

All reactions were monitored by thin layer chromatography using plastic sheets covered with silica gel 60 F<sub>254</sub> (Merck, Darmstadt, Germany) with UV detection at 254 nm. Silica gel L 100/250 (Lachema, Brno, Czech Republic) was used for column chromatography. Melting points were determined by Kofler apparatus (Nageman, Germany) and are uncorrected. <sup>1</sup>H NMR and <sup>13</sup>C NMR spectra were measured on a Bruker AM 400 spectrometer (Germany). FTIR spectra were recorded on Impact 400 (Nicolet Instrument Corporation, WI, USA) FT spectrophotometer. UV/VIS absorption spectra were measured on a Shimadzu 1650PC (Japan) spectrophotometer.

The content of BZS monomer in the copolymer was determined from <sup>1</sup>H NMR by comparison of integrated peak areas of separated three methylene groups (f-h) and aromatic hydrogens (a-d) of BZS with both aromatic and aliphatic styrene hydrogens (m-q) after subtraction of integral values of e and i-l protons signals of BZS which were overlapped by those to the styrene (m-q) (Figure 4).

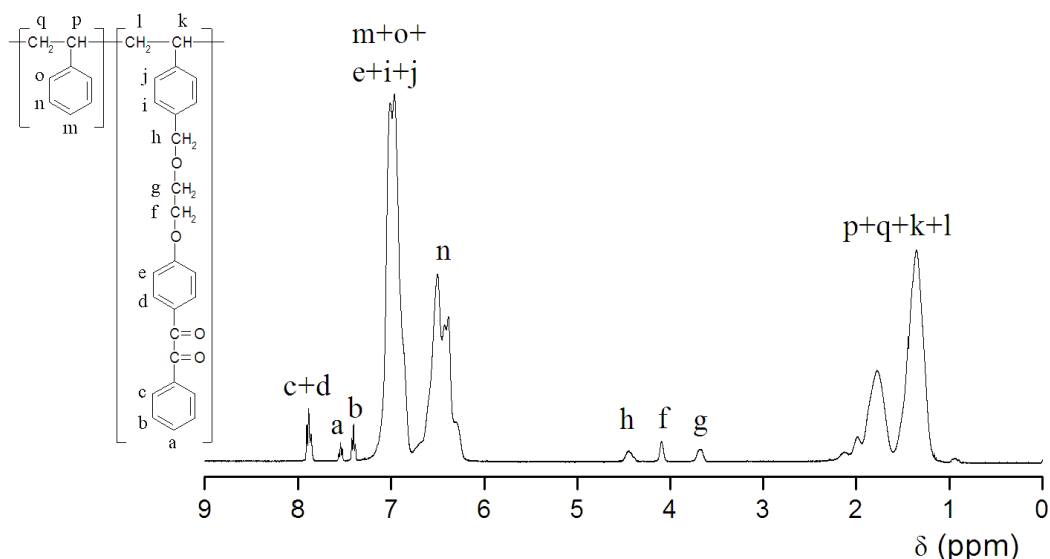


**Figure 4:** NMR spectrum of BZS/S copolymer with labelled peaks.

### 3.2.2 GPC measurements

Molar masses were estimated by GPC with THF as a mobile phase, series-connected PSS SDV 105 Å and PSS SDV 500 Å columns ( $d = 8$  mm,  $l = 300$  mm), a Knauer 64 pump (1 ml/min, 3.3 – 3.4 MPa), and MALS + RI WATERS 410 detector. Samples were prepared by diluting of 2 mg of polymer in 1 ml of THF.

### 3.2.3 Preparation of films

Films consisting of 40 mg or 100 mg of polymer were prepared by casting from 1 ml solution (benzene or chloroform) on a glass plate ( $10$  cm<sup>2</sup> area) in the dark. The plate was covered by a Petri dish to slow the solvent evaporation. This procedure resulted in films with good optical quality. The self-supporting polymer films were separated from the glass by dipping into distilled water. Films were dried to constant weight at room temperature under vacuum. They were used in chapter 4 and 7.

Films were prepared also by compression moulding of 200 mg of polymer at  $20$  cm<sup>2</sup> in a paper window between two Teflon sheets during 1 min at  $150$  °C under 200 bar. The thickness of the films was about  $100$  μm. They were used in chapters 5-7.

### 3.2.4 Irradiation devices

A homemade “merry-go-round” apparatus was employed in irradiation experiments to study the photoperoxidation step (chapter 4, 7). It consists of three concentric quartz walls reactor in which a 125 W medium pressure mercury arc in the inner cylinder was placed. In the inner walls of the reactor (surrounding the space for the mercury arc) circulated cooling water. In the outer walls a 1 cm thick layer of a liquid filter (500 g NaBr plus 3 g  $\text{Pb}(\text{NO}_3)_2$  per 1000 ml aqueous solution) transmitting  $\lambda > 330$  nm was placed (Figure 5). The distance of each sample (placed in rotating 8-rectangular holder) from arc is about 8 cm. The radiation was filtered with a monochromatic glass filter Hg Mon 436 (Carl Zeiss, Jena, Germany) transmitting  $\lambda = 436$  nm placed in front of the sample (Figure 5). Films were irradiated at ambient temperature in air.

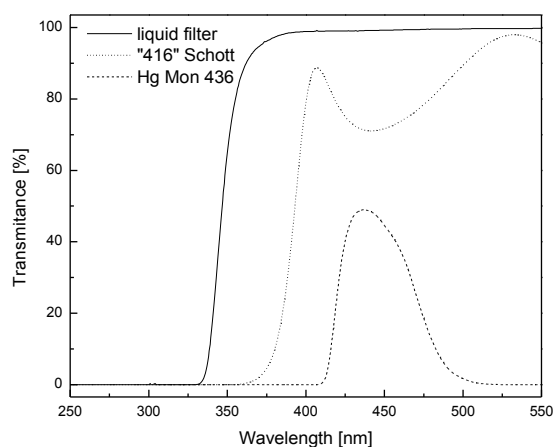


**Figure 5:** Transmittance spectra of the liquid filter (solid), “416” Schott filter (dot) and Hg Mon 436 filter (dash).

Another irradiation device was a SEPAP apparatus used in majority of studies (chapters 5-7). It had a cylindrical structure at elliptic base made of highly reflective aluminium. The source of light was a 400 W medium pressure mercury arc (Tesla, Holešovice, Czech Republic) filtered by a borosilicate glass envelope that emits radiation of wavelength higher than 300 nm. This source was fixed on the first focal axis of the device whereas a “merry-go-round” was fixed on the second focal axis located at approximately 10 cm. At this distance, the received energy was between 20-30  $\text{mW}/\text{cm}^2$ . Source chamber and merry-go-round chamber were separated by a glass filter “614” Schott (Figure 5). The temperature of the irradiated samples was fixed approximately at 35 °C due to the temperature regulator connected to a thermocouple located under the “merry-go-round”. Samples were placed in aluminium holders and fixed to the “merry-go-round”.

### ***3.2.5 Thermal decomposition of peroxides***

Thermal decomposition of the formed peroxides in the irradiated films (prepared from solution) was conducted in air at  $91 \pm 1$  °C in standard aerated oven. To take advantage of the comparison of our new results with already published data, the same temperature was used. Moreover, this temperature was chosen to be lower than  $T_g$  of PS to avoid the shrinkage of the film.

Thermal decomposition of the formed peroxides in the irradiated films (prepared by compression moulding) was conducted at 110 °C in standard aerated oven.

### ***3.2.6 Melt rheology measurements***

Molecular changes were monitored by melt viscoelasticity experiments in oscillatory shear mode using a rotational controlled stress rheometer (StressTech/Rheologica, Lund, Sweden) equipped with a parallel plate geometry. Their diameter was 10 mm and the gap between the plates was 1.000 mm. In all cases, the values of the stress amplitude were checked to ensure that all measurements were conducted within the linear viscoelastic region. A frequency sweep extending from 0.01 to 30 Hz was performed at different temperatures 150-170-200 °C. The temperature 170 °C was considered as a referential temperature. IRIS 2006 (Innovative Rheological Interface Software) was used to create master curves by the automatic time-temperature superposition.

Initial copolymers were placed in rheometer in powder form. They were molten at 170 °C and thermally equilibrated 5 min before measurement.

At the experimental temperature 170 °C, peroxidic species are not stable. Final networks were prepared in situ from photoperoxidised copolymer films in the rheometer by thermal treatment at 170 °C for 15 min before measurement.

### ***3.2.7 DSC measurements***

A Mettler-Toledo DSC 30 apparatus was used to carry out the thermal analysis. It was equipped with a liquid nitrogen cooling unit permitting to scan temperatures ranging from -170 to 500 °C. A cooling/heating rate  $0.7$  °C.min<sup>-1</sup> was adopted. This rate value has been determined to be slow enough to keep the system under a continuous thermodynamically equilibrium state.

Calibration, in terms of temperature and heat, was performed using *n*-heptane (-90.6 °C, 140.5 J.g<sup>-1</sup>), indium (156.6 °C, 28.45 J.g<sup>-1</sup>) and zinc (419.2 °C, 107.5 J.g<sup>-1</sup>) as references. A dedicated software allows various calculations (onset, heat, peak temperature, etc.) from the original recorded DSC curves.

Thermoporometry is a technique using DSC. About 10 mg of swollen gel with a slight excess of CCl<sub>4</sub> were introduced into an aluminium DSC crucible. The temperature program was applied to record the DSC thermograms of the CCl<sub>4</sub> confined inside the polymeric gel. The depression freezing temperature is often higher than that of melting. For this reason, we adopted the cooling process to conduct the thermoporometry experiments. To avoid overlapping of confined and free solvent peaks, starting temperature was -50 °C where both confined and free solvents are frozen. Heating to -24 °C causes confined solvent to melt while the free solvent remains frozen. The following DSC program was chosen:

- 1) -50 °C → -24 °C (0.7 °C/min)
- 2) -24 °C → -40 °C (-0.7 °C/min)

### ***3.2.8 Swelling measurements***

Swelling is a classic method for the analysis of crosslinked polymers. Crosslinked polymer was dipped into CCl<sub>4</sub> for 48 h. Insoluble part was extracted several times with CCl<sub>4</sub>. The gel was weighted during 5 min in 30 s intervals. The weight of gel  $M_{\infty}$  was calculated by extrapolation to the time zero. Then, the gel was dried under vacuum at 100 °C to constant weight to estimate the weight of insoluble part  $M_0$ .

### ***3.2.9 Densitometry measurements***

Densitometry is a technique used to follow the diminution of the soluble part of polymers resulting from crosslinking. Crosslinking, by increasing the molecular weight of the polymeric chains, decreases indeed the solubility of the material. After crosslinking, a sample of the polymer film was introduced into a glass phial together with carbon tetrachloride, which is a good solvent of the uncrosslinked polymer. The amount of carbon tetrachloride was adjusted in order to have the same specific concentration for all the mixtures; typically 100 mg/10 ml. The phials were then hermetically closed and hidden from the daylight for 48 h. Using a vibrating tube density meter

DMA 58 (Anton Paar, Graz, Austria) allowing a very accurate measurement ( $\pm 0.00001 \text{ g}\cdot\text{cm}^{-3}$ ), the densities of the liquid phases of the mixtures were determined at 20.00 °C. Before crosslinking occurs, the polymer is soluble and the density of the solution is the lowest. As the crosslinking occurs, the polymer becomes more and more insoluble and consequently the density of the liquid phase increases and finally tends towards that of the pure solvent.

## 4 STUDY OF PHOTOPEROXIDATION

### 4.1 Introduction

All already prepared styrene copolymers bearing BZ moiety are not chemically homogeneous<sup>16,17,18</sup>. In the monomer mixture, corresponding monomers are more reactive than styrene. Monomer 1-phenyl-2-{4-[2-(4-vinylbenzyloxy)ethoxy]phenyl}ethane-1,2-dione (BZS) was proposed as an analogue of VBz that reacts faster with styrene in a monomer mixture<sup>18</sup>. As a result, chemically less homogeneous copolymer is obtained. The reason of high reactivity of VBz is a strongly deactivating substituent in the *para* position of styrene structure<sup>20</sup>. Therefore, it was supposed that styrene copolymer with BZS would have a better distribution of photoreactive units than VBz/S.

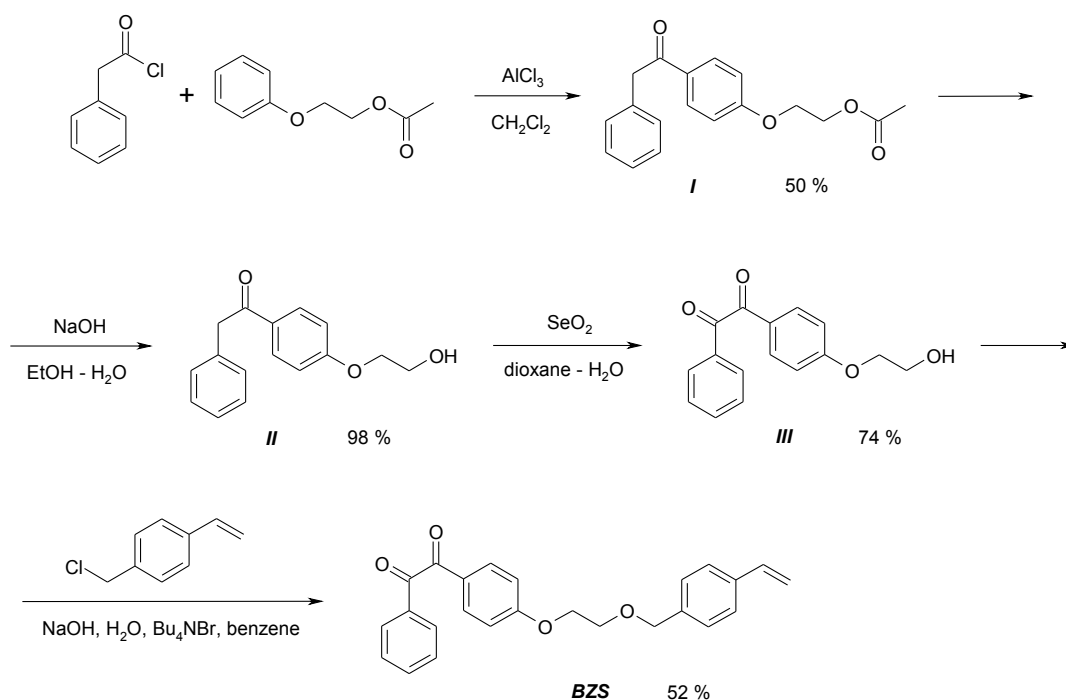
The aim of this chapter is to synthesise monomer BZS and its styrene copolymer BZS/S. Another objective was to study its unique photoperoxidation followed by thermal crosslinking of synthesised copolymer. In previous studies<sup>16-18</sup>, the photoperoxidation was accompanied by a partial crosslinking. For an attempt to prepare a soluble photoperoxidised copolymer, the longest irradiation wavelength possible where BZ still absorbs ( $\lambda = 436$  nm) was used.

### 4.2 Synthesis of the monomer BZS

For the synthesis of the monomer BZS, etherification of 1-[4-(2-hydroxyethoxy)phenyl]-2-phenylethan-1,2-dione (**III**) with 4-vinylbenzyl chloride was proposed (Scheme 15). Intermediates are known compounds and were prepared according to the literature<sup>102,103,104</sup>. The yields were much higher than those mentioned in the literature. Overall yield of the synthesis was 19 %.

In the first step, 2-(4-phenylacetylphenoxy)ethyl acetate (**I**) was prepared by Friedel-Crafts acylation of 2-phenoxyethyl acetate with phenylacetyl chloride in dichloromethane<sup>102</sup>. The product was distilled under vacuum and crystallised from ethanol to yield 50 %. Probably, less side products would be formed if a catalyst less reactive than  $\text{AlCl}_3$  was used.

In the next step, the ester **I** was hydrolysed with NaOH in aqueous ethanol<sup>104</sup>. The product **II** was not purified. The yield was almost quantitative (98 %).



**Scheme 15:** Synthesis of the monomer BZS.

The third step was an oxidation of  $\alpha$ -methylene group of 1-[4-(2-hydroxyethoxy)phenyl]-2-phenylethanone (**II**) with selenium dioxide in dioxane with a small amount of water under reflux condition<sup>103</sup>. After 10 h, the reactant is not detected by TLC. Yellow product 1-[4-(2-hydroxyethoxy)phenyl]-2-phenylethan-1,2-dione (**III**) was crystallised from methanol yielding 74 %.

The last step was an etherification of **III** with 4-vinylbenzyl chloride in the presence of an alkalic solution and phase transfer catalyst  $(C_4H_9)_4NBr$ . An attempt without solvent and minimum amount of water necessary to dissolve NaOH was unsuccessful. The reaction mixture polymerised. Neither an attempt with benzene as organic solvent was successful. Finally, BZS was prepared by using of benzene and NaOH solution with lower concentration. Monomer was afforded in 52 % yield after purification by chromatography with dichloromethane as an eluent.

#### 4.2.1 Synthesis of 2-(4-phenylacetylphenoxy)ethyl acetate (**I**)

Phenylacetyl chloride (53.0 ml, 0.4 mol) was added to a suspension of dichloromethane (120 ml) and  $AlCl_3$  (53.3 g, 0.4 mol) cooled in a ice bath and stirred with a mechanical stirrer. Then, a solution of 2-phenoxyethyl acetate (72.1 g, 0.4 mol) in dichloromethane (60 ml) was added dropwise while the temperature of reaction mixture did not exceed 5 °C. The reaction mixture was stirred for 3 h. Reaction was quenched by pouring the reaction mixture onto ice (300 ml). Organic

layer was separated and water layer was extracted by chloroform (3×100 ml). Combined organic layers were washed with water (50 ml), dried over Na<sub>2</sub>SO<sub>4</sub>, filtered and concentrated. Impurities with lower boiling point were removed by distillation at 30 mbar. Product was distilled from a sand bath at 210 °C at 0.13 torr and crystallised from ethanol to yield 60.1 g (50 %) of white crystalline compound 2-(4-phenylacetylphenoxy)ethyl acetate (**I**) with mp = 89-92 °C (lit. 93-94 °C).

**R<sub>f</sub>** = 0,45 (silica, ethylacetate/isohexane 1:2)

**<sup>1</sup>H NMR** (CDCl<sub>3</sub>): δ (ppm) = 8.00 (d, *J* = 9 Hz, 2H, CO-C<sub>ipso</sub>-CH), 7.35-7.23 (m, 5H, C<sub>6</sub>H<sub>5</sub>), 6.94 (d, *J* = 9 Hz, 2H, CH-C<sub>ipso</sub>-O), 4.44 (t, *J* = 4.5 Hz, 2H, CH<sub>2</sub>OAc), 4.25-4.20 (m, 4H, CH<sub>2</sub>-CO + Ar-OCH<sub>2</sub>), 2.10 (s, 3H, CH<sub>3</sub>)

**IR** (KBr): 1736 cm<sup>-1</sup> (C=O, ester), 1682 cm<sup>-1</sup> (C=O, ketone), 1603 cm<sup>-1</sup> (C=C)

#### 4.2.2 Synthesis of 1-[4-(2-hydroxyethoxy)phenyl]-2-phenylethanone (**II**)

Solution of NaOH (14.1 g, 0.353 mol) in water (20 ml) was added to a solution of the compound **I** (60.1 g, 0.202 mol) dissolved in 350 ml of hot ethanol (60 °C). Reaction mixture was stirred for 15 min, neutralised with HCl and concentrated. Chloroform (200 ml) and water (60 ml) were added. Organic layer was separated, dried with Na<sub>2</sub>SO<sub>4</sub> and concentrated. White crystalline compound 1-[4-(2-hydroxyethoxy)phenyl]-2-phenylethanone (**II**) was obtained in 98 % yield (50.6 g) with mp = 94-96 °C (lit. 97-98 °C).

**R<sub>f</sub>** = 0.46 (silica, ethylacetate/isohexane 2:1)

**<sup>1</sup>H NMR** (CDCl<sub>3</sub>): δ (ppm) = 8.00 (d, *J* = 9 Hz, 2H, CO-C<sub>ipso</sub>-CH), 7.35-7.23 (m, 5H, C<sub>6</sub>H<sub>5</sub>), 6.95 (d, *J* = 9 Hz, 2H, CH-C<sub>ipso</sub>-O), 4.24 (s, 2H, CH<sub>2</sub>-CO), 4.14 (t, *J* = 4.5 Hz, 2H, ArOCH<sub>2</sub>), 4.03-3.97 (m, 2H, CH<sub>2</sub>OH), 2.00 (t, *J* = 6 Hz, 1H, OH)

**FTIR** (KBr): 3420 cm<sup>-1</sup> (O-H), 1684 cm<sup>-1</sup> (C=O), 1599 cm<sup>-1</sup> (C=C)

#### 4.2.3 Synthesis of 1-[4-(2-hydroxyethoxy)phenyl]-2-phenylethan-1,2-dione (**III**)

Unpurified compound **II** (30.3 g, 118.2 mmol) was dissolved in hot dioxane (30 ml). Selenium dioxide (14.4 g, 130 mmol) was dissolved in a mixture of hot dioxane (40 ml) and water (2.4 ml). Combined solutions were refluxed in a dark place for 10 h. Majority of formed selenium was removed by decantation. A hot reaction mixture was filtered through a short column of silica,

silica column was washed with hot ethanol and the solution was concentrated. Crystallisation from methanol yielded to 23.8 g (74 %) of yellow crystalline product 1-[4-(2-hydroxyethoxy)phenyl]-2-phenylethan-1,2-dione (**III**) with mp = 102-105 °C (lit. 104.5-105.5 °C).

$R_f = 0.43$  (silica, ethylacetate/isohexane 2:1)

$^1\text{H NMR}$  ( $\text{CDCl}_3$ ):  $\delta$  (ppm) = 8.00-7.93 (m, 4H,  $\text{CH-C}_{\text{ipso}}\text{-CO-CO-C}_{\text{ipso}}\text{-CH}$ ), 7.65 (tt,  $J = 7.5, 1.5$  Hz, 1H,  $\text{H}_{\text{para}}$ ), 7.51 (t,  $J = 7.5$  Hz, 2H,  $\text{H}_{\text{meta}}$ ), 7.00 (d,  $J = 9$  Hz, 2H,  $\text{CH-C}_{\text{ipso}}\text{-O}$ ), 4.17 (t,  $J = 4.5$  Hz, 2H,  $\text{ArOCH}_2$ ), 4.01 (t,  $J = 4.5$  Hz, 2H,  $\text{CH}_2\text{OH}$ ), 1.94 (br.s, 1H, OH)

$\text{FTIR}$  (KBr): 3368  $\text{cm}^{-1}$  (O-H), 1679  $\text{cm}^{-1}$  (C=O), 1652  $\text{cm}^{-1}$  (C=O), 1601  $\text{cm}^{-1}$  (C=C)

### ***4.2.4 Synthesis of 1-phenyl-2-{4-[2-(4-vinylbenzyloxy)ethoxy]phenyl}-ethane-1,2-dione (BZS)***

See chapter 4.3.

## **4.3 Synthesis, photoperoxidation and crosslinking of styrene copolymer with pendant BZ moieties**

This chapter is in the form of a publication. The article “Synthesis, photoperoxidation and crosslinking of styrene copolymer with pendant benzil moieties” has been accepted for publication in *Journal of Photochemistry and Photobiology A: Chemistry*<sup>105</sup>.

Available online at [www.sciencedirect.com](http://www.sciencedirect.com)

Journal of  
Photochemistry  
and  
Photobiology  
A: Chemistry

Journal of Photochemistry and Photobiology A: Chemistry xxx (2007) xxx–xxx

[www.elsevier.com/locate/jphotochem](http://www.elsevier.com/locate/jphotochem)

## Synthesis, photoperoxidation and crosslinking of styrene copolymer with pendant benzil moieties

B. Husár, I. Lukáč\*

*Polymer Institute, Slovak Academy of Sciences, Dúbravská cesta 9, 842 36 Bratislava, Slovakia*

Received 3 September 2007; accepted 1 October 2007

### Abstract

A new benzil-containing (BZ) styrene monomer, 1-phenyl-2-[4-[2-(4-vinylbenzyloxy)ethoxy]phenyl]-ethane-1,2-dione (BZS) and its copolymer with styrene (BZS/S) were prepared. BZS concentration in the monomer mixtures is almost identical to the concentration in the copolymers and therefore the chemically homogeneous styrene copolymers are produced. When irradiated ( $\lambda = 436$  nm) in the air, the pendant BZ groups of the BZS/S copolymer are transformed into benzoyl peroxide (BP) groups. The BP groups can be converted to esters and benzoic acid moieties during subsequent thermal treatment, resulting in highly crosslinked films.

© 2007 Elsevier B.V. All rights reserved.

**Keywords:** Benzil; Crosslinking of polystyrene; Photoperoxidation

### 1. Introduction

Methods of polystyrene (PS) crosslinking using a small amount of copolymerized crosslinker are scarce. According to our knowledge, vinyl benzocyclobutene structure incorporated into PS chains was used for its crosslinking [1,2]. Crosslinking of these materials proceeds at a temperature exceeding 200 °C via a coupling reaction of two benzocyclobutene structures, which was exploited for the preparation of architecturally defined nanoparticles via intramolecular chain collapse [1]. A generalized approach for the applications of these materials to the modification of solid surfaces, such as a wide variety of metal, metal oxide, semiconductors, and polymeric surfaces is described [2]. Also in a chloroform solution the formation of crosslink between PS chains with phenylindene pendant groups via their photo-dimerization was studied [3].

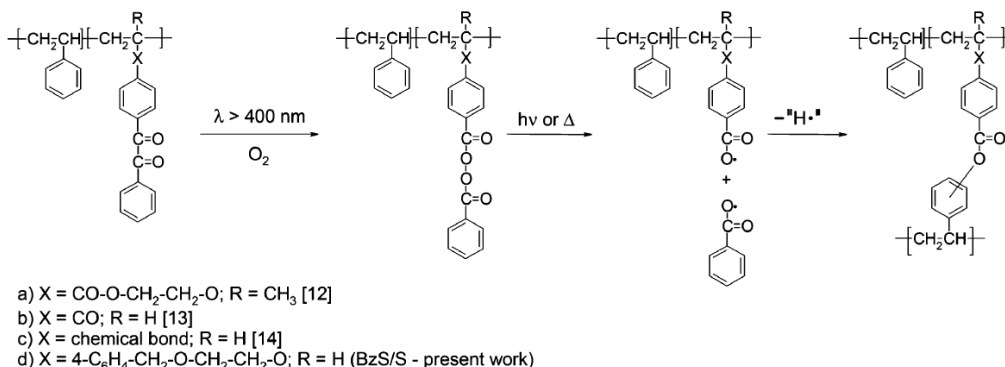
Polymers bearing BZ units in the main chain or as pendant groups have been examined as potential negative [4] or positive [5] resist materials based on photo degradation of their polymer networks. They were exploited as water-soluble polymeric photoinitiators [6]. Also, thermoporometry with carbon tetra-

chloride as a liquid probe has been used to study the crosslinking of polymers bearing BZ units [7]. Finally, the photochemical properties of copolymers bearing BZ pendant groups have been investigated in solution [8].

BZ is an industrially important member of the class of molecules with 1,2-dicarbonyl functionality. The solution-phase photochemistry of BZ has been investigated extensively, both in the presence and absence of molecular oxygen. BZ is photostable in absence of molecular oxygen without hydrogen donor. When molecular oxygen is available, photooxidation of BZ in benzene leads to phenyl benzoate, benzoic acid, biphenyl and a small amount of benzoyl peroxide (BP) [9]. However, in aerated glassy polymer films upon irradiation at  $\lambda > 400$  nm (i.e., the long wavelength edge of the  $n \rightarrow \pi^*$  absorption band, where BP does not absorb), BZ can be converted almost quantitatively to BP [10,11]. Covalently attached BP pendant groups have also been formed by irradiation of copolymer films containing BZ structures [12–14].

Whereas a decomposition of low molecular peroxides doped into PS film results in a net decrease in polymer molecular weight [12,15], the decomposition of pendant BP groups in copolymers is an efficient method of polymer crosslinking [12–14] (Scheme 1). Complete crosslinking of copolymers with pendant BZ groups was also achieved in only one step by irradiation at a shorter wavelength (366, 313 or 254 nm) [13,14]. At a shorter wavelength, the incident light simultaneously decomposes the

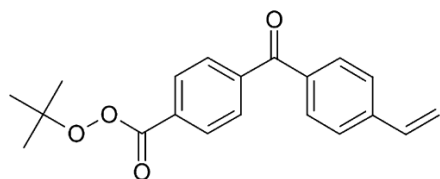
\* Corresponding author. Tel.: +421 2 54777404; fax: +421 2 54775923.  
E-mail address: [ivan.lukac@savba.sk](mailto:ivan.lukac@savba.sk) (I. Lukáč).



Scheme 1. Photoperoxidation of copolymers bearing pendant BZ groups followed by thermal or photochemical crosslinking.

formed peroxides. As in the previous cases [12–14], the copolymer of styrene with low percentages of *p*-vinylbenzophenone-*p'*-*tert*-butyl perbenzoate (Scheme 2) has been observed to crosslink efficiently with light [16–18]. While it is possible to presume similar crosslinking efficiency between perester [16] (Scheme 2) and BZ pendant groups [12–14] (Scheme 1), the synthesis of the monomer without potentially explosive perester group (Scheme 2) seems to be more convenient.

It has been found in all studies performed to date [12–14] that monomers bearing BZ structures are more reactive than styrene in free radical initiated copolymerizations. Consequently, the concentration of the monomer units bearing BZ structures was higher in the copolymer than in the monomer mixture (at less than complete conversions of the monomers). To avoid chemical heterogeneity of the formed copolymer, a new monomer with presumed lower reactivity than previous monomers [12–14], 1-phenyl-2-{4-[2-(4-vinylbenzyloxy)ethoxy]phenyl}-ethane-1,2-dione (BZS) and its copolymer with styrene (BZS/S) were prepared. The photoperoxidation of the 1,2-dicarbonyl moieties of the BzS/S copolymer, and the process of BP groups decomposition leading to the efficient crosslinking was studied. The new monomer BZS can overcome the difficulties in the preparation of chemically homogeneous copolymers with styrene, and facilitate preparation of copolymers of equal reproducible quality. Therefore, a more regular network than previously obtained [12–14] can be formed. To minimize the extent of the side reactions during the photoperoxidation step [8–10], the lowest possible energy irradiation wavelength of 436 nm was selected.

Scheme 2. Structural formula of *p*-vinylbenzophenone-*p'*-*tert*-butyl perbenzoate.

## 2. Experimental

### 2.1. Materials

1-[4-(2-Hydroxyethoxy)phenyl]-2-phenylethane-1,2-dione was prepared as reported previously [19,20]. 4-Vinylbenzyl chloride (Aldrich), *tert*-butylammonium bromide (Lachema, Brno, Czech Republic), 2,2'-azobis(2-methylpropionitrile) (AIBN) (Aldrich), tetrahydrofuran (THF, HPLC grade), benzene, chloroform, dichloromethane, ethanol and methanol (analytical grade) were used as received. Stabilized styrene (Aldrich) was washed with diluted sodium hydroxide solution and water, dried with anhydrous MgSO<sub>4</sub> and distilled.

### 2.2. Instrumentation

FTIR spectra were recorded on an Impact 400 spectrophotometer (Nicolet Instrument Corporation, WI, USA). <sup>1</sup>H and <sup>13</sup>C NMR spectra were measured on a Bruker AM 300 spectrometer (Germany) using chloroform-*d* as a solvent and tetramethylsilane (TMS) as internal standard. UV/vis absorption spectra were measured on a Shimadzu 1650PC spectrophotometer (Japan). Melting points are uncorrected and were measured on a hot stage apparatus. Molecular weights were estimated by gel permeation chromatography (GPC) with THF as a mobile phase, a PSS SDV 5 μm column (*d* = 8 mm, *l* = 300 mm), a Waters 515 pump, and a Waters refractive index detector. The instrument was calibrated with PS standards (Polymer Standards Service, Mainz, Germany).

### 2.3. Monomer synthesis

1-Phenyl-2-{4-[2-(4-vinylbenzyloxy)ethoxy]phenyl}-ethane-1,2-dione (BZS) was prepared according to Scheme 3. Benzene (200 mL), 4-vinylbenzyl chloride (10.7 g, 70 mmol), 1-[4-(2-hydroxyethoxy)phenyl]-2-phenylethane-1,2-dione (10 g, 37 mmol) and Bu<sub>4</sub>NBr (1.2 g, 3.7 mmol) were added to 20 mL of a stirred aqueous NaOH (7.4 g, 185 mmol) solution. The reaction mixture was stirred for 10 days in the dark at room temperature. The benzene layer was separated, washed with



Scheme 3. Synthesis of BZS.

water, dried with anhydrous  $\text{MgSO}_4$ , filtered, and concentrated. The product was isolated by column chromatography on silica gel with dichloromethane as an eluent to afford 7.4 g (52%) of yellowish powder, mp 128–130 °C.

$^1\text{H}$  NMR ( $\text{CDCl}_3$ ):  $\delta$  (ppm) = 8.00–7.91 (m, 4H,  $\text{CH}-\text{C}_{\text{ipso}}-\text{CO}-\text{CO}-\text{C}_{\text{ipso}}-\text{CH}$ ), 7.65 (tt,  $J=7.5, 1.5$  Hz, 1H,  $\text{H}_{\text{para}}$ ), 7.51 (t,  $J=7.5$  Hz, 2H,  $\text{H}_{\text{meta}}$  from  $\text{C}_6\text{H}_5$ ), 7.40 (d,  $J=8$  Hz, 2H,  $\text{CH}-\text{C}_{\text{ipso}}-\text{CH}=\text{CH}_2$ ), 7.31 (d,  $J=8$  Hz, 2H,  $\text{OCH}_2-\text{C}_{\text{ipso}}-\text{CH}$ ), 7.00 (d,  $J=9$  Hz, 2H,  $\text{CH}-\text{C}_{\text{ipso}}-\text{O}$ ), 6.71 (dd,  $J=17.5, 11$  Hz, 1H,  $\text{CH}=\text{CH}_2$ ), 5.75 (dd,  $J=17.5, 1$  Hz, 1H,  $\text{ArCH}=\text{CH}_2$  (Z)), 5.24 (dd,  $J=11, 1$  Hz, 1H,  $\text{ArCH}=\text{CH}_2$  (E)), 4.61 (s, 2H,  $\text{OCH}_2\text{Ar}$ ), 4.22 (t,  $J=4.5$  Hz, 2H,  $\text{ArOCH}_2$ ), 3.84 (t,  $J=4.5$  Hz, 2H,  $\text{CH}_2-\text{CH}_2-\text{O}-\text{CH}_2$ ).

$^{13}\text{C}$  NMR ( $\text{CDCl}_3$ ):  $\delta$  (ppm) = 194.8 (C=O), 193.1 (C=O), 164.2 ( $\text{C}_{\text{ipso}}-\text{O}$ ), 137.3 ( $\text{C}_{\text{ipso}}$ ), 137.2 ( $\text{C}_{\text{ipso}}$ ), 136.5 ( $\text{CH}=\text{CH}_2$ ), 134.7 ( $\text{C}_{\text{para}}$ ), 133.2 ( $\text{C}_{\text{ipso}}$ ), 132.3 ( $\text{C}_{\text{ar}}$ ), 129.9 ( $\text{C}_{\text{ar}}$ ), 128.9 ( $\text{C}_{\text{ar}}$ ), 128.0 ( $\text{C}_{\text{ar}}$ ), 126.3 ( $\text{C}_{\text{ar}}$ ), 126.3 ( $\text{C}_{\text{ipso}}$ ), 114.9 ( $\text{C}_{\text{ar}}$ ), 114.0 ( $\text{CH}=\text{CH}_2$ ), 73.2 ( $\text{CH}_2$ ), 68.0 ( $\text{CH}_2$ ), 67.9 ( $\text{CH}_2$ ).

IR (KBr): 1677 (C=O), 1659 (C=O), 1630 (C=C, vinyl), 1601  $\text{cm}^{-1}$ .

MS ( $m/z$ ): 425 (M + K), 409 (M + Na), 242.

UV/vis ( $\text{CHCl}_3$ ):  $\lambda_{\text{max}}$ [nm] ( $\log \epsilon$ ) = 289 (4.26), 387 (2.05).

#### 2.4. Polymerization

An ampoule containing BZS (0.200 g, 0.517 mmol), styrene (4.545 g, 43.64 mmol) and AIBN (5 mg) was sealed under argon and polymerized at 60 °C for 6.5 h. The copolymer was precipitated three times from chloroform solution into methanol to yield 1.31 g (28%) of slightly yellow copolymer. Residual BZS monomer still present in the copolymer was removed by Soxhlet extraction with ethanol. The content of BZS in the copolymer was determined to be 3.9 wt.% by  $^1\text{H}$  NMR using the integrated peak areas of separated 3 methylene groups and the aromatic hydrogens of BZS and aromatic styrene hydrogens. GPC:  $M_n = 2.1 \times 10^5$  g  $\text{mol}^{-1}$  and  $M_w = 4.0 \times 10^5$  g  $\text{mol}^{-1}$ .

$^1\text{H}$  NMR ( $\text{CDCl}_3$ ):  $\delta$  (ppm) = 7.98 (t, 4H-arom. of BZS), 7.64 (t, 1H-arom. of BZS), 7.50 (t, 2H-arom. of BZS), 7.43–6.88 (m, 3H-arom. of S + 6H-arom. of BZS), 6.88–6.29 (m, 2H-arom. of S), 4.54 (br.s,  $\text{CH}_2$  of BZS), 4.19 (br.s,  $\text{CH}_2$  of BZS), 3.76 (br.s,  $\text{CH}_2$  of BZS), 1.85 (br.s, CH of S + CH of BZS), 1.43 (br.s,  $\text{CH}_2$  of S +  $\text{CH}_2$  of BZS).

$^{13}\text{C}$  NMR ( $\text{CDCl}_3$ ):  $\delta$  (ppm) = 164.1 ( $\text{C}_{\text{ipso}}-\text{O}$  of BZS), 145.2 ( $\text{C}_{\text{ipso}}$  of S), 134.6 ( $\text{C}_{\text{para}}$  of BZS), 133.1 ( $\text{C}_{\text{ipso}}$  of BZS), 132.3 ( $\text{C}_{\text{ar}}$  of BZS), 129.8 ( $\text{C}_{\text{ar}}$  of BZS), 128.9 ( $\text{C}_{\text{ar}}$  of BZS), 127.9 ( $\text{C}_{\text{ar}}$  of S), 127.5 ( $\text{C}_{\text{ar}}$  of S), 126.1 ( $\text{C}_{\text{ar}}$  of BZS), 125.6 ( $\text{C}_{\text{ar}}$  of S), 114.8 ( $\text{C}_{\text{ar}}$  of BZS), 73.3 ( $\text{CH}_2$  of BZS), 67.8 ( $2 \times \text{CH}_2$  of BZS), 43.8 ( $\text{CH}_2$  of S), 40.3 (CH of S). Owing to the low concentration, several peaks corresponding to BZS structure (both C=O and

most of  $\text{C}_{\text{ipso}}$ ) are not visible in the spectrum.

IR (film): 1678 (C=O).

#### 2.5. Irradiations and measurements

Films of 40 mg of BZS/S copolymer with good optical quality about 40  $\mu\text{m}$  thick, were prepared by casting from 1 mL benzene solutions onto a glass plate (10  $\text{cm}^2$  area). The plate was covered by a Petri dish to slow solvent evaporation. The self-supporting polymer films were separated from the glass by dipping into distilled water. Films were dried to a constant weight at room temperature under vacuum and were irradiated at ambient temperature in air. A homemade “merry-go-round” apparatus was employed. It consisted of a 125 W medium pressure mercury arc placed in a circulating-water-jacketed quartz tube which was surrounded by a 1 cm-thick layer of a liquid filter (500 g NaBr and 3 g  $\text{Pb}(\text{NO}_3)_2$  per 1000 mL aqueous solution) transmitting at  $\lambda > 330$  nm. The distance of each sample (placed in rotating 8-rectangular holders) from arc was about 8 cm. Finally, a glass filter Hg Mon 436 (Carl Zeiss, Jena, Germany) transmitting in region 410–510 nm with maximum at  $\lambda = 436$  nm (46.5%) was placed in front of each sample. Thermal decomposition of the formed peroxides in the irradiated films was conducted in the air at  $91 \pm 1$  °C in the column oven of a Shimadzu gas chromatograph.

### 3. Results and discussion

#### 3.1. Synthesis and characterization of the BZS/S copolymer

The contents of BZS in the monomer mixture and in the copolymer are compared with published results from radical copolymerizations of other BZ containing monomers and styrene [12–14] in Table 1. Similarly to BZS/S copolymer in Table 1, a copolymer with higher content of BZS was prepared as well (not included in this work). The content of BZS in the monomer mixture was 13.25 wt.% and in the copolymer it was 12.8 wt.% at 19% conversion. The small difference between the concentrations of the monomer mixtures and in the copolymer at a low conversion enables us to confirm our assumption that the rates of conversion of the two monomers are about equal and that the new BZS/S copolymer exhibits a statistical distribution of BZ pendant groups in its polymer chains. The mutual reactivity of styrene with its 4-substituted derivatives is known to depend on the nature of the substituent [21]; reactivity increases with the decreasing electron donating character of the substituent. The substituent of BZS (4- $\text{CH}_2\text{OR}$  group) is slightly electron donating. Therefore, BZS should be slightly less reactive than styrene and substantially less reactive than 4-vinyl benzil containing strongly deactivating 1,2-dicarbonyl structures in position 4 (X

Table 1  
Content of BZS in the monomer mixture and in its copolymer with styrene as well as data for related copolymers of monomers bearing BZ group and styrene

X <sup>a</sup>	R <sup>a</sup>	Conversion (wt.%)	Mol% of BZ monomer		Reference
			In monomer mixture	In copolymer	
CO–O–CH <sub>2</sub> –CH <sub>2</sub> –O	CH <sub>3</sub>	29.5	1.68	3.7	[12]
CO	H	17.9	3.8	11.1	[13]
Chemical bond	H	51.6	2.44	4.9	[14]
4-C <sub>6</sub> H <sub>4</sub> –CH <sub>2</sub> –O–CH <sub>2</sub> –CH <sub>2</sub> –O	H	27.6	1.17	1.1	Present work

<sup>a</sup> See Scheme 1.

is chemical bond and R=H in Scheme 1) [14]. It is known that the reactivity of methacryl (X=CO–O–CH<sub>2</sub>–CH<sub>2</sub>–O and R=CH<sub>3</sub>) [12] and of vinyl carbonyl (X=CO and R=H) [13] derivatives is higher than that of styrene in copolymerization with styrene [21]. Our results are consistent with this trend. Therefore, the monomer BZS must be distributed almost statistically in the BZS/S copolymers.

### 3.2. Photoperoxidation of BZS/S copolymer (Scheme 1)

During the irradiation of the BZS/S copolymer films in air (Fig. 1), the loss of intensity from BZ carbonyl stretching bands at 1650–1690 cm<sup>-1</sup> and the growth of BP carbonyl stretching bands at 1750–1800 cm<sup>-1</sup> are clearly seen in FTIR spectra. In the subtracted spectra (Fig. 2), the decrease in aromatic absorption (1597 and 1574 cm<sup>-1</sup>) is caused by a lower extinction coefficient of the product (BP structures) in comparison with the starting BZ structures. An increase of the absorption at 1607 cm<sup>-1</sup>, as the result of the product absorption shift, is also seen in the subtracted spectra (Fig. 2). The development of the spectra during irradiation is similar to that of the free BZ in PS [10,11] and BZ pendant groups in copolymer films [12–14]. The advantage of the BZS/S copolymer in comparison with methacrylate and vinyl carbonyl derivatives (case a and b in Scheme 1) is that the copolymer does not contain other groups (e.g. ester or other carbonyl) absorbing in the region of the main changes

in IR spectra. Therefore, the monitoring of photoperoxidation and the decomposition of peroxides in BZS/S copolymer by means of IR spectroscopy is much simpler as in previously mentioned copolymers. After the dissolution of the irradiated BZS/S copolymer in chloroform, an insoluble (crosslinked) part was clearly seen in the solution, which was determined to be 23%.

One aim of this research was to prepare peroxide-containing polymers that retain their solubility in organic solvents. As seen in Fig. 1 and better in Fig. 2, it was impossible to avoid the formation of some side products (1700–1750 cm<sup>-1</sup>) which led to crosslinking even using the mildest possible radiation (436 nm) which is absorbed only by the red edge of the BZ *n* →  $\pi^*$  absorption band. Therefore, similarly as it was at  $\lambda > 400$  nm [12–14], even at  $\lambda = 436$  nm (present work) it is impossible to avoid partial crosslinking in the photoperoxidation step near the complete conversion.

What is the origin of this crosslinking? The main reaction of benzil excited triplet state in the presence of a hydrogen donor in inert atmosphere is hydrogen abstraction under ketyl and alkyl radical formation [22–25]. Benzil excited triplet state cannot abstract aromatic hydrogen [22–26] and formed alkyl radical on the polystyrene backbone prefer to disproportionate (main chain scission), not recombine (crosslinking) [15]. Therefore hydrogen abstraction probably does not participate in the crosslinking.

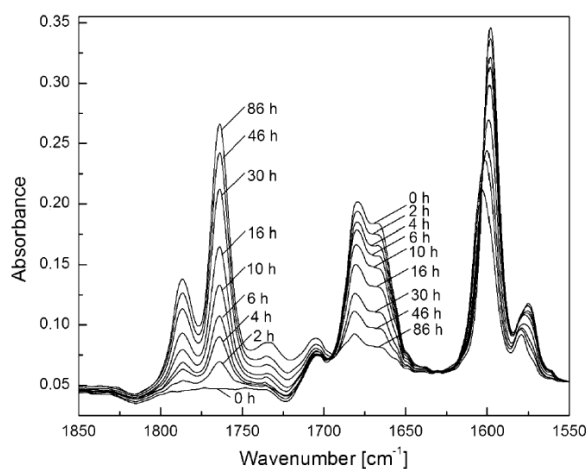


Fig. 1. Changes in FTIR spectra of a BZS/S copolymer film during irradiation ( $\lambda = 436$  nm) at room temperature in air. The spectrum of PS was subtracted.

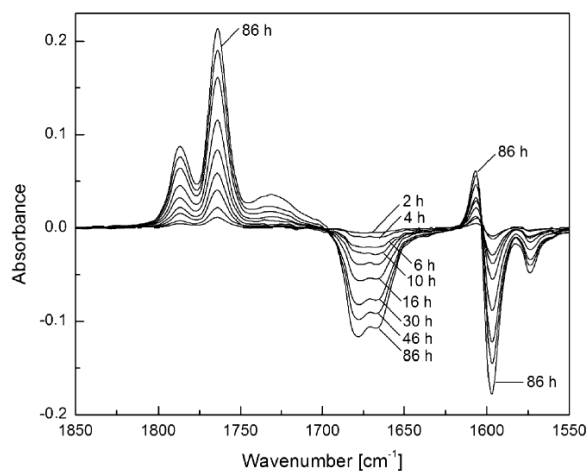


Fig. 2. Changes in FTIR spectra of BZS/S copolymer films irradiated at room temperature in air at  $\lambda = 436$  nm. The spectrum of the unirradiated copolymer was subtracted.

During the 103 h of irradiation of free BP in PS film at the same condition, no decomposition of BP was observed. Therefore, the crosslinks are not formed by thermal nor direct photochemical decomposition of BP during irradiation.

Because the majority of the side product is formed at the end of irradiation at the highest BP concentration, the side products are formed probably from labile BP. There is also experimental support for this hypothesis. The side product absorbs in the same region as the decomposition products of BP do ( $1700\text{--}1750\text{ cm}^{-1}$ ). At the lowest concentration of BZ the decomposition of BP is most important. Therefore excited BZ (singlet, or triplet) states, at the given conditions, probably do not sensitize the decomposition of BP. This conclusion supports also the sensitized decomposition of BP studies [27,28]. Some new absorbing species as possible sensitizing structures (conjugated double bonds?) present to the end of 436 nm light irradiation in irradiated film (Fig. 4) probably can sensitize decomposition of peroxide structures via efficient singlet energy transfer.

The depletion of the original dicarbonyl concentration in BZS structures (negative values) and the formation of a product (bound BP structures, positive values) are also proven in the changes recorded in Fig. 3. For the free BZ in PS (spectrum not given), a decrease is observed at  $1209\text{ cm}^{-1}$  and an increase at  $1223\text{ cm}^{-1}$  only. The same changes as for the free unsubstituted BZ are also observed in very similar region during irradiation of BZS/S copolymer film. Therefore, the changes at  $1212\text{ cm}^{-1}$  and  $1227\text{ cm}^{-1}$  correspond to the bonding of carbonyl to the unsubstituted phenyl ring in BZS structure. In the BZS structure, beside the carbonyl bound to phenyl ring, there is yet another carbonyl bound to the phenyl substituted in position 4 (Scheme 1). The rest of the peaks corresponds to bonds of the initial carbonyl structure of BZS attached to an ethoxy substituted phenyl ring ( $1165\text{ cm}^{-1}$ ) and to carbonyl groups connected to the ethoxy substituted phenyl ring in bound BP structures ( $1240\text{ cm}^{-1}$ ).

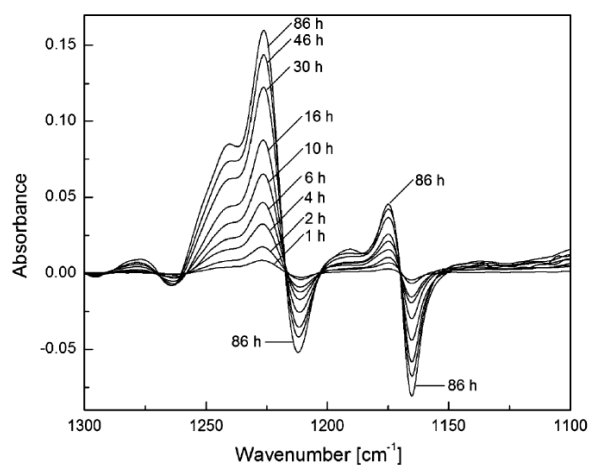


Fig. 3. Changes in FTIR spectra of BZS/S copolymer films irradiated at room temperature in air at  $\lambda = 436\text{ nm}$ . The spectrum of the unirradiated copolymer was subtracted.

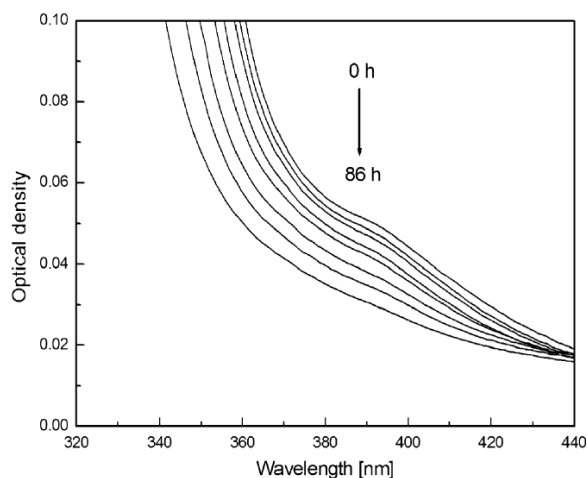


Fig. 4. Changes in UV/vis spectra of BZS/S copolymer films irradiated at room temperature in air at  $\lambda = 436\text{ nm}$ .

Also, the decrease of electronic absorption in the regions of the  $n \rightarrow \pi^*$  and  $\pi \rightarrow \pi^*$  bands (Fig. 4) during irradiation can be attributed to the conversion of BZ to BP moieties.

### 3.3. Thermal crosslinking of photoperoxidized BZS/S copolymer

The BP structures in the BZS/S copolymer formed during irradiation in the air were decomposed in a subsequent thermal step at  $91\text{ }^\circ\text{C}$ . The loss of BP and the formation of new products can be followed easily by means of FTIR spectroscopy (Fig. 5). The decrease of the absorption of carbonyl groups in BP ( $1750\text{--}1800\text{ cm}^{-1}$ ) and the formation of aromatic esters structures (stretching band of the carbonyl of the ester groups with absorption maximum at  $1735\text{ cm}^{-1}$ ) and benzoic acid structures (stretching band of the carbonyl of carboxylic acid groups at  $1660\text{--}1690\text{ cm}^{-1}$ ) can be seen in the FTIR spectra.

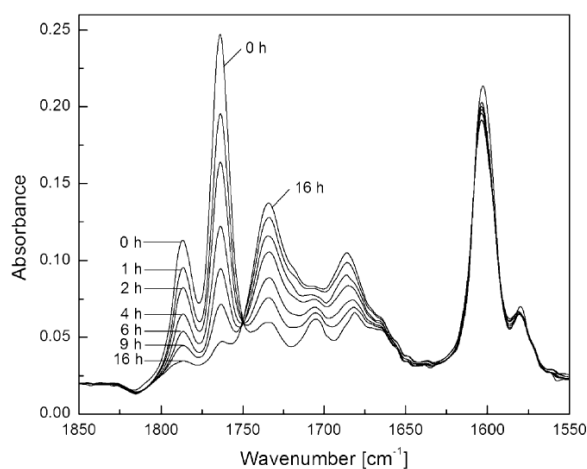


Fig. 5. Evolution of FTIR spectra due to the thermal decomposition of BP groups in a preirradiated BZS/S copolymer at  $91\text{ }^\circ\text{C}$ . The spectrum of PS was subtracted.

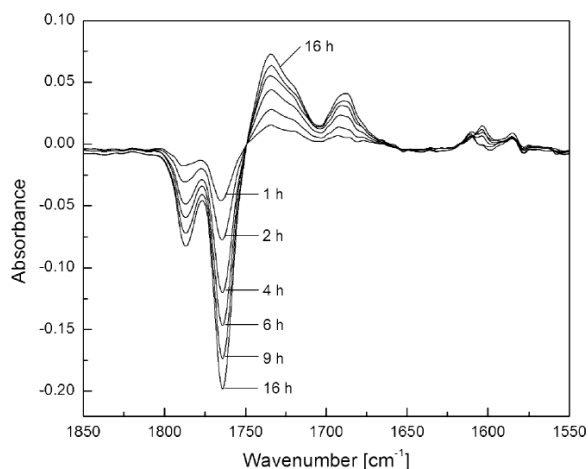


Fig. 6. Evolution of FTIR spectra due to the thermal decomposition of BP groups in a preirradiated BZS/S copolymer at 91 °C. The spectrum of the preirradiated copolymer was subtracted.

The subtracted spectra are more suitable to follow the BP transformations (Fig. 6).

A first-order rate constant for thermal decomposition of BP groups,  $k_t = 0.20 \pm 0.01 \text{ h}^{-1}$ , was calculated (Fig. 7) from IR peak intensity changes at  $1763 \text{ cm}^{-1}$  (Fig. 5). It is a bit lower than that obtained at the same temperature for the equally 4-substituted BP structure (with the same BZ type photoperoxidized group;  $0.26 \text{ h}^{-1}$ ), which was bound to a methacryl group [12]. Because at a low content of bound BP structures, statistically distributed along the polymer chain in the photoperoxidized BZS/S copolymer, the induced decomposition [29] (chain decomposition – decomposition of BP by the formed radicals) of BP structures can be presumed to be absent or suppressed. At about 4 times higher content of the BP groups (first row in Table 1), not statistically distributed, the contribution of the induced decomposition may be higher as in the later case.

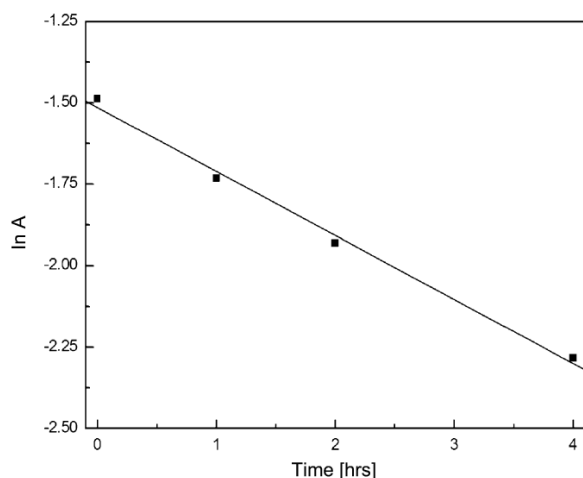


Fig. 7. Semilog plot for the thermolysis of photoperoxidized BZS/S film at 91 °C. Absorbance (A) is at  $1763 \text{ cm}^{-1}$  (Fig. 5).

Also an evaluation of the BP groups decomposition rate constant by means of IR spectroscopy may be less precise in the presence of methacryl carbonyl groups absorbing closely to the carbonyl of peroxide.

After the thermal treatment, the polymer films are completely insoluble in organic solvents due to extensive crosslinking, which is induced by the decomposition of the BP groups. For the BZS/S copolymer as well as for the copolymers described earlier [12–14], a common crosslinking scheme (discussed previously [14]) can be imagined (Scheme 1).

What is the advantage of this method of crosslinking? The PS crosslinking based on the decomposition of a small amount of the covalently bound peroxide or perester group and the subsequent addition of formed polymeric benzoyloxy radical to an aromatic ring of PS seems to be easier and more probable as the known methods of photo-crosslinking based on cycloadditions [18]. The main reason of lower efficiency for cycloadditions is that the reactants at a low concentration present in the copolymer can find their counterpart only with difficulties. In this connection it is interesting to mention the high crosslinking efficiency of surface nano-layers caused by the thermal coupling reaction of two benzocyclobutene structures in PS structure in melt [2]. Some features of the crosslinking of PS according the Scheme 1 are equal to that of the direct methods of the photochemical formation of reactive species, which can react directly with the polymeric substrate under the formation of a network [16,18] (nitrenes, carbenes, excited triplet state of carbonyl compound, or a sensitized decomposition of perester). From these methods only photosensitized decomposition of peresters was sufficiently efficient [16]. At the decomposition of BP and perester structures, the same active species (polymeric benzoyloxy radicals) are formed and their concentrations do not differ much, so it is possible to deduce similar efficiency for both systems. For the modification of surfaces, the method of crosslinking of copolymers with pendant BZ groups based on the access of oxygen in both photoperoxidation and the addition of formed benzoyloxy radical to aromatic ring steps [12–14], seems to be advantageous. An investigation of the influence of variation in chemical heterogeneity of the starting copolymer on the crosslink density of the irradiated and heated films of BZS/S copolymer is in progress.

#### 4. Conclusions

A new monomer BZS, bearing BZ group, has been copolymerized with styrene and has been found to be of comparable reactivity during free-radical polymerization as styrene. As a consequence, the copolymers are much more chemically homogeneous than previously prepared copolymers with styrene in which the other monomers containing a BZ group were used. BZ structural units in films of BZS/S copolymer were converted to BP structures upon irradiation in the air. The use of mild irradiation conditions ( $\lambda = 436 \text{ nm}$ ) did not completely stop the formation of species, which led to partial crosslinking during irradiation. Pendant BP structures are thermally unstable, and treatment at 91 °C resulted in significant crosslinking of their copolymers as indicated by the complete insolubility of the films in organic solvents and by IR spectra.

**Acknowledgments**

The authors thank Grant Agency Vega for the support through project 2/6015/26 and 2/5108/25 and Dr. R.G. Weiss, Georgetown University, Washington DC, USA for reading the manuscript. NMR measurements provided by the Slovak State Program Project No. 2003SP200280203 are also gratefully acknowledged.

**References**

- [1] E. Harth, B. Van Horn, V.Y. Lee, D.S. Germack, C.P. Gonzales, R.D. Miller, C.J. Hawker, *J. Am. Chem. Soc.* 124 (2002) 8653–8660.
- [2] D.Y. Ryu, K. Shin, E. Drockenmuller, C.J. Hawker, T.P. Russell, *Science* 308 (2005) 236–239.
- [3] R. Schinner, T. Wolff, D. Kuckling, *Ber. Bunsenges Phys. Chem.* 102 (1998) 1710–1714.
- [4] H. Simbürger, W. Kern, K. Hummel, C. Hagg, *Polymer* 41 (2000) 7883–7897.
- [5] J. Mosnáček, I. Lukáč, Š. Chromík, I. Kostič, P. Hrdlovič, *J. Polym. Sci. Part A: Polym. Chem.* 42 (2004) 765–771.
- [6] F. Catalina, C. Peinado, M. Blanco, N.S. Allen, T. Corrales, I. Lukáč, *Polymer* 39 (1998) 4399–4408.
- [7] B. Husár, S. Commereuc, I. Lukáč, Š. Chmela, J.M. Nedelec, M. Baba, *J. Phys. Chem. B* 110 (2006) 5315–5320.
- [8] I. Lukáč, P. Hrdlovič, W. Schnabel, *Macromol. Chem. Phys.* 195 (1994) 2233–2245.
- [9] J. Saltiel, H.C. Curtis, *Mol. Photochem.* 1 (1969) 239–243.
- [10] I. Lukáč, C. Kósa, *Macromol. Rapid Commun.* 15 (1994) 929–934.
- [11] C. Kósa, I. Lukáč, R.G. Weiss, *Macromol. Chem. Phys.* 200 (1999) 1080–1085.
- [12] C. Kósa, I. Lukáč, R.G. Weiss, *Macromolecules* 33 (2000) 4015–4022.
- [13] J. Mosnáček, R.G. Weiss, I. Lukáč, *Macromolecules* 35 (2002) 3870–3875.
- [14] J. Mosnáček, R.G. Weiss, I. Lukáč, *Macromolecules* 37 (2004) 1304–1311.
- [15] H.C. Haas, *J. Polym. Sci.* 54 (1961) 287–299.
- [16] I. Gupta, S.N. Gupta, D.C. Neckers, *J. Polym. Sci.: Polym. Chem. Ed.* 20 (1982) 147–157.
- [17] D.C. Neckers, *J. Radiat. Curing* 10 (1983) 19–24.
- [18] A. Reiser, *Photoreactive Polymers. The Science and Technology of Resists*, John Wiley and Sons, New York, 1989.
- [19] I. Lukáč, I. Zvara, P. Hrdlovič, *Eur. Polym. J.* 18 (1982) 427–433.
- [20] I. Lukáč, M. Kačuráková, E. Malík, *Collect. Czech. Chem. Commun.* 52 (1987) 756–760.
- [21] R.Z. Greenley, in: J. Brandrup, E.H. Immergut, E.A. Grulke (Eds.), *Polymer Handbook*, 4th ed., Wiley-Interscience, New York, 1999, pp. II/181–308.
- [22] C. Kósa, I. Lukáč, *Chem. Listy* 90 (1996) 287–294.
- [23] M.B. Rubin, *Top. Curr. Chem.* 129 (1985) 1–56.
- [24] M.B. Rubin, *Top. Curr. Chem.* 13 (1969) 251–306.
- [25] B.M. Monroe, *Adv. Photochem.* 8 (1971) 77–108.
- [26] Y. Sawaki, C.S. Foote, *J. Org. Chem.* 48 (1983) 4934–4940.
- [27] J.E. Leffler, J.W. Miley, *J. Am. Chem. Soc.* 93 (1971) 7005–7012.
- [28] J.E. Leffler, *An Introduction to Free Radicals*, John Wiley & Sons, New York, 1993.
- [29] M. Lázár, in: S. Patai (Ed.), *The Chemistry of Functional Groups, Peroxides*, John Wiley & Sons, New York, 1983, pp. 778–806.

### 4.4 Conclusion

A BZS monomer bearing benzil moiety was synthesised in 4 steps in 19 % overall yield. Its copolymerization with styrene affords BZS/S copolymer that has almost regular distribution of benzil units. When irradiated in air with a light  $\lambda = 436$  nm, pendant benzil groups of BZS/S are transformed almost quantitatively into benzoyl peroxide groups. Use of the longest possible wavelength where benzil still absorbs did not suppress the formation of side products responsible for partial crosslinking. Probably, it is caused by a sensitised decomposition of peroxide structures. Thermal treatment of photoperoxidised copolymers leads to a notable crosslinking.

## 5 STUDY OF CROSSLINKING

### 5.1 Introduction

The aim of this part was to study the crosslinking process of BZS/S copolymer. We have chosen thermoporometry to characterise the insoluble part of a swollen crosslinked polymer. It is a relatively new technique largely developed in LPMM. Originally, thermoporometry was proposed to study a morphology of a solid<sup>66</sup>. Then, the method was applied to measure mesh size of a soft matter, such as hydrogels, elastomers, polyolefins<sup>72-79</sup>.

At first, it was necessary to choose a good solvent. A good solvent completely dissolves uncrosslinked polymer, swells crosslinked polymer, does not cause the shrinkage of polymeric network, is available at high purity grade and thermogram peaks corresponding to free and confined solvent must be separated. Preferably, its thermal transition temperatures are not too low. Already calibrated solvents such as chloroform, *p*-xylene, cyclohexane, *n*-hexane, *n*-heptane, acetone are unsuitable. 1,4-Dioxane swells the crosslinked polymer but the results are not interpretable. Carbon tetrachloride was chosen as a probe liquid. Crosslinked polymer was swollen in CCl<sub>4</sub>. Bulk CCl<sub>4</sub> was largely studied and its thermal phase transitions are well characterised<sup>106</sup>. It exhibits a complex thermal transitions system. For our study, liquid-to-solid transition was employed.

### 5.2 Carbon Tetrachloride as Thermoporometry Liquid Probe to Study the Cross-Linking of Styrene Copolymer Networks

This chapter is in a form of a publication. The article “Carbon Tetrachloride as a Thermoporometry Liquid Probe To Study the Cross-Linking of Styrene Copolymer Networks” has been published in Journal of Physical Chemistry B<sup>107</sup>.

## Carbon Tetrachloride as a Thermoporometry Liquid Probe To Study the Cross-Linking of Styrene Copolymer Networks

B. Husár,<sup>†,‡</sup> S. Commereuc,<sup>†</sup> I. Lukáč,<sup>‡</sup> Š. Chmela,<sup>‡</sup> J. M. Nedelec,<sup>§</sup> and M. Baba<sup>\*,†</sup>

Laboratoire de Photochimie Moléculaire et Macromoléculaire, UMR CNRS 6505, Ecole Nationale Supérieure de Chimie de Clermont-Ferrand et Université Blaise Pascal, 24 Av. des Landais, 63174 Aubière Cedex, France, Polymer Institute, Centre of Excellence of Degradation of Biopolymers, Slovak Academy of Sciences, Dúbravská cesta 9, 842 36 Bratislava, Slovak Republic, and Laboratoire des Matériaux Inorganiques, UMR CNRS 6002, Ecole Nationale Supérieure de Chimie de Clermont Ferrand et Université Blaise Pascal, 24 Av. des Landais, 63174 Aubière Cedex, France

Received: October 4, 2005; In Final Form: January 16, 2006

Mesh size distributions (MSDs) of swollen cross-linked styrene copolymer networks have been measured by thermoporometry using CCl<sub>4</sub> as a probe liquid. All numerical relationships required for the calculation of the MSD were established for both the liquid-to-solid and the solid-to-solid thermal transitions of CCl<sub>4</sub> and successfully validated on test samples. It was found that the polymer network, for both thermally and photo-cross-linked materials, was completely built in about 4 h of exposure. A clear correlation was established between the average mesh size of the swollen polymer network on one hand and the benzoyl peroxide groups content and swelling ratio on the other hand.

### I. Introduction

Benzil (BZ) is an industrially important member of the class of molecules with 1,2-dicarbonyl functionality. It is used in the manufacture of photographic materials and polymer resists and as photoinitiator in radical polymerizations.

The synthesis of vinyl monomers bearing benzil pendant groups and their copolymerization with styrene has been described.<sup>1,2</sup> It was reported that covalently attached benzil pendant groups on the polymer backbone undergo efficient peroxidation through irradiation in air at  $\lambda > 400$  nm of the solid copolymer films. The conversion of  $\alpha$ -dicarbonyl on peroxy moieties is almost quantitative. Moreover, decomposition of resulting pendant benzoyl peroxide groups (BP) offers an efficient method of effective cross-linking of polymer. The cleavage of peroxy moieties (BP) can be induced either by thermal treatment or upon irradiation at  $\lambda > 300$  nm (photo-cross-linking). The photochemistry of copolymer films of these novel comonomers and styrene has been investigated. The ability of these materials to form images when irradiated through a mask has been demonstrated. In addition, these copolymers are expected to find applications in areas where controlled cross-linking is desired.

Hence, it is now necessary to characterize the final three-dimensional network in relation to the design and photoreactivity of the copolymer. Recently, the use of different techniques has been notified to reveal the network formation by cross-linking upon photooxidation of polymers. Swelling measurements,<sup>4,5</sup> viscosimetric analysis,<sup>5,6</sup> melt rheology,<sup>7</sup> thermoporometry,<sup>8,9</sup>

densitometry,<sup>10</sup> and electron spin resonance<sup>5</sup> have been explored. These methods were employed for providing deeper insight on gelation phenomenon, cross-linking extent, and network structure. On the basis of previous work,<sup>10</sup> we decided to choose thermoporometry with CCl<sub>4</sub> as a liquid probe because of its ability to swell the styrene copolymer materials.

One of the obvious advantages of this technique is to monitor the network structure on a mesoscopic scale assessing information about the size of the net. We illustrate the interest of this methodology in the case of poly(1-phenyl-2-[4-[2-(4-vinylbenzoyloxy)ethoxy]phenyl]ethane-1,2-dione-co-styrene), named poly(BZST-co-styrene) hereafter, shown in Scheme 1. In addition, chemical changes and network formation are easily followed by FTIR spectroscopy through the formation of ester groups as junctions units. In previous papers<sup>1,2</sup> very reactive monomers were used in which  $\alpha$ -dicarbonyl was directly attached to phenyl ring of styrene unit (benzil was attached directly to the main polymer chain) or the benzil was bearing a vinyl keto polymerizing group in *para* position. On the contrary, in the present work, monomer benzil is separated from the 4-alkylstyrene group by a spacer. The reactivity of the alkyl-substituted styrenes is similar to the reactivity of the unsubstituted styrene. This fact resulted in a copolymer with much more uniform distribution of new monomer bearing benzil in the copolymer with styrene.

In this paper, some kinetic parameters of the cross-linking reaction are given and the structure of the network obtained upon irradiation is discussed in comparison with those formed by thermal treatment. Finally, an attempt is done to correlate the final three-dimensional network to peroxy moieties (BP) content during the cross-linking step.

### II. Materials and Techniques

**2.1. Materials.** *2.1.1. Styrene Copolymer.* Synthesis of the new monomer and its copolymerization with styrene are described in ref 3. Poly(BZST-co-styrene) contains 2.6 wt %

\* To whom correspondence should be addressed. E-mail: mohamed.baba@univ-bpclermont.fr.

<sup>†</sup> UMR CNRS 6505, Ecole Nationale Supérieure de Chimie de Clermont-Ferrand et Université Blaise Pascal.

<sup>‡</sup> Centre of Excellence of Degradation of Biopolymers, Slovak Academy of Sciences.

<sup>§</sup> UMR CNRS 6002, Ecole Nationale Supérieure de Chimie de Clermont Ferrand et Université Blaise Pascal.

## SCHEME 1: Photoreactivity of Poly(1-phenyl-2-[4-[2-(4-vinylbenzyloxy)ethoxy]phenyl]ethane-1,2-dione-co-styrene)

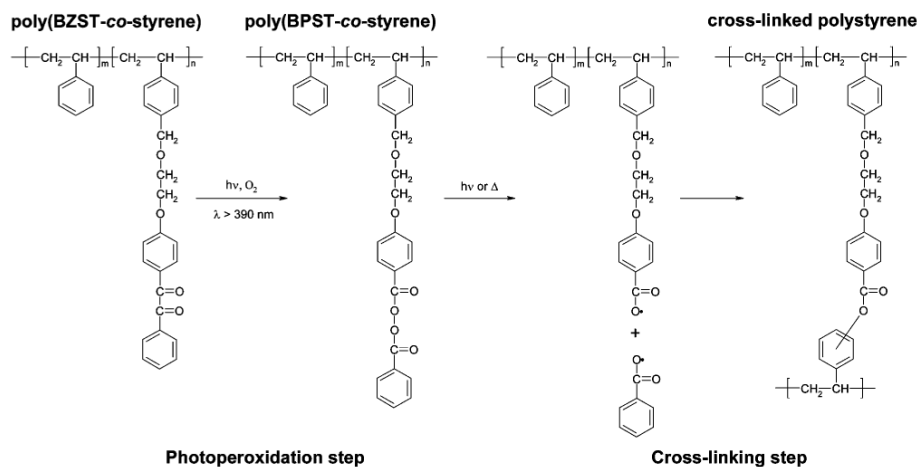


TABLE 1: Textural Data for the Nanoporous Calibration Samples

sample	SSA (m <sup>2</sup> ·g <sup>-1</sup> )	V <sub>p</sub> (cm <sup>3</sup> ·g <sup>-1</sup> )	R <sub>p</sub> (nm)
1	472.7	0.922	3.42
2	166.2	0.991	8.7
3	183.1	1.327	14.25
4	111.6	0.680	7.5
5	406.9	0.813	3.1

of benzil pendant groups on the basis of NMR determination. Molecular weights were determined by SEC measurements using a polystyrene calibration ( $M_n = 200\,000$ ,  $M_w = 450\,000$ ). Films were prepared by compression molding between two Teflon sheets during 1 min at 150 °C under 190 bar. The thickness of the films was about 100 μm.

**2.1.2. Porous Samples.** Nanoporous silica gels monoliths with tailored texture<sup>1-3</sup> were prepared as described elsewhere.<sup>11</sup> Additional commercial porous glass beads<sup>4</sup> were also used as reference material for the calibration procedure.

Commercial silica gel for chromatography<sup>5</sup> was used as a test sample to confirm the validity of the calibration procedure. The textural properties of the different materials have been measured by nitrogen gas sorption technique (BJH method) on a Quantachrome Autosorb6 apparatus, and results are given in Table 1. Nanoporous sol-gel derived silica samples are particularly valuable since their monolithic form allows easy handling.

CCl<sub>4</sub> (Aldrich) of HPLC quality was used without any supplementary purification.

**2.2. Analysis.** A Mettler-Toledo DSC 30 apparatus was used to carry out the thermal analysis. It was equipped with a liquid nitrogen cooling unit permitting to scan temperatures ranging from -170 to 500 °C. A cooling/heating rate 0.7 °C·min<sup>-1</sup> was adopted. This rate value has been determined to be slow enough to keep the system under a continuous thermodynamically equilibrium state.

Calibration, in terms of temperature and heat, was performed using *n*-heptane (-90.6 °C, 140.5 J·g<sup>-1</sup>), indium (156.6 °C, 28.45 J·g<sup>-1</sup>), and zinc (419.2 °C, 107.5 J·g<sup>-1</sup>) as references. A dedicated software allows various calculations (onset, heat, peak temperature, etc.) from the original recorded DSC curves.

An Impact 400 FTIR spectrophotometer, supplied by Nicolet Co. (Omnic software), was used to record the FTIR absorption spectra of the copolymer films after various photooxidation and curing times of the cross-linking process.

**2.3. Cross-Linking Procedure.** Irradiations were performed using a polychromatic light from SEPAP device (ATLAS Corp.) which has been described in ref 12.

An aerated oven was used for the heating experiments.

## III. Results and Discussion

**3.1. Thermoporometry Experiments.** The theoretical basis of this technique was already largely reported,<sup>13-15</sup> and it is admitted now that the thermoporometry (or thermoporosimetry) is a good tool to study divided medium. The technique relies on the experimental evidence that confined liquid, within a pore or "compartmentized" in a gel, freezes at a temperature lower than the one of bulk liquid. The shift of the transition temperature is related to the size of the confinement volume. Particularly, thermoporometry is a suitable method to study the soft and fragile materials provided that a proper liquid probe is chosen. Indeed, Scherer and co-workers<sup>16,17</sup> reported that a shrinkage can occur when the swelling liquid crystallizes. In the case of water for instance, and because of the higher molar volume of ice compared to liquid water, crystallization can provoke damage within the gel network.

We have chosen CCl<sub>4</sub> as liquid probe to explore the cross-linking of styrene copolymer materials. CCl<sub>4</sub> is a good solvent of non-cross-linked polystyrene; its thermal transition temperatures are not too low, and it is available at high purity grade. Furthermore, the solid CCl<sub>4</sub> being denser than its liquid form, and no important shrinkage is expected when the confined solvent crystallizes. Anyway, even if the swollen gel undergoes dimensional variations because of the thermal transition of the liquid probe, these variations must be small compared to the ones induced by swelling. Thermoporometry consequently remains an efficient and unique tool to compare the state of cross-linking of different polymeric samples. The mesh size distributions calculated from the thermoporometry formalism reflect the actual state of the sample taking in account the eventual shrinkage and the swelling equilibrium.

Bulk CCl<sub>4</sub> was studied before, and its thermal phase transitions were well characterized.<sup>18,19</sup> It exhibits a complex thermal transitions system as shown in Figure 1.

Takei et al.<sup>19</sup> showed that both solid-to-solid and liquid-to-solid transitions of CCl<sub>4</sub> were strongly dependent on the average pore size of the porous medium in which the liquid is confined. In particular, they demonstrated that the liquid-to-I<sub>a</sub> transition disappears when the pore radius is smaller than 16.5 nm that is the case of all our calibration samples (see Table 1).

## Cross-Linking of Styrene Copolymer Networks

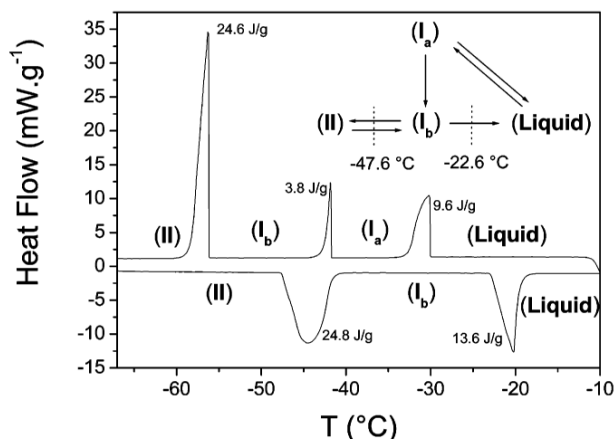


**Figure 1.** DSC thermogram showing the complex thermal transition system of bulk  $\text{CCl}_4$ . The scanning rate was  $0.7\text{ }^\circ\text{C}\cdot\text{min}^{-1}$ .

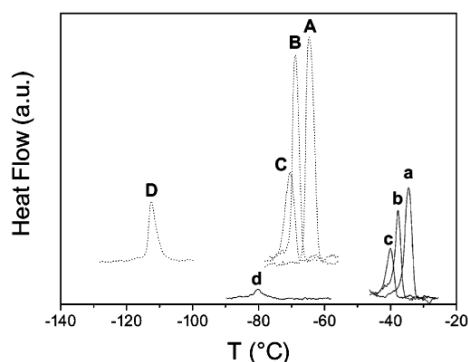


**Figure 2.** DSC thermograms of confined  $\text{CCl}_4$  within the calibration samples: (a, A) sample with 14.25 nm as pore radius; (b, B) 8.7 nm; (c, C) 7.5 nm; (d, D) 3.42 nm. Solid lines represent the liquid-to- $I_b$  and the dashed lines the  $I_b$ -to-II thermal transitions. The cooling rate was  $0.7\text{ }^\circ\text{C}\cdot\text{min}^{-1}$ .

**3.1.1. Calibration Procedure.** A direct calibration procedure using the silica gel samples having well-defined textural properties has been already described.<sup>14,19,20</sup> We applied the same procedure to establish the empirical relationships linking the pore radius ( $R_p$ ) and the shift of transition temperature of the confined  $\text{CCl}_4$  ( $\Delta T$ ).

Figure 2 shows the DSC thermograms related to the cooling of  $\text{CCl}_4$  confined in the calibration samples. For each calibration sample, two peaks are observed: a–d correspond to the liquid-to- $I_b$  crystallizations; A–D are attributed to the corresponding  $I_b$ -to-II allotropic transitions. As expected, the smaller the pore radius, the lower the temperature at which the confined liquid undergoes the transition. The similar behavior is observed for the two transitions. On the other hand, the area under peak, which is proportional to the released energy, decreases with respect to the pore radius.

Figure 3 shows the graphic representations of pore radius ( $R_p$ ) versus the transition point depression,  $\Delta T = T_p - T_0$ , related to the liquid-to- $I_b$  and the  $I_b$ -to-II transformations.  $T_0$  is the bulk  $\text{CCl}_4$  melting temperature (corresponding to the onset point of the fusion endotherm for liquid-to-solid transition), and  $T_p$  is the temperature of the phase transition inside the pore (taken at the top of the peak as recommended by Landry).<sup>21</sup> In the same figure, the data published earlier by Brun and co-workers<sup>18</sup> were also plotted. A good agreement can be seen between the two series.

No linear dependence was observed between the pore radius ( $R_p$ ) and the reciprocal shift of transition temperature ( $\Delta T^{-1}$ ).

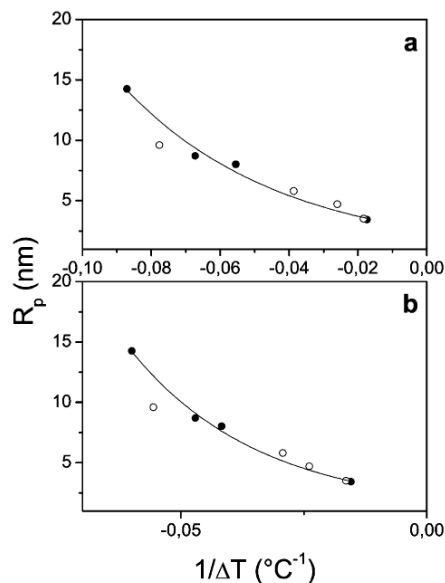


**Figure 3.** Dependence of pore radius against the depression transition point: (a) liquid-to-solid transition; (b) solid-to-solid transition. The opened symbols represent the data published by Brun and co-workers.<sup>18</sup>

**TABLE 2: Numerical Parameter Values of the Relationships between the Apparent Energy of Thermal Transitions ( $W_a$ ) and Their Depression Temperature ( $\Delta T$ ) and between the Pore Radii ( $R_p$ ) and  $\Delta T^{-1}$**

transitn	$R_p = t \exp(-b/\Delta T)$		$W_a = W_0 \exp(f/\Delta T)$	
	$t$ (nm)	$b$ ( $^\circ\text{C}$ )	$W_0$ ( $\text{J}\cdot\text{cm}^{-3}$ )	$f$ ( $^\circ\text{C}^{-1}$ )
liquid-to-solid	2.43	20.1	25.07	0.04
solid-to-solid	2.09	31.6	46.6	0.017

The same kind of relationship was already observed for several others thermoporometry liquid probes.<sup>9,22–24</sup> This observed nonlinearity could be related to the strong temperature dependence of the latent enthalpy of transition ( $W_a$ ). The apparent enthalpies of both liquid-to-solid and solid-to-solid transition have been calculated by following the same procedure described elsewhere.<sup>22</sup> Table 2 summarizes the expressions of  $R_p$  and  $W_a$  as function of  $\Delta T$ .

**3.1.2. Control of the Calibration.** To check the pertinence of the calibration empiric relationships, PSDs of two samples were calculated using the obtained numerical equations. The first one is a commercial silica gel powder used for column chromatography with 6.0 nm nominal pore diameter. The second control sample is a powdered porous glass, the textural properties of which can be found in Table 1. This sample being used for the calibration, the mean pore size is obviously well reproduced, but it is striking to note that the whole pore size distribution is indeed very well reproduced by thermoporometry using both transitions. Figure 4 gives a comparison between PSDs calculated from the gas adsorption technique with the BJH model and the thermoporometry experiments. The two series of data seem in good agreement, thus validating our calibration procedure. Figure 4b shows a certain discrepancy between the nitrogen gas sorption and thermoporometry results in the lowest  $R_p$  side. This observation may be explained by the  $R_p$  expression given in Table 2. The  $t$  value, 2.09 nm for the solid-to-solid transition, represents the lowest  $R_p$  which can be measured by thermoporometry method and which is reached when  $\Delta T$  tends toward infinity.

**3.2. Application to Styrene Copolymer Networks.** **3.2.1. Evolutions of the Mesh Sizes Distributions.** The poly(BZST-

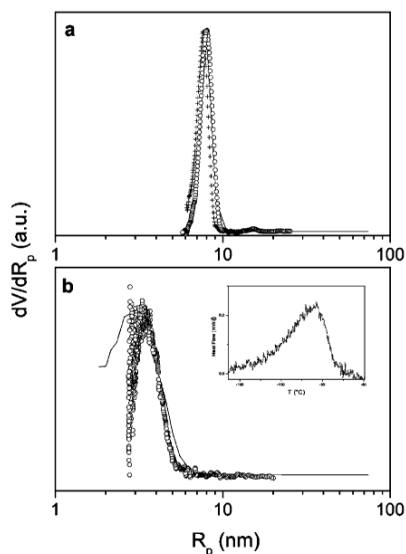


**Figure 4.** Pore size distributions derived from gas ( $N_2$ ) adsorption (lines) and from thermoporometry technique (symbols) for glassy beads with 7.5 nm of average pore radius (a) and for column chromatography silica gel (b). The inset figure shows the DSC thermogram of the solid-to-solid transition of  $CCl_4$  within silica gel powder.  $\circ$  represents the PSD calculated from the solid-to-solid transition, and  $+$ , the PSD calculated from the liquid-to-solid one in (b). Because of the weak intensity of the liquid-to-solid peak, only the solid-to-solid transition was used.

*co*-styrene) films, peroxidized at  $\lambda > 390$  nm and then cross-linked by heating at  $110$  °C or by irradiation at  $\lambda > 300$  nm, were swollen in  $CCl_4$  for 48 h. A 10–20 mg amount of the swollen gel was taken and set in the DSC crucible. The temperature program, described in the calibration section, was applied to record the DSC thermograms of the  $CCl_4$  confined inside the polymer gel. As it was assumed in several previous papers,<sup>9,22,25</sup> a formal analogy exists between the notion of the pore in the rigid porous material and that of the mesh in the swollen polymeric gel.  $CCl_4$ , swelling the soft material, is confined, and its degrees of freedom are reduced in the same way as when it is trapped inside the porous material. Even if there are no pores in the polymer gel, the mobility of the liquid is limited in the two cases. Mesh sizes distributions, calculated for various photo-cross-linked and thermally cross-linked poly-(BZST-*co*-styrene) samples, are presented in Figure 5. The exposure or the cure time increases from right to left. The inset, in Figure 5a, shows a typical DSC thermogram of  $CCl_4$  confined in the swollen gel. Only the liquid-to-solid thermal transition of  $CCl_4$  was used. At first glance, one can notice that the MSD globally shifts toward smaller values of mesh sizes (from 370 to 60 nm) when the time increases. This behavior reveals a densification of the polymer network corresponding to an increase of the cross-linking level. It is also noticeable that no significant variation of the MSD was detected after 4 h regardless of the cross-linking conditions. Both irradiation and heating treatment seems to have the same effect on the polymer matrix.

**3.2.2. Correlation between the Thermoporometry and the Results from FTIR Measurements.** According to the mechanism depicted in Scheme 1, the cross-linking is due to the cleavage of the benzoyl peroxide functions and the subsequent ester groups formation. Conversion of benzil pendant groups (BZ) during the photoperoxidation step (irradiation at  $\lambda > 300$  nm at  $35$  °C) was easily followed by FTIR spectroscopy. As the reaction proceeds, the intensity of the characteristic FTIR

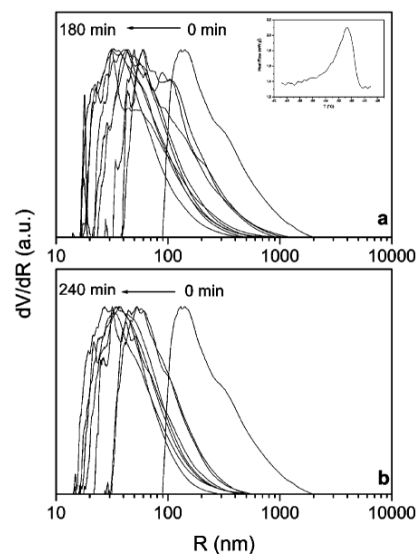


**Figure 5.** Mesh sizes distributions of the polymer networks of cross-linked poly(BZST-*co*-styrene) samples. The films were at first irradiated in air at  $\lambda > 390$  nm at  $35$  °C to transform the benzil pendant functions (BZ) into benzoyl peroxide groups (BP) and after then either thermally cross-linked at  $110$  °C (a) or photo-cross-linked by irradiation at  $\lambda > 300$  nm at  $35$  °C (b). The inset figure shows an example of a DSC thermogram of the liquid-to-solid transition of  $CCl_4$  swelling a thermally cross-linked copolymer sample.

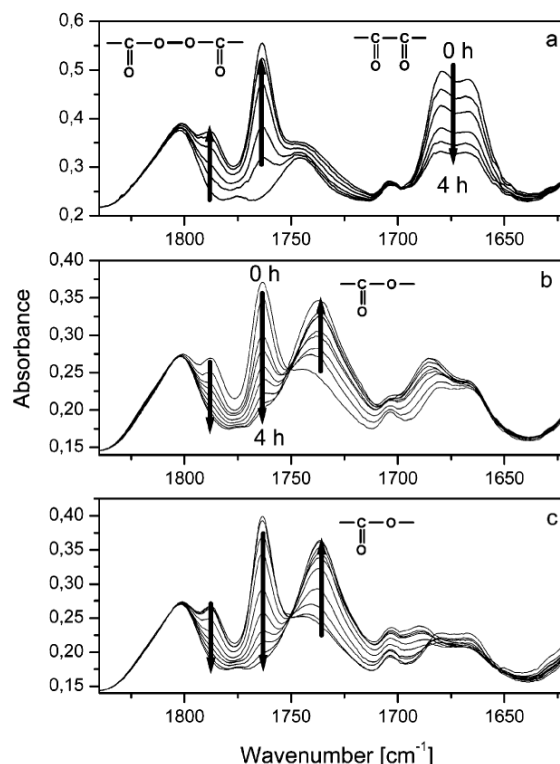


**Figure 6.** FTIR spectra of poly(VBZ-*co*-styrene) films. Peroxidation step: films were irradiated at  $\lambda > 390$  nm at  $35$  °C in air (a). Cross-linking step by thermal treatment: peroxidized films were heated at  $110$  °C in an aerated oven (b). Photo-cross-linking step: peroxidized films were irradiated at  $\lambda > 300$  nm at  $35$  °C in air (c). The periods of each treatment ranged between 0 and 240 min.

stretching band of 1,2-dicarbonyl groups at  $1675$   $cm^{-1}$  decreases (see Figure 6a). Formation of BP moieties is detected in FTIR

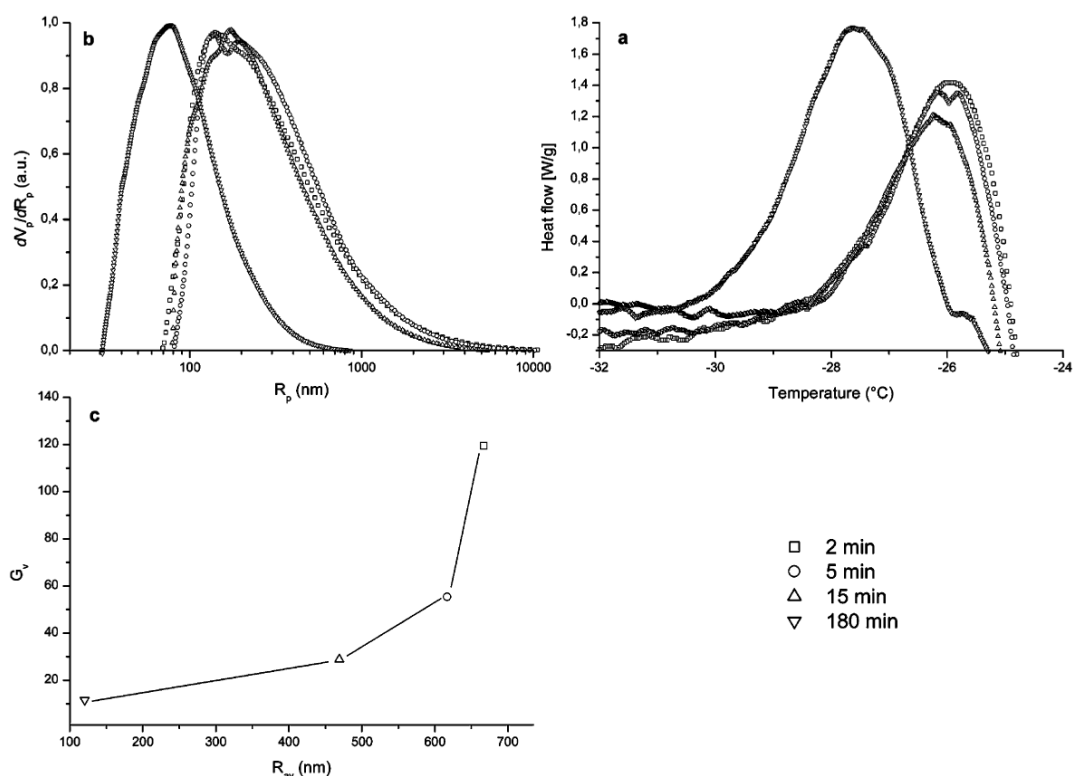


**Figure 7.** Correlation between the average mesh size of the network ( $R_{av}$ ) and the degree of swelling ( $G_v$ ): (a) DSC exotherms of solidification of the confined  $\text{CCl}_4$  for four irradiated and swollen samples ( $\square$ , 2 min;  $\circ$ , 5 min;  $\triangle$ , 15 min;  $\nabla$ , 180 min); (b) corresponding mesh size distributions; (c) plot of the degree of swelling measured by the gravimetric method ( $G_v$ ) versus the average mesh size ( $R_{av}$ ) derived from thermoporometry.

spectra by the growth of new absorption bands at 1765 and 1785  $\text{cm}^{-1}$  ascribed to benzoyl peroxide groups.

The cross-linking step leads to significant changes in the IR absorption spectra. Figure 6 displays the chemical evolution of peroxidized sample poly(BPST-*co*-styrene) upon either thermal cross-linking at 110 °C either photo-cross-linking at  $\lambda > 300$  nm at 35 °C.

The thermal decomposition of BP groups is detected by the decrease of the peroxide absorption bands in the region 1750–1800  $\text{cm}^{-1}$  and the increase of an absorption band at 1740  $\text{cm}^{-1}$  assigned to the ester links formation. The thermal decomposition of photochemically generated BP groups in poly(BZST-*co*-styrene) film is achieved upon 4 h of treatment at 110 °C.

Similar results are obtained through the photo-cross-linking process. Figure 6c monitors the phototransformation of BP groups (absorbing in the region 1750–1800  $\text{cm}^{-1}$ ) into ester bridges (at 1740  $\text{cm}^{-1}$ ) linking the macromolecular chains to each other. After 4 h of UV exposure at  $\lambda > 300$  nm, the peroxide moiety is no longer detected in the FTIR spectrum.

To correlate the disappearance of benzoyl peroxide (BP) and the morphological evolution of the polymer matrix, the average size ( $R_{av}$ ) of the mesh of the network was calculated from each MSD. Our assumption is that the average size of the mesh is related to the degree of swelling and can be used as cross-linking indicator: the smaller  $R_{av}$ , the denser the polymeric network. To confirm this assumption, prior to use of the  $R_{av}$  data, some experiments have been performed to compare the thermoporometry results with gravimetric swelling measurement, which is the more conventional method to characterize the three-dimensional network. For four new samples, irradiated respectively for 2, 5, 15, and 180 min, the degrees of swelling ( $G_v$ ) were determined by the gravimetric method. The same samples were then submitted to the thermoporometry procedure, and their

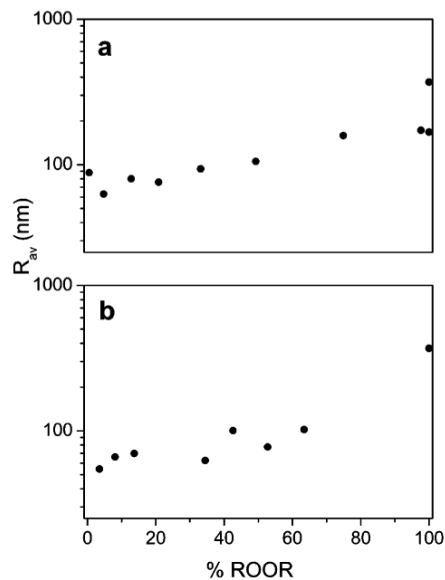


**Figure 8.** Correlation between the relative homolyzed benzoyl peroxide concentration (% ROOR) and the average mesh size ( $R_{av}$ ) of the polymer network during irradiation at  $\lambda > 300$  nm at 35 °C (a) and heating at 110 °C in air (b). The films were at first peroxidized at  $\lambda > 390$  nm at 35 °C in air.

average mesh size was been calculated. Figure 7 summarizes the results of these experiments. As can be seen in Figure 7c, it can be pointed out that  $R_{av}$  increases with the degree of swelling, thus confirming our working hypothesis.

Figure 8 presents the evolution of  $R_{av}$  with respect to the relative homolyzed benzoyl peroxide concentration (% ROOR).

The % ROOR was determined on the basis of IR analysis by rationing absorbances at  $1765\text{ cm}^{-1}$  as follows:

$$\% \text{ ROOR} = \frac{A(t)}{A_0} \times 100$$

Here  $A(t)$  is the absorbance at  $1765\text{ cm}^{-1}$  for a given exposure time ( $t$ ) and  $A_0$  the initial absorbance.

Regardless of the cross-linking conditions (heating or irradiation), an actual correlation can be observed between the cleaved peroxide content of the matrix and the average mesh size of the network. The origin of cross-linking is then clearly established. Thus, we assume that while peroxide cleavage is clearly responsible for cross-linking, the BP content defines the structure of the final network. Besides, Figure 8a exhibits two distinct values of  $R_{av}$  corresponding apparently to an identical percentage of ROOR (100%). A possible explanation of this observation may be the better sensitivity of the thermoporometry by comparison with the IR spectroscopy. In fact, a small diminution in % ROOR, not detectable by IR investigation, can cause a noticeable morphological modification in the polymeric network which may be measurable by thermoporometry.

## Conclusion

Films of poly(BZST-co-styrene) were irradiated at  $\lambda > 390\text{ nm}$  to transform pendant benzil dicarbonyl groups (BZ) into pendant benzoyl peroxide groups (BP). The pendant benzoyl peroxide groups were converted, either by irradiation at  $\lambda > 300\text{ nm}$  or heating at  $110\text{ }^\circ\text{C}$ , into ester functions linking the macromolecular chains to each other and leading to a cross-linked material. This chemical evolution is conventionally monitored by FTIR spectroscopy or gravimetric swelling method. Thermoporometry, giving the mesh size distribution of the polymer network for different irradiation or curing times, is an alternative and complementary way to follow these alterations. A pertinent correlation between these three approaches was clearly established.

$\text{CCl}_4$ , as thermoporometry liquid probe, seems to be very suitable to study the cross-linking of the styrene copolymers. All the numerical relationships, needed to perform the calculation of the mesh sizes distributions from DSC thermograms,

were established, and their validity was successfully checked for the two thermal transitions of  $\text{CCl}_4$ .

**Acknowledgment.** The authors are grateful to the VEGA agency for financial support through Grant 2/5108/25. Financial support from the French ANR under project Nanothermomécanique (ACI Nanosciences No. 108) is gratefully acknowledged.

## References and Notes

- (1) Mosnáček, J.; Weiss, R. G.; Lukáč, I. *Macromolecules* **2002**, *35*, 3870.
- (2) Mosnáček, J.; Weiss, R. G.; Lukáč, I. *Macromolecules* **2004**, *37*, 1304.
- (3) Husár, B.; Lukáč, I. *Polym. Photochem. Photobiol., A: Chem.* Submitted for publication.
- (4) Giurginca, M.; Zaharescu, T. *Polym. Degrad. Stab.* **2002**, *75*, 267.
- (5) Chipara, M. I.; Georgescu, L.; Oproiu, C.; Chipara, M. D.; Niculescu, A.; Galatanu, N.; Reyes, J. R.; Secu, C. E. *NIM Phys. Res.* **1997**, *B131*, 188.
- (6) Adam, C.; Lacoste, J.; Lemaire, J. *Polym. Degrad. Stab.* **1991**, *32*, 51.
- (7) Commereuc, S.; Bonhomme, S.; Verney, V.; Lacoste, J. *Polymer* **2000**, *41*, 917.
- (8) Baba, M.; Gardette, J. L.; Lacoste, J. *Polym. Degrad. Stab.* **1999**, *63*, 121.
- (9) Baba, M.; Nedelec, J. M.; Lacoste, J.; Gardette, J. L. *J. Non-Cryst Solids* **2003**, *315* (3), 228.
- (10) Baba, M.; Gardette, J. L.; Lacoste, J. *Polym. Degrad. Stab.* **1999**, *65*, 421.
- (11) Hench, L. L. In *Sol-gel silica: processing, properties and technology transfer*; Noyes Publications: New York, 1998.
- (12) Lemaire, J.; Arnaud, R.; Gardette, J. L.; Lacoste, J.; Seiner. *Kunstst.-Ger. Plast.* **1986**, *76*, 149.
- (13) Kunh, W. Peterli, E.; Majer, H. *J. Polym. Sci.* **1955**, *16*, 539–548.
- (14) Brun, M.; Lallemand, A.; Quinson, J. F.; Eyraud, C. *Thermochim. Acta* **1977**, *21*, 59.
- (15) Rudman, R.; Post, B. *Science* **1966**, *154*, 1009.
- (16) Scherer, G. W. *J. Non-Cryst. Solids* **1993**, *155*, 1–25.
- (17) Scherer, G. W.; Smith, D. M.; Stein, D. *J. Non-Cryst. Solids* **1995**, *186*, 309–315.
- (18) Brun, M.; Quinson, J. F.; Martinie, B.; Eyraud, C. *J. Chim. Phys.* **1978**, *75*, 469–475.
- (19) Takei, T.; Ooda, Y.; Fuji, M.; Watanabe, T.; Chikazawa, M. *Thermochim. Acta* **2000**, *352–353*, 199–204.
- (20) Denoyel, R.; Pellenq, R. *J. Langmuir* **2002**, *18*, 2710.
- (21) Landry, R. *Thermochim. Acta* **2005**, *433*, 27–50.
- (22) Billamboz, N.; Nedelec, J.-M.; Grivet, M.; Baba, M. *ChemPhys-Chem* **2005**, *6*, 1–7.
- (23) Billamboz, N.; Baba, M.; Grivet, M.; Nedelec, J. M. *J. Phys. Chem. B* **2004**, *108*, 12032–12037.
- (24) Bahloul, N.; Baba, M.; Nedelec, J. M. *J. Phys. Chem. B* **2005**, *109*, 16227–16229.
- (25) Baba, M.; Nedelec, J. M.; Lacoste, J.; Gardette, J. L.; Morel, M. *Polym. Degrad. Stab.* **2003**, *2*, 80.

### 5.3 Correlation of thermoporometry with densitometry results

Thermoporometry and densitometry are complementary methods. Thermoporometry studies insoluble part of crosslinked polymer, densitometry studies soluble part of crosslinked material. Densitometry is an alternative method to measure of insolubility during crosslinking. Instead of weighting the gel fraction, densitometry measures the density of uncrosslinked soluble part of a sample. The density of a solution of uncrosslinked sample can be higher or lower than the density of a pure solvent. More the sample is crosslinked, the density of sample becomes more similar to the density of pure solvent. For our study, the same sample was used for both measurements. As  $\text{CCl}_4$  has a high density, the density of BZS/S solution was lower. We wanted to compare the results obtained by both methods. For better understanding of thermoporometry results, average mesh size was calculated from mesh size distribution curve. Figure 6 displays the density of the extract and average mesh size of crosslinked BZS/S as a function of time of treatment: photoperoxidation followed by photo- or thermo-crosslinking.

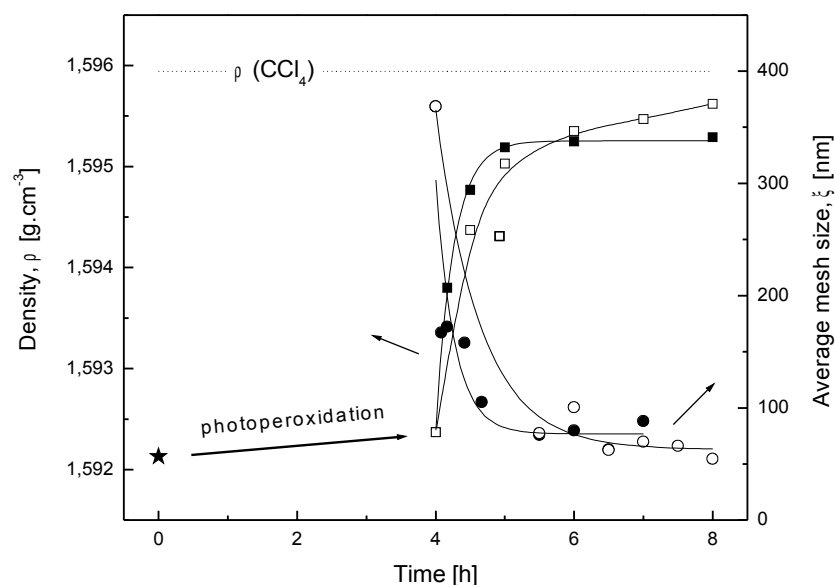


**Figure 6:** Correlation of thermoporometry with densitometry. Density of the extract ( $\square$ ,  $\blacksquare$ ) and average mesh size  $\zeta$  of crosslinked sample ( $\circ$ ,  $\bullet$ ) as a function of time. Interval 0-4 h is a photoperoxidation step ( $\lambda > 390$  nm), initial copolymer BZS/S is labelled as ( $\star$ ). Interval 4-8 h is a thermo-crosslinking (110 °C, hollow) or photo-crosslinking step ( $\lambda > 300$  nm, solid).

The solution of unirradiated BZS/S ( $\star$ ) has the lowest density. After photoperoxidation during 4 h, its density increases slightly. During first hour of crosslinking, the polymer becomes

more and more insoluble, so a rapid increase of density is observed. After reaching the gel point, polymer becomes nearly insoluble and only a small increase of density or a plateau can be observed. After thermo-crosslinking process (□), the density is higher than after photo-crosslinking (■).

It is shown that thermo-crosslinking (○) is almost equally efficient as photo-crosslinking (●) under given experimental conditions. Network formed by thermo-crosslinking is slightly denser. However, a higher density of network could be expected for photo-crosslinking while consumption of moiety during photoperoxidation process was only 60 %. The remaining 40 % of original BZ (according to IR spectroscopy) could be used to produce a denser network during photo-crosslinking process while it is not possible for thermo-crosslinking. One can conclude that densitometry results correlate with thermoporometry results.

## 5.4 Conclusion

Thermoporometry, an alternative to swelling measurements, was used to follow the crosslinking process of BZS/S copolymer by characterising the mesh size of its swollen polymeric network. Carbon tetrachloride was chosen as a probe liquid. It seems to be very suitable solvent for this purpose. All numerical relations necessary for the calibration were established.

After photoperoxidation step, a slightly crosslinked polymer is obtained. During crosslinking step, a rapid process of crosslinking is observed during first hour of treatment ( $\lambda > 300$  nm at 35 °C or 110 °C). After 1 h, a densification of formed network can be observed. Thermo-crosslinking seems to be more efficient than photo-crosslinking. Correlating results were observed using densitometry – a complementary method that measure the density of soluble part of a crosslinked material. A correlation between thermoporometry and FTIR was established as well.

## 6 STUDY OF FINAL POLYMER NETWORK

### 6.1 Introduction

This chapter handles about the characterisation of final network of crosslinking. The aim was to compare the networks of copolymers BZS/S with different content of photoreactive BZ group. For that reason, a series of different copolymers was prepared under the same conditions (except one sample) and all copolymers were crosslinked in the same manner as well to ensure the comparability. Characterisation was performed on the initial, photoperoxidised and crosslinked copolymers. Melt rheology was chosen to characterise the final network. It is a sensitive method to all evolutions of the molecular structure. Rheological results were compared with the results obtained by the analysis of a soluble part (densitometry) and an insoluble part (swelling, thermoporometry).

Another aim of this chapter is to compare networks of copolymers prepared by a conventional free radical polymerization with copolymers prepared by nitroxide mediated living radical polymerization (NMP). Living polymerization routes permit the synthesis of well-defined macromolecules possessing predictable molar masses, narrow molar mass distribution, controlled chemical composition, possibility to choose capped functional groups or arrangement of different monomeric units in macromolecule. This enhanced control is a direct consequence of a very fast coupling reaction of nitroxide radicals with growing polymer chain-end radicals. Temporarily capped living radical in the form of thermally labile alkoxyamine decomposes into original nitroxide radical and growing radical, which is able to add some monomer molecules at the time of its existence. Connection of macroradical with nitroxide decreases the steady state concentration of macroradical and almost completely eliminates non-reversible termination reactions between growing macroradicals. Repetition of these reaction steps results in “living” character of polymerization.

### 6.2 Synthesis of copolymers

A series of the copolymers BZS/S with BZ bearing monomer (BZS) and styrene were

prepared either by conventional free-radical polymerization or by living free-radical polymerization (Table 3). As the mutual reactivity of BZS and styrene are almost equal, the polymerizations can be carried to the high conversions. The free radical polymerizations were carried out at 92 °C with *tert*-butyl peroxybenzoate (TBPB) as an initiator and toluene as a solvent to dilute the polymerization mixture to allow stirring even at high conversions. BZS/S with the highest content of BZS (13 wt%) was prepared by free radical polymerization in bulk at 60 °C with AIBN as an initiator. For a comparison, two “living” copolymers were prepared at 125 °C; two types of mediators were used: BTXNOR and StNO. BTXNOR is a novel type of mediator bearing a fluorescent benzothioxanthene chromophore. StNO is a stable free radical, a 4-stearoyloxy derivative of 2,2,6,6-tetramethyl-1-piperidinyloxy. The length of alkyl chain does not affect the effectivity of mediator.

***Free radical polymerization in solution (PS, BZS/S 0.5%, BZS/S 1%, BZS/S 2%, BZS/S 4%, BZS/S 8%)***

A solution of BZS, styrene, TBPB (0.4 wt%) in toluene (see Table 3) was deaerated with argon and polymerised at 92 °C under argon. The conversion was monitored by precipitation of the polymer from 1 ml solution of reaction mixture into methanol. After cooling, polymerization mixtures were diluted with chloroform and precipitated twice into methanol. Polymers prepared in this manner still contain the residual BZS as it can be seen from <sup>1</sup>H NMR spectra. They were purified by Soxhlet extraction with ethanol.

***Free radical polymerization in bulk (BZS/S 13%)***

An ampoule containing BZS (0.417 g, 1.08 mmol), styrene (2.731 g, 26.2 mmol) and AIBN (3 mg) was sealed under argon and polymerised at 60 °C for 10 h. The copolymer was precipitated 4 times from chloroform solution into methanol to yield 0.61 g (19 %) of the copolymer. Residual BZS monomer was removed by Soxhlet extraction with ethanol.

***Nitroxide mediated polymerization (BZS/S 4% BTXNOR, BZS/S 4% StNO)***

A solution of BZS (0.3 g), styrene (7.5 ml) and StNO (14.5 mg) or BTXNOR (18.5 mg) was deaerated with argon, sealed in an ampoule and polymerised at 125 °C. After cooling, polymerization mixtures were diluted with chloroform and precipitated twice into methanol.

Precipitated polymers were purified by Soxhlet extraction with ethanol to remove residual BZS and mediator.

**Table 3:** Polymerization conditions for a series of copolymers BZS/S.

<i>Copolymer sample</i>	<i>Mediator</i> [ $4.4 \times 10^{-3}$ mol/l]	<i>BZS</i> [g]	<i>Styrene</i> [ml]	<i>Toluene</i> [ml]	<i>Temperature</i> [°C]	<i>Polymerization</i> <i>time</i> [h]	<i>Conversion</i> [%]
PS	-	0	50	100	92	61	82
BZS/S 0.5%	-	0.02	4	8	91	49	36
BZS/S 1%	-	0.04	4	8	91	49	34
BZS/S 2%	-	2	100	200	92	53	81
BZS/S 4%	-	2	50	100	92	53	70
BZS/S 8%	-	2	25	50	92	93	36
BZS/S 13%	-	0.417	3	-	60	10	19
BZS/S 4% BTXNOR	BTXNOR	0.3	7.5	-	125	14	68
BZS/S 4% StNO	StNO	0.3	7.5	-	125	14	77

The content of BZS in copolymer was determined by means of NMR (see Table 4). It can be clearly seen that the content of BZS in copolymer is practically the same as in the monomer mixtures and does not depend very much on conversion and BZS content in monomer mixture. It is a reflection of very similar reactivity of both comonomers resulting in statistical copolymer with regular distribution of BZS in polymer chains.

**Table 4:** Content of BZS in monomer mixture and in copolymer BZS/S.

<i>Copolymer sample</i>	<i>BZS in monomer</i> <i>mixture</i> [wt%]	<i>BZS in copolymer</i> [wt%]	<i>BZS in monomer</i> <i>mixture</i> [mol%]	<i>BZS in copolymer</i> [mol%]
PS	0	0.0	0	0
BZS/S 0.5%	0.55	0.5	0.15	0.13
BZS/S 1%	1.11	1.0	0.30	0.27
BZS/S 2%	2.17	2.0	0.59	0.54
BZS/S 4%	4.25	4.0	1.18	1.1
BZS/S 8%	8.15	8.0	2.33	2.3
BZS/S 13%	13.25	12.8	3.96	3.8
BZS/S 4% BTXNOR	4.25	4.0	1.18	1.1
BZS/S 4% StNO	4.25	4.0	1.18	1.1

## 6.3 Characterisation of molecular parameters of initial BZS/S

Mostly used method for characterisation the average molar masses and their distribution of the synthesised polymers is GPC. It is a chromatographic method in which particles are separated based on their size, or in more technical terms, on their hydrodynamic volume. GPC can be used as a measure of both the size and the polydispersity of a synthesised polymer - that is, the distribution of sizes of polymer molecules.

Alternatively, molecular parameters of polymers can be characterised by a rheology using a Cole-Cole plot. Cole-Cole representation provides a value of a zero shear viscosity  $\eta_0$  which is a function of mass average molecular weight  $M_w$  and the value of a distribution parameter  $h$  that is a function of the polydispersity index.

### 6.3.1 Gel permeation chromatography

Behaviour of a polymer during crosslinking are dependent on molar mass. To compare a series of copolymers, it is necessary to have similar molar masses. Synthesised copolymers BZS/S were characterised by GPC with MALS and RI detector. GPC results are presented in Table 5.

**Table 5:** PS equivalent molar masses and polydispersities of a series of copolymers BZS/S (0-13 wt% of BZS) determined by GPC using MALS + RI detector.

<i>Copolymer sample</i>	$M_w$ [g/mol]	$M_n$ [g/mol]	<i>PDI</i>
PS	148700	88400	1.68
BZS/S 0.5%	123800	82000	1.51
BZS/S 1%	98300	67400	1.46
BZS/S 2%	154000	83500	1.84
BZS/S 4%	156800	80400	1.95
BZS/S 8%	86200	47800	1.80
BZS/S 13%	650000 <sup>(*)</sup>	230000 <sup>(*)</sup>	2.8 <sup>(*)</sup>
BZS/S 4% BTXNOR	164600	123100	1.34
BZS/S 4% StNO	189900	145000	1.31

<sup>(\*)</sup> Sample measured separately in different conditions.

Copolymers with 0 %, 2 %, 4 % content of BZS and copolymers prepared by NMP have similar  $M_w$ ; NMP copolymers have higher  $M_n$ . Molar masses of copolymers with 0.5 %, 1 % and

8 % content of BZS are notably lower. These copolymers were prepared in smaller quantities, the conversions were smaller and prolongation of the polymerization time did not lead to the conversion increase. BZS/S 13%, prepared in bulk, has the highest  $M_w$ ,  $M_n$ .

As presumed, the polydispersities of NMP copolymers ( $\sim 1.3$ ) are much lower than those prepared by a conventional polymerization ( $\sim 1.5 - 2.0$ ). It is also well seen from Figure 7 that chromatograms of NMP “living” copolymers are narrower than the others. BZS/S 13%, prepared in bulk, has the highest polydispersity.

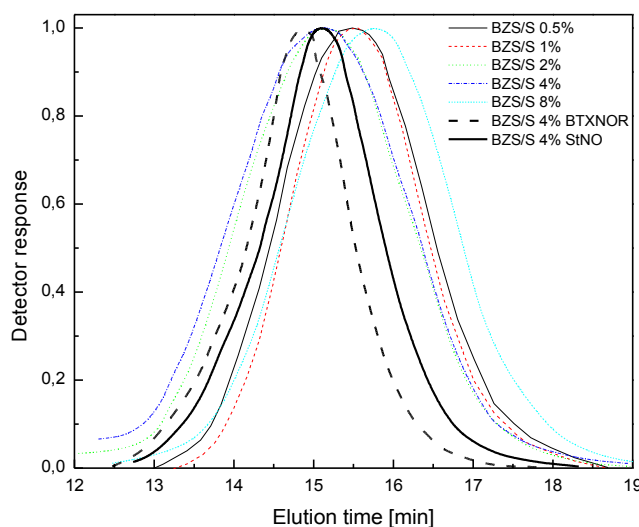


**Figure 7:** Chromatograms of a series of BZS/S copolymers (MALS + RI detector).

An advantage of BZS/S 4% BTXNOR copolymer is the presence of a fluorescent benzothioxanthene chromophore that allows us to calculate the percentage of the chain ends containing this chromophore.

First, a calibration curve was constructed: peak area from fluorescent or UV/VIS spectra (395-520 nm) of THF solution of BTXNOR as a function of BTXNOR concentration. Peak area from fluorescent or UV/VIS spectrum of BZS/S 4% BTXNOR copolymer solution allowed us to estimate benzothioxanthene concentration in copolymer and knowing the concentration of the copolymer solution we were able to calculate theoretical number average molecular weight  $M_n$  of copolymer under assumption that all polymer chains are marked with benzothioxanthene chromophore. The percentage of polymer chains bearing the chromophore was calculated as a ratio of  $M_n$  determined by GPC to calculated  $M_n$  of copolymer having all polymer chains marked with chromophore.

The extent of “livingness” calculated on the base of data obtained from fluorescence as well

as UV/VIS absorption measurement was almost the same and the values 64 % (fluorescence) and 60 % (UV/VIS absorption) were obtained. It means that at given conversion just 60 % of polymer chains are ended by fluorescence probe.

### 6.3.2 Rheological master curves

Figures 9-15 show rheological master curves of a series of initial copolymers BZS/S and Figure 8 shows rheological master curves of PS. These curves display similar rheological behaviour typical for melt polymers. The point of intersection divides the curve into terminal zone (low frequencies) and rubbery plateau region (high frequencies). Copolymers with lower molar masses have the weak rubbery plateaus (Figures 9, 10, 13). It was necessary to gain maximum points in the terminal zone to make a good extrapolation in the case of Cole-Cole plot.

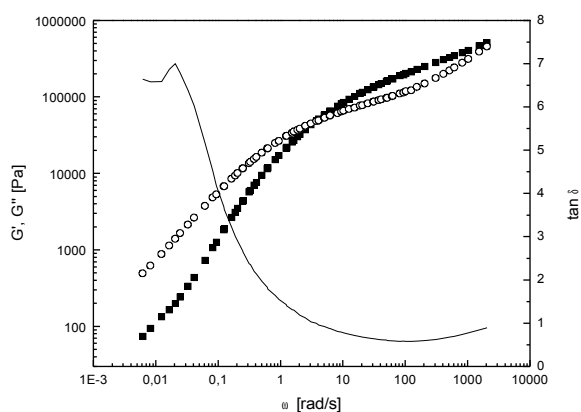


**Figure 8:** Storage ( $G'$ , ■) and loss ( $G''$ , ○) moduli as a function of frequency pulsation  $\omega$  for PS. The reference temperature was 170 °C.

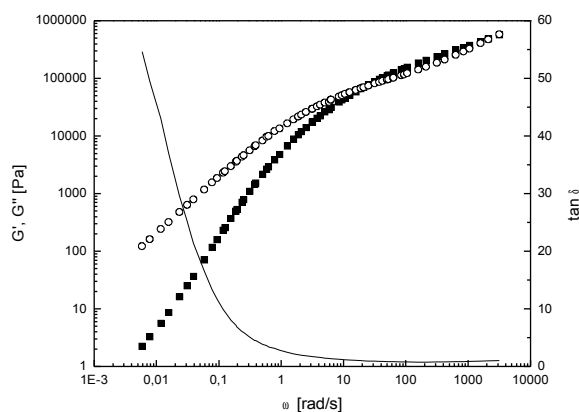


**Figure 9:** Storage ( $G'$ , ■) and loss ( $G''$ , ○) moduli as a function of frequency pulsation  $\omega$  for initial BZS/S 0.5%. The reference temperature was 170 °C.

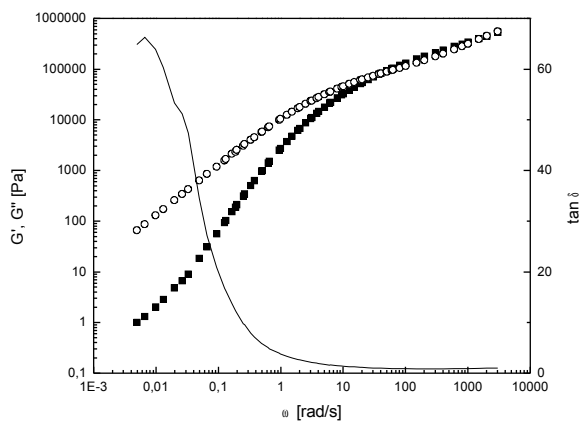


**Figure 10:** Storage ( $G'$ , ■) and loss ( $G''$ , ○) moduli as a function of frequency pulsation  $\omega$  for initial BZS/S 1%. The reference temperature was 170 °C.

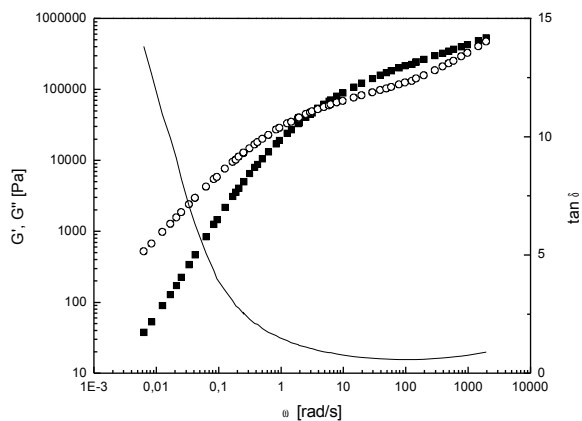


**Figure 11:** Storage ( $G'$ , ■) and loss ( $G''$ , ○) moduli as a function of frequency pulsation  $\omega$  for initial BZS/S 2%. The reference temperature was 170 °C.

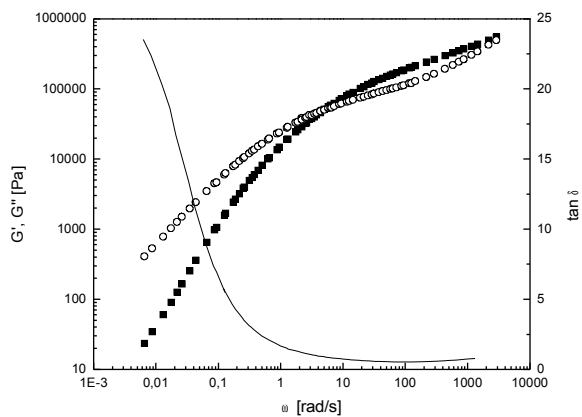


**Figure 12:** Storage ( $G'$ , ■) and loss ( $G''$ , ○) moduli as a function of frequency pulsation  $\omega$  for initial BZS/S 4%. The reference temperature was 170 °C.

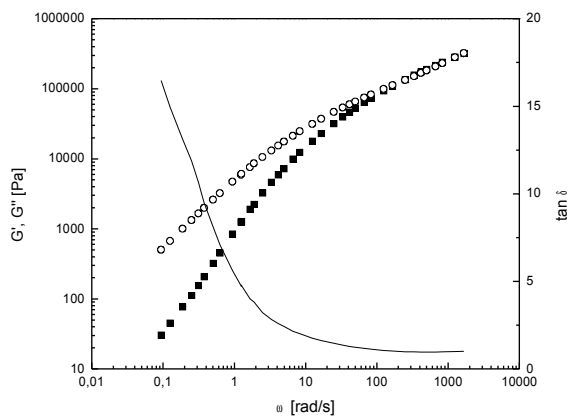


**Figure 13:** Storage ( $G'$ , ■) and loss ( $G''$ , ○) moduli as a function of frequency pulsation  $\omega$  for initial BZS/S 8%. The reference temperature was 170 °C.

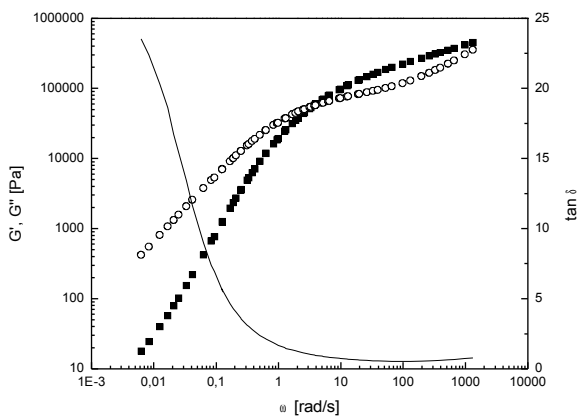


**Figure 14:** Storage ( $G'$ , ■) and loss ( $G''$ , ○) moduli as a function of frequency pulsation  $\omega$  for initial BZS/S 4% BTXNOR. The reference temperature was 170 °C.

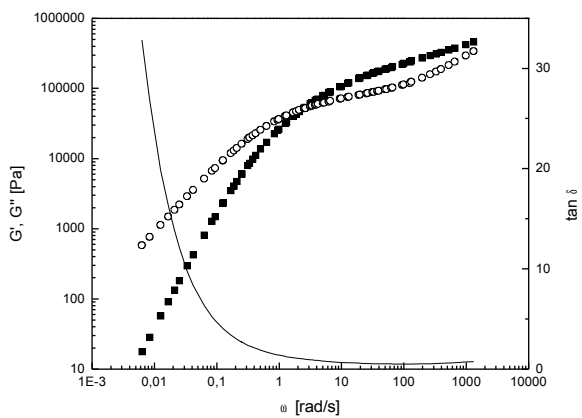


**Figure 15:** Storage ( $G'$ , ■) and loss ( $G''$ , ○) moduli as a function of frequency pulsation  $\omega$  for initial BZS/S 4% StNO. The reference temperature was 170 °C.

### 6.3.3 Cole-Cole representation

An empirical rheological model used to fit dynamic data is the Cole-Cole distribution. A Cole-Cole plot is constructed by plotting of imaginary component of dynamic viscosity  $\eta''$  ( $\eta'' = G''/\omega$ ) versus real component of dynamic viscosity  $\eta'$  ( $\eta' = G'/\omega$ ). In the complex plane, this model predicts the variation of the viscosity components ( $\eta''$  vs.  $\eta'$ ) to be an arc of circle. From this representation it is possible to determine the parameters of the distribution:  $\eta_0$  is obtained through the extrapolation of the arc of the circle on the real axis and the distribution parameter  $h$  through the measurement of the angle  $\Phi = h\pi/2$  between the real axis and the radius going from the origin of the axis to the centre of the arc of the circle.

Parameter  $h$  is a function of the polydispersity. Zero shear viscosity  $\eta_0$  depends on the mass average molecular weight  $M_w$  and obeys a power law ( $\eta_0 \propto M_w^{3.4}$ )<sup>95</sup>.

The Cole-Cole plot of a series of BZS/S samples is shown in Figure 16. It confirms the results of GPC. All results are summarised in Table 6. Zero shear viscosity  $\eta_0$  is compared with  $M_w$  and the distribution parameter  $h$  is compared with the polydispersity index.

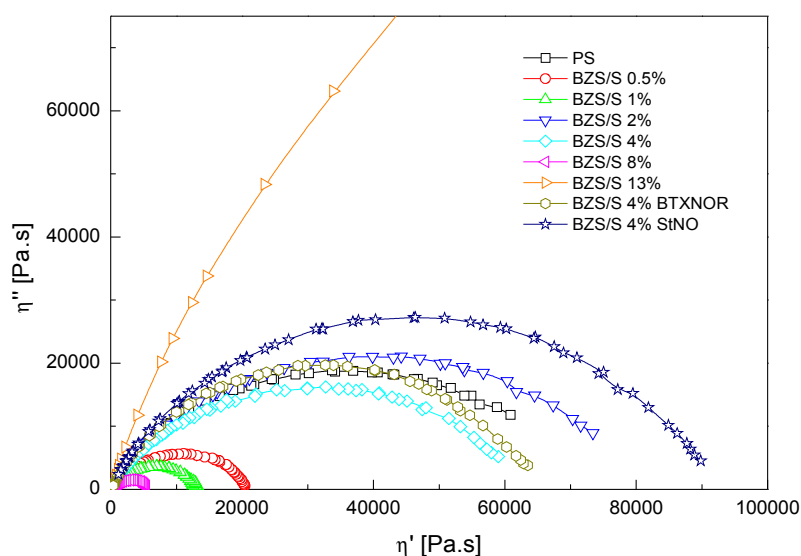


**Figure 16:** Cole-Cole plot of the initial copolymers BZS/S: Imaginary component of dynamic viscosity ( $\eta''$ ) as a function of real component of dynamic viscosity ( $\eta'$ ).

The distribution parameter  $h$  of NMP copolymers (0.31, 0.32) is lower than of those prepared by a conventional polymerization (0.37 – 0.40) that confirms the “living” character of NMP copolymers. BZS/S 13%, having the highest polydispersity has the lowest  $h$  but the

extrapolation in this case was inaccurate because of lack of data points.

**Table 6:** Comparison of zero shear viscosity  $\eta_0$  with weight average molar mass  $M_w$  and comparison of distribution parameter  $h$  with polydispersity index of initial copolymers.

Copolymer sample	$\eta_0$ [Pa.s]	$M_w$ [g/mol]	$h$	PDI
PS	71600	148700	0.37	1.68
BZS/S 0.5%	21100	123800	0.37	1.51
BZS/S 1%	13400	98300	0.37	1.46
BZS/S 2%	80200	154000	0.37	1.84
BZS/S 4%	62800	156800	0.38	1.95
BZS/S 8%	5800	86200	0.40	1.80
BZS/S 13%	911000	650000	0.29	2.8
BZS/S 4% BTXNOR	64800	164600	0.31	1.34
BZS/S 4% StNO	92200	189900	0.32	1.31

The fit of the plot of  $\log \eta_0$  versus  $\log M_w$  should give a straight line with a slope of theoretical value of 3.4 according to the power law  $\eta_0 \propto M_w^{3.4}$ . Molar masses gave a good fit with a slope  $k = 3.64$  that is reasonably close to the theoretical value 3.4 (Figure 17).

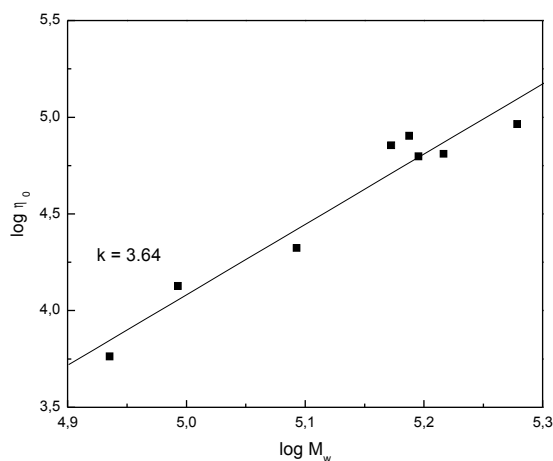


**Figure 17:** Logarithmic plot of zero shear viscosity ( $\eta_0$ ) against weight-average molar mass ( $M_w$ ) for initial BZS/S copolymers.

#### 6.3.4 Number of BZ units per polymer chain

A very suitable parameter of initial copolymers is number of BZ units per chain. It was

calculated from BZ content in copolymer and  $M_n$  and  $M_w$  determined by GPC. The results are summarised in Table 7. We can also calculate theoretical crosslinking index  $\gamma$ . It is defined as a number of crosslinked units per primary molecule in the system as a whole. Crosslinking index  $\gamma$  is a relative degree of crosslinking defined for bifunctional crosslinks ( $f' = 2$ ) with concentration  $c$  (mol/g) as

$$\gamma = f' c M_w$$

When pendant BP group is thermally decomposed into low molecular benzoyloxy radical and benzoyloxy macroradical (Scheme 10), only one of them can be bound to another polymer chain. Only benzoyloxy macroradical can cause crosslinking (Scheme 11). So, the probability that one BP group will cause crosslinking is 50 %. Thus, the theoretical crosslinking index  $\gamma$  is equivalent to the number of BZ units per chain (from  $M_w$ ).

We have to take into account also the degree of BZ transformation to BP because only BP contributes to crosslinking (Table 8).

**Table 7:** Number of BZ units per polymer chain.

<i>Copolymer sample</i>	<i>BZS in copolymer [mol%]</i>	<i><math>M_n</math> [g/mol]</i>	<i>Number of BZ units per chain (from <math>M_n</math>)</i>	<i><math>M_w</math> [g/mol]</i>	<i>Number of BZ units per chain (from <math>M_w</math>)</i>	<i>Theoretical crosslinking index <math>\gamma</math></i>
PS	0	88400	0	148700	0	0
BZS/S 0.5%	0.13	82000	1.1	123800	1.6	1.6
BZS/S 1%	0.27	67400	1.7	98300	2.5	2.5
BZS/S 2%	0.54	83540	4.3	154000	8.0	8.0
BZS/S 4%	1.1	80400	8.3	156800	16.2	16.2
BZS/S 8%	2.3	47800	9.9	86200	17.8	17.8
BZS/S 13%	3.8	230000	76	650000	215	215
BZS/S 4% BTXNOR	1.1	123100	13	164600	17.0	17.0
BZS/S 4% StNO	1.1	145000	15	189900	19.7	19.7

## 6.4 Characterisation of molecular parameters of photoperoxidised BZS/S

Only phototransformed pendant BZ groups are responsible for the crosslinking. Due to the fact that the phototransformation of BZ to BP was not quantitative after the fixed curing time, it is necessary to estimate the BZ conversion and BP formation respectively.

### 6.4.1 Content of BP in photoperoxidised copolymers

All samples were photoperoxidised by an irradiation in the SEPAP device for 4 h. BZ conversion during irradiation was calculated from IR spectra from the peak areas of the initial and the photoperoxidised copolymer (peak area of PS was subtracted) in the 1710-1640  $\text{cm}^{-1}$  region (Figure 18). BP formation can be characterised by the absorbance at 1763  $\text{cm}^{-1}$  of BP carbonyl groups in the films with the same thickness (Table 8). BZ transformation to BP was accompanied by a partial decomposition of BP into esters absorbing in the region 1750-1700  $\text{cm}^{-1}$ .

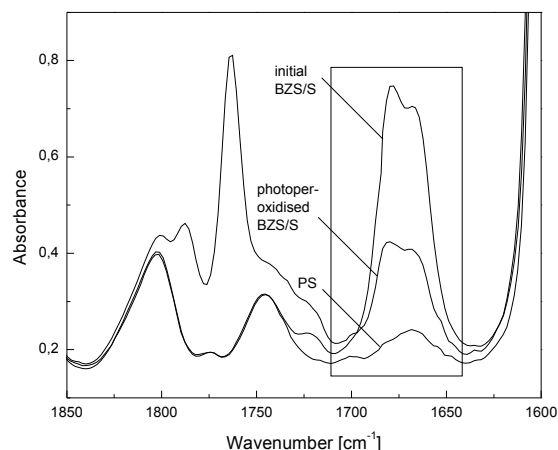


**Figure 18:** FTIR spectra used to calculate the conversion of BZ group. Band corresponding to BZ group is situated in the rectangle.

**Table 8:** BZ conversion and BP formation (absorbance of BP carbonyl groups at 1763  $\text{cm}^{-1}$ ) in BZS/S copolymers irradiated for 4 h. Theoretical crosslinking index  $\gamma$  recalculated with a regard to the yield of phototransformation of BZ.

Copolymer sample	BZ conversion	BP formation: Absorbance at 1763 $\text{cm}^{-1}$	Theoretical crosslinking index $\gamma$
PS	0 %	0	0
BZS/S 0.5%	65 %	0.09	1.0
BZS/S 1%	69 %	0.19	1.8
BZS/S 2%	67 %	0.34	5.3
BZS/S 4%	64 %	0.61	10.3
BZS/S 8%	53 %	0.88	9.5
BZS/S 13%	47 %	1.20	101
BZS/S 4% BTXNOR	46 %	0.46	7.8
BZS/S 4% StNO	64 %	0.64	12.5

BZ conversion is decreasing with increasing BZS content in a copolymer (all films had the same thickness and were irradiated for 4 h). It can be explained by internal screening effect. Therefore, BP formation is not increasing linearly with increasing BZS content in a copolymer. Slower BZ conversion of BZS/S 4% BTXNOR in comparison to other copolymers bearing 4 wt% of BZS is caused by a presence of benzothioxanthene chromophore that acts as a filter and absorbs a part of incident light.

Theoretical crosslinking index  $\gamma$  from chapter 6.3.4 was multiplied by BZ conversion to give lower value of  $\gamma$  with regard to the yield of phototransformation of BZ. The value of  $\gamma$  at the gel point is equal to 1. Thus, at 100 % efficiency of crosslinking, BZS/S 0.5% should reach the gel point and other copolymers should be crosslinked.

## 6.5 Characterisation of the final network of crosslinked BZS/S

As mentioned previously, the crosslinking results in a multiplication of crosslinks between the macromolecular chains induced the important modifications of material properties. The study of the crosslinking is often based on knowledge of the properties of final crosslinked material. Dynamic melt viscoelasticity is a powerful method to assess some specific parameters of a crosslinking process (gel time, crosslinking density). Classical methods based upon low frequency slopes variations, such as the Winter and Chambon method, was successfully applied. An alternative method based upon the high frequency slope variation of the Cole-Cole plot was used as well. The swelling measurement still remains the most widely used method to evaluate the crosslinking process even if it gives only average values and it is often difficult to perform. The equilibrium degree of swelling represents the ratio of swollen crosslinked polymer and dried crosslinked polymer. The measurement of the density is based on the progressive loss of the solubility of polymer during crosslinking. The thermoporometry uses a swelling solvent as a probe placed inside the polymeric swollen network in order to describe its texture.

### 6.5.1 Analysis of the global network

Peroxidised samples were placed in the rheometer at 170 °C and were crosslinked for 15 min. Immediately after the thermal treatment, rheological measurements were performed to analyse the global network using Winter-Chambon criterion based on low frequencies slopes, Cole-Cole plot based on high frequencies slopes and theoretical rheological model using the value of plateau  $G_e$ . Then, the samples were dipped into carbon tetrachloride. Soluble part of crosslinked sample was characterised by densitometry. Swollen insoluble part was characterised by swelling measurements and thermoporometry.

### 6.5.1.1 Rheological master curves

The most sensitive region of the rheological curve reflecting the molecular changes during a crosslinking process is the terminal zone. First,  $G'$  is always smaller than  $G''$ , as the initial polymer has more viscous behaviour and both moduli vanish at low frequencies  $\omega$  (terminal zone,  $G' \propto \omega^2$ ,  $G'' \propto \omega$ ). As crosslinking process proceeds,  $G'$  increases rapidly and becomes larger than  $G''$ , which is a characteristic feature of the crosslinked system that has a more elastic behaviour (Figure 19). Also,  $G_e$  increases more rapidly than  $G_N^0$  because the latter is being increased by crosslinks only whereas the former is increased by both crosslinks and the entrapment of entanglements.

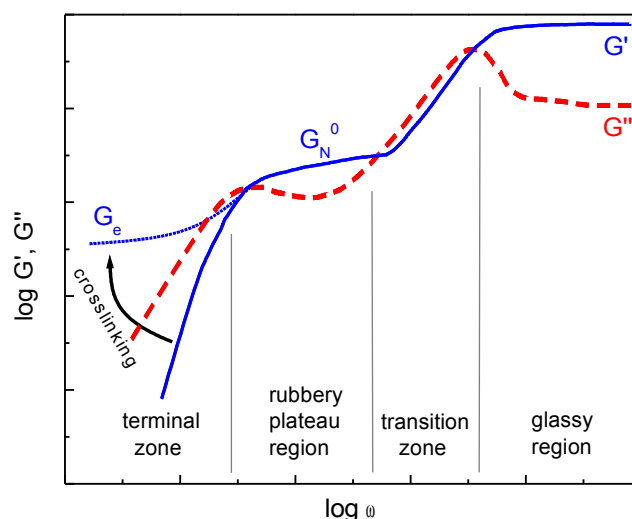


**Figure 19:** Logarithmic plot of the storage ( $G'$ ) and loss ( $G''$ ) moduli as a function of frequency pulsation  $\omega$  showing the changes in the terminal zone of a crosslinked polymer.

Figure 20-27 shows rheological master curves of thermally treated photoperoxidised copolymers ( $G'$  (■),  $G''$  (○)). Figures 20 and 21 show curves of uncrosslinked polymers, although the slopes of  $\log G'$  are decreased from the theoretical value of 2 to the value of 1.3 (BZS/S 0.5%) resp. 1.0 (BZS/S 1%). Figure 22 shows a sample (BZS/S 2%) that just exceeded the gel point ( $G'$ ,  $G''$  in terminal zone are almost parallel) but a plateau is observed at low values of  $\omega$ . Figures 23-27 display typical rheological behaviour of the crosslinked polymers. The points of intersection disappeared. The modulus of the fully crosslinked samples  $G'$  appears frequency independent (Figure 25).

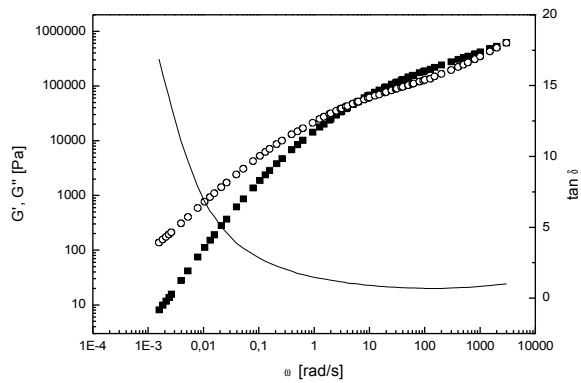


**Figure 20:** Storage ( $G'$ , ■) and loss ( $G''$ , ○) moduli as a function of frequency pulsation  $\omega$  for photoperoxidised and thermally treated BZS/S 0.5%. The reference temperature was 170 °C.

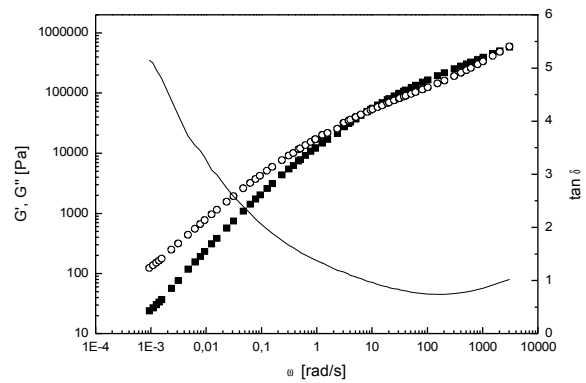


**Figure 21:** Storage ( $G'$ , ■) and loss ( $G''$ , ○) moduli as a function of frequency pulsation  $\omega$  for photoperoxidised and thermally treated BZS/S 1%. The reference temperature was 170 °C.

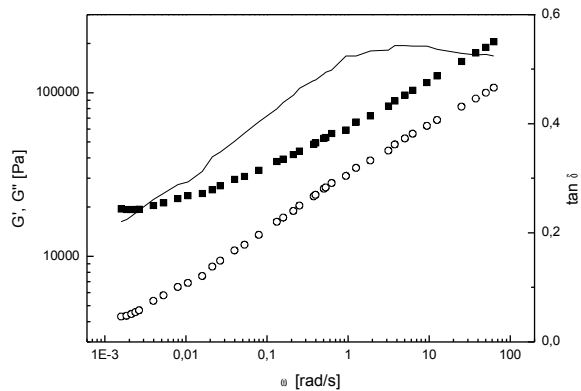


**Figure 22:** Storage ( $G'$ , ■) and loss ( $G''$ , ○) moduli as a function of frequency pulsation  $\omega$  for crosslinked BZS/S 2%. The reference temperature was 170 °C.

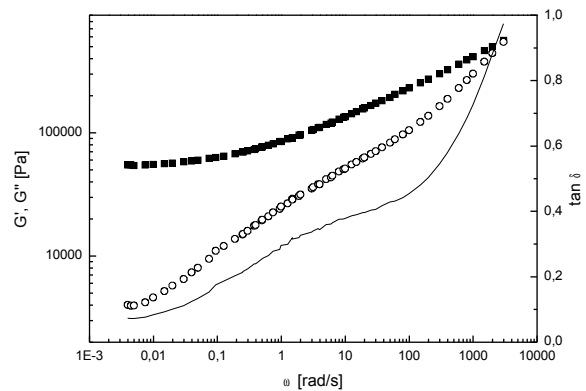


**Figure 23:** Storage ( $G'$ , ■) and loss ( $G''$ , ○) moduli as a function of frequency pulsation  $\omega$  for crosslinked BZS/S 4%. The reference temperature was 170 °C.

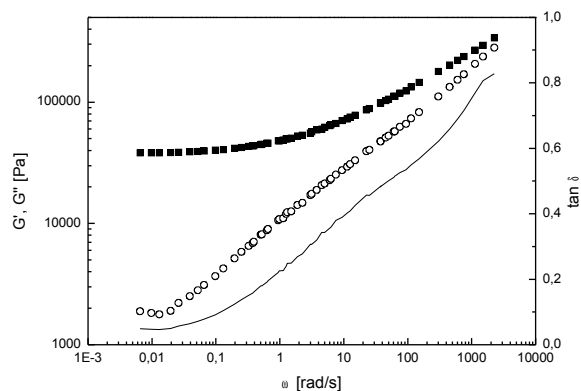


**Figure 24:** Storage ( $G'$ , ■) and loss ( $G''$ , ○) moduli as a function of frequency pulsation  $\omega$  for crosslinked BZS/S 8%. The reference temperature was 170 °C.

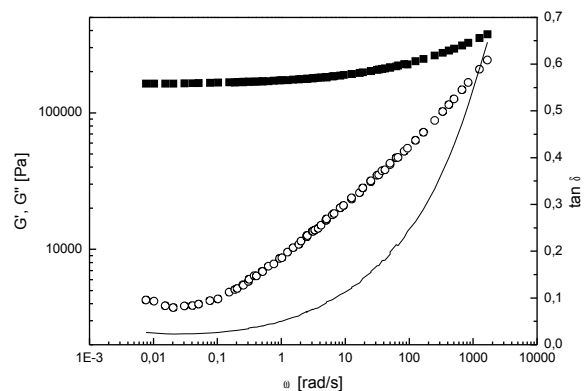


**Figure 25:** Storage ( $G'$ , ■) and loss ( $G''$ , ○) moduli as a function of frequency pulsation  $\omega$  for crosslinked BZS/S 13%. The reference temperature was 170 °C.

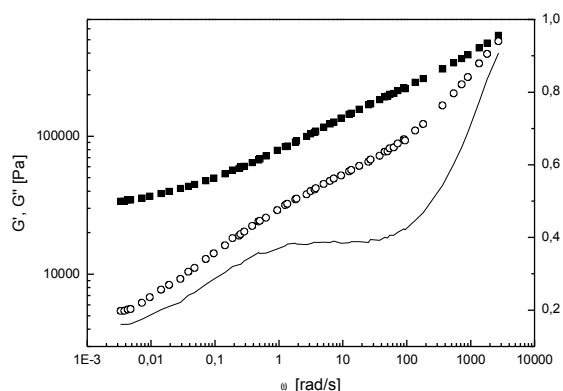


**Figure 26:** Storage ( $G'$ , ■) and loss ( $G''$ , ○) moduli as a function of frequency pulsation  $\omega$  for crosslinked BZS/S 4% BTXNOR. The reference temperature was 170 °C.

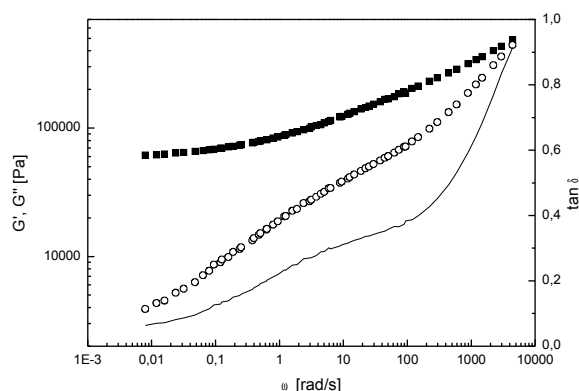


**Figure 27:** Storage ( $G'$ , ■) and loss ( $G''$ , ○) moduli as a function of frequency pulsation  $\omega$  for crosslinked BZS/S 4% StNO. The reference temperature was 170 °C.

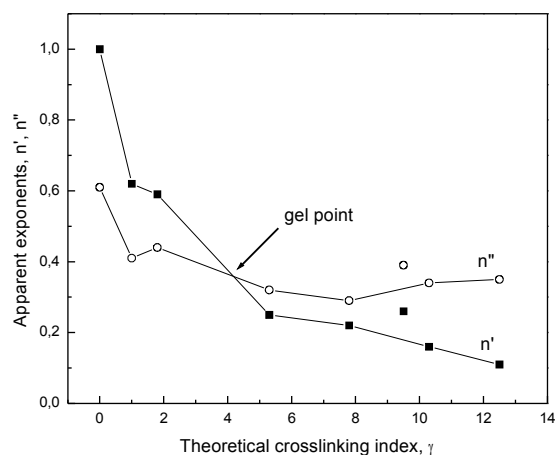
### 6.5.1.2 Winter-Chambon criterion

Primarily, Winter-Chambon criterion is proposed for determining of the gel point. For the initial polymer,  $G'$  is smaller than  $G''$  in the terminal zone and their apparent exponents are  $n' = 2$ ,  $n'' = 1$  ( $G' \propto \omega^{n'}$ ,  $G'' \propto \omega^{n''}$ ). During crosslinking process,  $G'$  increases rapidly. At the gel point,  $G'$  and  $G''$  exhibit a power law behaviour with a common exponent  $n$  ( $G' \propto G'' \propto \omega^n$ ). The loss tangent  $\tan \delta$  becomes independent on frequency pulsation  $\omega$ . On completion of the curing,  $G'$  is significantly larger than  $G''$ ,  $n'$  is lower than  $n''$ , characteristic of crosslinked systems.

Calculated apparent exponents  $n'$ ,  $n''$  are summarised in Table 9. Apparent exponent  $n'$  has the highest value for PS in which crosslinking process does not take place. With an increasing content of BZS in the initial copolymer,  $n'$  is rapidly decreasing till a value of  $n' = 0.25$  corresponding to BZS/S 2%, then it's decreasing slowly to a value of 0.06 (BZS/S 13%). Lower molecular weight of BZS/S 8% caused a shift of  $n'$ ,  $n''$  to higher values. A minimum BZS content for creating the gel under given experimental conditions can be found as an intersection of the both curves (Figure 28). The critical exponent  $n' = n'' = n$ , equals to 0.35 and under given conditions of crosslinking, the minimum essential content of crosslinker is 4 BP groups per chain (from  $M_w$ ). It is also seen that BZS/S 4% StNO bearing the same content of BZS as BZS/S 4%, has a lower  $n'$  because of higher  $M_w$ .

**Table 9:** Apparent exponents  $n'$  for storage and  $n''$  for loss moduli of the thermally treated photoperoxidised BZS/S.

Crosslinked copolymer sample	$n'$	$n''$	Interval [rad/s]
PS	1.00	0.61	0.1 – 3
BZS/S 0.5%	0.62	0.41	1 – 20
BZS/S 1%	0.59	0.44	1 – 40
BZS/S 2%	0.25	0.32	0.1 – 3
BZS/S 4%	0.16	0.34	0.1 – 4
BZS/S 8%	0.26	0.39	10 – 150
BZS/S 13%	0.06	0.30	0.1 – 10
BZS/S 4% BTXNOR	0.22	0.29	0.1 – 4
BZS/S 4% StNO	0.11	0.35	0.1 – 3

**Figure 28:** Calculated slopes at low frequencies ( $n'$ ,  $n''$ ) as a function of theoretical crosslinking index  $\gamma$ . Experimental points for BZS/S 13% are not shown. A minimum value of  $\gamma$  to reach the gel point is indicated by an arrow.

### 6.5.1.3 Cole-Cole representation

Another way for characterising of the crosslinked polymer is the Cole-Cole representation. While for uncrosslinked polymers Cole-Cole plot gives an arc of circle (chapter 6.3.3), for crosslinked polymer Cole-Cole plot gives a straight line, i.e. an arc of infinite circle and we are unable to extrapolate the curve to determine the zero shear viscosity  $\eta_0$  because the molecular weight of the crosslinked polymer becomes infinite. This method is preferable for polymers that reached the gel point. The use of Winter-Chambon criterion is suitable for a determining of the gel point but less accurate for dense networks.

**Table 10:** Zero shear viscosity  $\eta_0$  and distribution parameter  $h$  of initial and thermally treated photoperoxidised BZS/S that did not reach the gel point.

Copolymer sample	Initial copolymer		Thermally treated photoperoxidised copolymer	
	$\eta_0$ [Pa.s]	$h$	$\eta_0$ [Pa.s]	$h$
BZS/S 0.5%	21100	0.37	85000	0.46
BZS/S 1%	13400	0.37	128000	0.53

Complex viscosity components using the Cole-Cole representation of the initial copolymers gives an arc of circle (Figure 16). After the thermal treatment of photoperoxidised copolymers,  $\eta_0$

became much higher for BZS/S 0.5% and BZS/S 1% that did not reach the gel point (Table 10, Figure 29). From the power law:  $\eta_0 \propto M_w^{3.4}$ , one can determine that  $M_w$  of BZS/S 0.5% is increased by 50 % and  $M_w$  of BZS/S 1% is nearly doubled. The distribution parameter is increasing from 0.37 (for both copolymers) to 0.46 and 0.53 respectively. It means that the polydispersity is increasing too that is characteristic for crosslinking process.

**Table 11:** Slopes of Cole-Cole representation of the thermally treated photoperoxidised BZS/S.

Crosslinked copolymer sample	Slope
BZS/S 0.5%	1.1
BZS/S 1%	1.2
BZS/S 2%	2.2
BZS/S 4%	5.5
BZS/S 8%	9.4
BZS/S 13%	32
BZS/S 4% BTXNOR	3.2
BZS/S 4% StNO	7.5

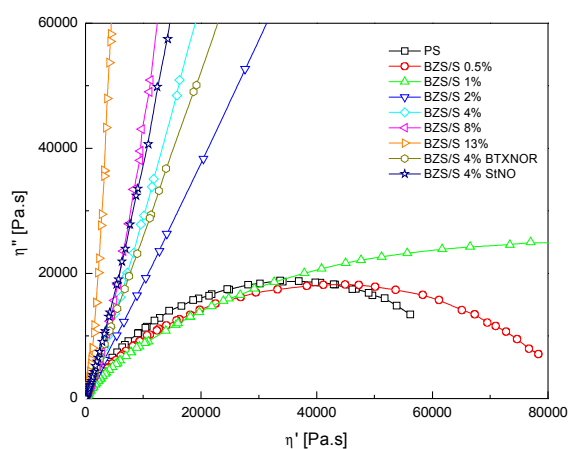


**Figure 29:** Cole-Cole plot of the thermally treated photoperoxidised copolymers BZS/S: Imaginary component of dynamic viscosity ( $\eta''$ ) as a function of the real component of dynamic viscosity ( $\eta'$ ).

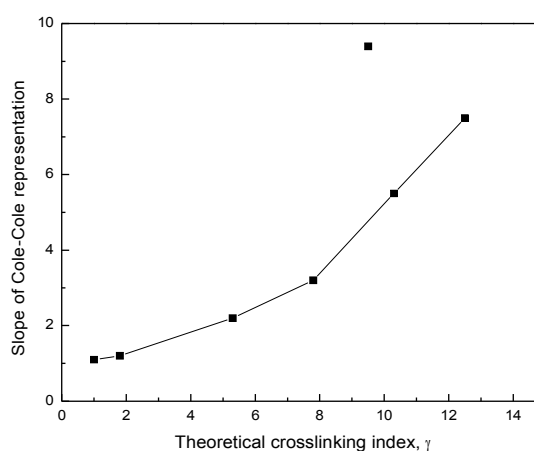


**Figure 30:** Slopes calculated from the Cole-Cole plot as a function of theoretical crosslinking index  $\gamma$ .

Other polymers are crosslinked and we can observe only a straight line (Figure 29). Determined slopes from the Cole-Cole plot are given in Table 11. The slopes of uncrosslinked polymers are calculated using the first several points of the high frequencies (low  $\eta'$ ,  $\eta''$ ). These slopes are plotted versus theoretical crosslinking index  $\gamma$  in the Figure 30. An increase of the crosslink density exhibits a strong increase of a slope calculated from the Cole-Cole plot. Contrary

to the result from the Winter-Chambon criterion, the network of BZS/S 8% seems to be denser than BZS/S 4%.

#### 6.5.1.4 Theoretical rheological model

The classical theory of rubberlike elasticity specifies for idealised network with fixed crosslinks that the equilibrium shear modulus in infinitesimal deformations is given by

$$G_e = g \nu RT$$

where  $g$  is a constant ( $g \approx 1$ ),  $R$  is the universal gas constant ( $8.314 \text{ JK}^{-1}\text{mol}^{-1}$ ),  $T$  is the thermodynamic temperature (443 K). In the idealised network,  $\nu$  is the density of strands that are terminated at both ends by chemical crosslinks. This simple relationship do not account for contributions from trapped entanglements which may be introduced during the crosslinking reaction.

**Table 12:** Value of plateau  $G_e$ , elastically effective strands density  $\nu$ , molecular weight between crosslinks  $M_c$  determined from rheology.

Crosslinked copolymer sample	$G_e$ [Pa]	$\nu$ [mol/ml]	$M_c$ [g/mol]
BZS/S 2%	19300	$5.24 \times 10^{-6}$	200000
BZS/S 4%	54400	$1.48 \times 10^{-5}$	71100
BZS/S 8%	38300	$1.04 \times 10^{-5}$	101000
BZS/S 13%	163500	$4.44 \times 10^{-5}$	23600
BZS/S 4% BTXNOR	33800	$0.92 \times 10^{-6}$	114000
BZS/S 4% StNO	61400	$1.67 \times 10^{-5}$	63000

From the statistical rubber elasticity theory, it is possible to determine the crosslink density from rheology using a theoretical model. A crosslinked polymer storage modulus reaches a plateau  $G_e$  lower than the rubbery plateau of uncrosslinked material  $G_N^0$ . The value of  $G_N^0$  for entangled polystyrene is 200000 Pa. The amount of chemical crosslinks per ml  $\nu_c$  can be calculated as follows:

$$\nu = 2\nu_c \left( I - \frac{\rho}{\nu_c M_n} \right) + \frac{G_N^0}{RT} \left( I - \frac{\rho}{\nu_c M_n} \right)^2$$

where  $\rho$  is a density of polystyrene (1.05 g/ml) and  $M_n$  is the number average molar mass before crosslinking determined by GPC (Table 5).

**Table 13:** Value of plateau  $G_e$ , crosslink density  $\nu_c$ , molecular weight between crosslinks  $M_c$  determined from rheology.

<i>Crosslinked copolymer sample</i>	$G_e$ [Pa]	$\nu_c$ [mol/ml]	$M_c$ [g/mol]	$\gamma$
BZS/S 2%	19300	$1.47 \times 10^{-5}$	35800	4.3
BZS/S 4%	54400	$1.83 \times 10^{-5}$	28800	5.4
BZS/S 8%	38300	$2.72 \times 10^{-5}$	19300	4.5
BZS/S 13%	163500	$1.42 \times 10^{-5}$	36900	18
BZS/S 4% BTXNOR	33800	$1.14 \times 10^{-5}$	46100	3.6
BZS/S 4% StNO	61400	$1.17 \times 10^{-5}$	45000	4.2

From Table 13 it is seen that the network crosslink density is increasing and  $M_c$  is decreasing with increasing quantity of BZS in copolymer from BZS/S 2% to BZS/S 8%. Surprisingly, last 3 copolymers seem to have lower crosslink density  $\nu_c$  than BZS/S 2% that should have the lowest  $\nu_c$ . This is caused by lower  $M_n$  of first 3 samples. Thus, the factor  $(1 - \rho/\nu_c M_n)$  becomes a lower number and subsequently  $\nu_c$  has to increase markedly. The factor  $(1 - \rho/\nu_c M_n)^2$  becomes almost negligible for copolymers with low  $M_n$  but important for copolymers with high  $M_n$ . This means that the contribution of trapped entanglements decreases the mobility of polymer chains that decreases the efficiency of crosslinker by preventing BP to crosslink.

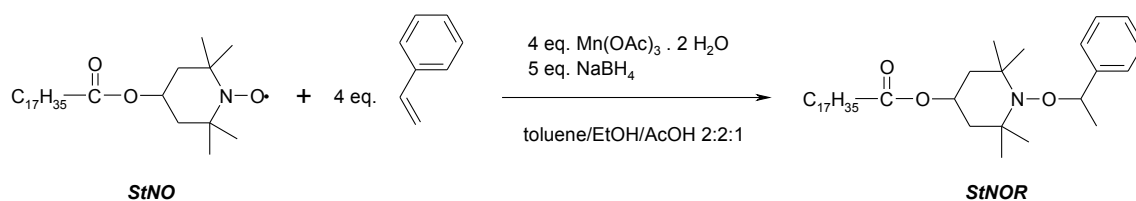
### 6.5.2 Analysis of the global network of additional series of NMP copolymers

Global network of a series of copolymers prepared by NMP was characterised by rheology to compare with previous results. They were prepared with two different contents of BZS (2 and 4 wt %), in the presence of three different mediators (StNOR, BTXNOR and HONOR) and with two concentrations of mediator ( $4.4 \times 10^{-3}$  and  $1.1 \times 10^{-2}$  mol/l). Use of a higher concentration of mediator led to lower molar masses.

#### 6.5.2.1 Synthesis of mediator StNOR

Synthesis of StNOR from StNO was accomplished by the addition of styrene in the presence of  $Mn(OAc)_3$  as a catalyst (Scheme 16). The most efficient conditions were obtained using a solvent mixture ethanol/toluene/acetic acid 2:2:1. Acetic acid increases the solubility of the  $Mn(OAc)_3$ , so

only a four-fold excess of  $\text{Mn}(\text{OAc})_3$  and styrene is needed.



**Scheme 16:** Synthesis of the mediator StNOR.

StNO (0.5 g, 1.14 mmol) was dissolved in a mixture of solvents toluene/EtOH/AcOH 2:2:1. Styrene (0.52 ml, 4.56 mmol, 4 eq.) and  $\text{Mn}(\text{OAc})_3$  (1.06 g, 4.56 mmol, 4 eq.) was added to create a red suspension. During 30 min,  $\text{NaBH}_4$  (0.22 g, 0.58 mmol, 5 eq.) was added in parts. Reaction mixture was stirred overnight and became colourless. White precipitate was filtered and solvents were evaporated on a vacuum rotatory evaporator. Dichloromethane was added and the rest of AcOH was neutralised with 10 % aqueous solution of  $\text{NaHCO}_3$ . Separated organic phase was washed with water, dried with  $\text{MgSO}_4$  overnight, filtered and concentrated. The product was isolated by column chromatography on silica gel with hexane - ethyl acetate 15:1 to yield 0.42 g (68 %) of a white powder with mp 42-49 °C.

$R_f = 0.78$  (silica, isohexane-ethyl acetate 15:1)

$^1\text{H NMR}$  ( $\text{CDCl}_3$ ):  $\delta$  (ppm) = 7.33-7.19 (m, 5H, Ph), 5.00 (m, 1H,  $\text{CH-O-CO}$ ), 4.76 (q,  $J = 6.7$  Hz, 1H,  $\text{CH-Ph}$ ), 2.24 (t,  $J = 7.7$  Hz, 2H,  $\text{CH}_2\text{-CO}$ ), 1.90-1.68 (m, 2H,  $\text{CH}_{\text{eq}}$ ), 1.67-1.44 (m, 2H,  $\text{CH}_{\text{ax}}$ ), 1.60 (s, 3H,  $\text{CH}_{3\text{eq}}$ ), 1.48 (d,  $J = 6.7$  Hz, 3H,  $\text{CH}_3\text{-CH-Ph}$ ), 1.33 (s, 3H,  $\text{CH}_{3\text{eq}}$ ), 1.34-1.20 (m, 30H,  $\text{CH}_3(\text{CH}_2)_{15}$ ), 1.12 (s, 3H,  $\text{CH}_{3\text{ax}}$ ), 0.88 (t,  $J = 6.7$  Hz, 3H,  $\text{CH}_3\text{-CH}_2$ ), 0.66 (s, 3H,  $\text{CH}_{3\text{ax}}$ ).

$^{13}\text{C NMR}$  ( $\text{CDCl}_3$ ):  $\delta$  (ppm) = 173.5 ( $\text{C=O}$ ), 145.4 ( $\text{C}_{\text{ipso}}$ ), 128.1 ( $2 \times \text{C}_{\text{meta}}$ ), 127.0 ( $\text{C}_{\text{para}}$ ), 126.6 ( $2 \times \text{C}_{\text{ortho}}$ ), 83.3 ( $\text{CH-Ph}$ ), 66.5 ( $\text{CH-O-CO}$ ), 60.2 ( $\text{C-N}$ ), 60.0 ( $\text{C-N}$ ), 44.6 ( $\text{CH}_2\text{-CH-O}$ ), 34.6 ( $\text{CH}_2\text{-CO-O}$ ), 34.4 ( $\text{CH}_{3\text{eq}}$ ), 34.1 ( $\text{CH}_{3\text{ax}}$ ), 31.9 ( $\text{CH}_3\text{-CH}_2\text{-CH}_2$ ), 29.7-29.1 ( $14 \times \text{CH}_2$ ), 25.0 ( $\text{CH}_{3\text{eq}}$ ), 23.3 ( $\text{CH}_3\text{-CH-Ph}$ ), 22.7 ( $\text{CH}_3\text{-CH}_2$ ), 21.1 ( $\text{CH}_{3\text{ax}}$ ), 14.1 ( $\text{CH}_3\text{-CH}_2$ ).

### 6.5.2.2 Synthesis and characterisation of NMP copolymers

A solution of BZS, styrene (5 ml) and appropriate mediator StNOR, BTXNOR or HONOR was deaerated with argon, sealed in an ampoule and polymerised for 12 h at 125 °C (Table 14). After cooling, polymerization mixtures were diluted with THF and precipitated into 10 $\times$  excess of methanol. Polymers prepared in this manner still contained the monomer BZS as it could be seen

from  $^1\text{H}$  NMR spectra. They were purified by Soxhlet extraction with ethanol.

**Table 14:** Polymerization data for a series of NMP copolymers BZS/S.

<i>Copolymer sample</i>	<i>Mediator</i>	<i>Mediator concentration [mol/l]</i>	<i>BZS in monomer mixture [wt%]</i>	<i>BZS in copolymer [wt%]</i>	<i>Conversion [%]</i>
VZ1	StNOR	$4.4 \times 10^{-3}$	2.16	2.0	74
VZ2	BTXNOR	$4.4 \times 10^{-3}$	2.16	2.0	76
VZ3	HONOR	$4.4 \times 10^{-3}$	2.16	2.0	73
VZ4	StNOR	$1.1 \times 10^{-2}$	2.16	2.0	72
VZ5	BTXNOR	$1.1 \times 10^{-2}$	2.16	2.0	74
VZ6	HONOR	$1.1 \times 10^{-2}$	2.16	2.0	71
VZ7	StNOR	$4.4 \times 10^{-3}$	4.23	4.0	77
VZ8	BTXNOR	$4.4 \times 10^{-3}$	4.23	4.0	75
VZ9	HONOR	$4.4 \times 10^{-3}$	4.23	4.0	74

The copolymers were characterised by GPC and by rheology using Cole-Cole representation. The Cole-Cole plot (Figure 31) displays a variety of arcs of circles. The smallest arcs signifying the lowest molecular weights belong to copolymers VZ4-VZ6.

The results of GPC and Cole-Cole parameters are given in Table 15. Zero shear viscosity  $\eta_0$  can be compared with  $M_w$  and distribution parameter  $h$  can be compared with the polydispersity index.

**Table 15:** GPC results for polymers VZ1-VZ9 using MALS + RI detector and the comparison with zero shear viscosity  $\eta_0$  and distribution parameter  $h$ .

<i>Polymer sample</i>	$\eta_0$ [Pa.s]	$h$	$M_w$ [g/mol]	$M_n$ [g/mol]	<i>PDI</i>
VZ1	67400	0.27	142000	105400	1.35
VZ2	97000	0.28	155800	113200	1.38
VZ3	75200	0.26	144700	116600	1.24
VZ4	6100	0.27	62800	53600	1.17
VZ5	14700	0.27	80900	71400	1.13
VZ6	6100	0.27	62800	59300	1.06
VZ7	48600	0.28	136200	101600	1.34
VZ8	121500	0.28	164000	128800	1.27
VZ9	61000	0.27	137400	101300	1.36

The “living” character of the polymers is proven by a low value of  $h$  (0.26 – 0.28) and low polydispersities (1.06 – 1.38), especially for VZ4-VZ6 (PDI = 1.06 – 1.17) prepared in the presence

of higher concentration of the mediator.

The lowest molar masses are those of VZ4-VZ6 because of higher concentration of the mediators. Other polymers VZ1-VZ3 and VZ7-VZ9 have very similar molar masses.

The fit of the plot of  $\log \eta_0$  versus  $\log M_w$  should give a straight line of a slope with a theoretical value 3.4. The correlation gave a good fit with a slope  $k = 2.96$  (Figure 32).

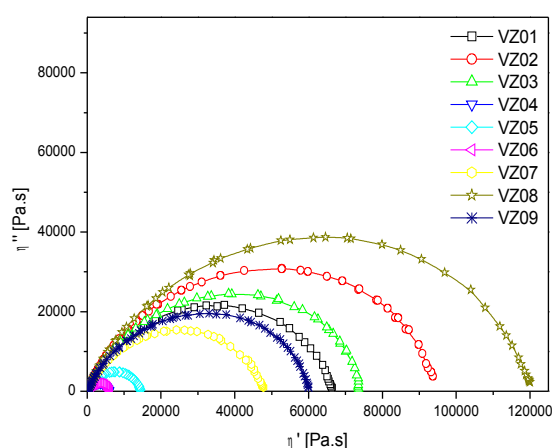


**Figure 31:** Cole-Cole plot of the initial copolymers BZS/S prepared by NMP: Imaginary component of dynamic viscosity ( $\eta''$ ) as a function of real component of dynamic viscosity ( $\eta'$ ). Sample VZ4 is overlapped by VZ6.

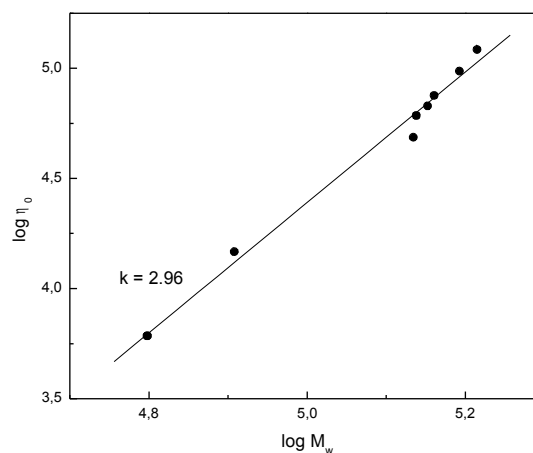


**Figure 32:** Logarithmic plot of the zero shear viscosity ( $\eta_0$ ) against the weight-average molar mass ( $M_w$ ) for initial polymers VZ1-VZ9.

Presence of a fluorescent benzothioxanthene chromophore in copolymers VZ2, VZ5, VZ8 permits to calculate the percentage of the chains containing this chromophore by UV/VIS or fluorescence spectroscopy. The extent of “livingness” calculated on the base of data obtained from fluorescence as well as UV/VIS absorption measurement was almost the same and the value 60 % was obtained for VZ2 and VZ8. It means that at given conversion, only 60 % of polymer chains are ended by fluorescence probe. Higher concentration of BTXNOR in the monomer feed (sample VZ5) caused a better control over polymerization process (lower polydispersity) and subsequently more chains contain benzothioxanthene chromophore (80 %).

### 6.5.2.3 Characterisation of molecular parameters of photoperoxidised samples

All samples were photoperoxidised by an irradiation in the SEPAP device for 4 h and BTXNO bearing copolymers for 6 or 9 h. It corresponds to about 60 % conversion of BZ (Table 16). BZ transformation to BP was accompanied by a partial decomposition of BP into esters absorbing in

the region 1750-1700  $\text{cm}^{-1}$ .

BZ conversion during irradiation was calculated from IR spectra from the peak areas of the initial and the photoperoxidised copolymer (peak area of PS was subtracted) in the 1710-1640  $\text{cm}^{-1}$  region (Figure 18). BP formation can be characterised by the absorbance at 1763  $\text{cm}^{-1}$  of BP carbonyl groups in the films with the same thickness (Table 16). Theoretical crosslinking index  $\gamma$ , an equivalent to the number of photo-converted BZ units per chain (from  $M_w$ ), was calculated as well.

**Table 16:** BZ conversion, BP formation (absorbance of BP carbonyl groups at 1763  $\text{cm}^{-1}$ ) in BZS/S copolymers irradiated during 4, 6 or 9 h and theoretical crosslinking index  $\gamma$ .

<i>Copolymer sample</i>	<i>Time of irradiation [h]</i>	<i>BZ conversion after irradiation</i>	<i>BP formation: Absorbance at 1763 <math>\text{cm}^{-1}</math></i>	<i>Theoretical crosslinking index <math>\gamma</math></i>
VZ1	4	63 %	0.30	4.6
VZ2	4	47 %	0.24	3.8
VZ3	6	61 %	0.29	4.9
VZ4	4	61 %	0.29	4.6
VZ5	4	60 %	0.29	1.9
VZ6	4	42 %	0.18	1.8
VZ7	9	67 %	0.27	2.8
VZ8	4	59 %	0.29	1.9
VZ9	4	61 %	0.58	8.6
	4	44 %	0.44	7.5
	6	57 %	0.54	9.7
	4	58 %	0.56	8.2

#### 6.5.2.4 Characterisation of final network by rheology

Final networks of VZ1-VZ9 were characterised by Winter-Chambon criterion and by Cole-Cole representation.

For the initial polymer,  $G'$  is smaller than  $G''$  in the terminal zone and their apparent exponents are  $n' = 2$ ,  $n'' = 1$  ( $G' \propto \omega^{n'}$ ,  $G'' \propto \omega^{n''}$ ). During crosslinking,  $G'$  increases rapidly. At the gel point,  $G'$  and  $G''$  exhibit a power law behaviour with a common exponent  $n$  ( $n = n' = n''$ ). For a crosslinked polymer,  $G'$  is higher than  $G''$ ,  $n'$  is lower than  $n''$ . Calculated apparent exponents  $n'$ ,  $n''$  and the interval where calculated are given in Table 17. Copolymers prepared in the presence of 2.5 $\times$  concentration of mediator (VZ4-VZ6) are uncrosslinked ( $n' > n''$ ). They also have about 2 times lower molecular weights. Other thermally treated photoperoxidised copolymers are

crosslinked. VZ1, VZ2 (irradiated for 6 h) and VZ3 are in the vicinity of the gel point ( $n' = n''$ ). 4 wt % BZS containing copolymers give clearly denser network.

While for uncrosslinked polymers Cole-Cole plot gives an arc of circle (Figure 31), for crosslinked polymer Cole-Cole plot gives a straight line, i.e. an arc of infinite circle. After the thermal treatment of photoperoxidised copolymers containing 2 wt% of BZS prepared in the presence of higher concentration of mediator,  $\eta_0$  became much higher for VZ4, VZ5, VZ6 that did not reach the gel point. From the power law:  $\eta_0 \propto M_w^{3.4}$ , it was determined that  $M_w$  of VZ5 is increased by 50 % and  $M_w$  of VZ4, VZ6 is about tripled. The distribution parameter is increasing from 0.27 to 0.47 (VZ5) or to 0.61 (VZ4, VZ6). It means that the polydispersity is increasing too. Other polymers are crosslinked and we can observe only a straight line. Determined slopes from the Cole-Cole plot are given in Table 17. The slopes of uncrosslinked polymers are calculated using the first several points of the high frequencies (low  $\eta'$ ,  $\eta''$ ).

**Table 17:** Apparent exponents  $n'$  for storage and  $n''$  for loss moduli and slope of Cole-Cole representation of the thermally treated photoperoxidised BZS/S.

<i>Crosslinked copolymer sample</i>	<i>Time of irradiation [h]</i>	<i>Interval of <math>\omega</math> [rad/s]</i>	$n'$	$n''$	<i>Slope of Cole-Cole representation</i>
VZ1	4	0.1 – 3	0.31	0.31	2.1
VZ2	4	0.1 – 2	0.40	0.30	1.5
	6	0.1 – 2	0.32	0.32	1.7
VZ3	4	0.1 – 3	0.32	0.32	2.0
VZ4	4	2 – 80	0.59	0.42	0.60
VZ5	4	1 – 25	0.74	0.45	–
	9	1 – 25	0.49	0.37	1.0
VZ6	4	2 – 80	0.59	0.41	0.55
VZ7	4	0.1 – 4	0.20	0.34	3.6
VZ8	4	0.1 – 1.5	0.26	0.30	2.6
	6	0.1 – 1.5	0.16	0.33	4.6
VZ9	4	0.1 – 4	0.21	0.31	3.4

The results from the new series of NMP copolymers (chapter 6.5.2.2) are compared with a series of copolymers prepared by conventional free radical polymerization in solution and two NMP copolymers prepared in bulk (chapter 6.2). Apparent exponents  $n'$ ,  $n''$  as a function of theoretical crosslinking index  $\gamma$  are plotted in Figure 33. Additional experimental points improved the determination of the gel point. It can be reached for copolymers crosslinked under given conditions with a theoretical crosslinking index  $\gamma = 4.8$ . Slopes of Cole-Cole representation as a function of theoretical crosslinking index  $\gamma$  are plotted in Figure 34. It can be well seen that NMP copolymers

VZ1-VZ9 are consistent with previous data.

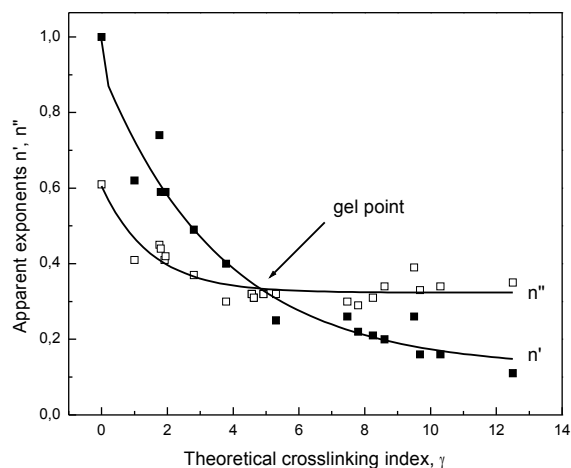


**Figure 33:** Apparent exponents ( $n'$  - ■,  $n''$  - □) as a function of theoretical crosslinking index  $\gamma$  for copolymers prepared by conventional free radical polymerization and by NMP.

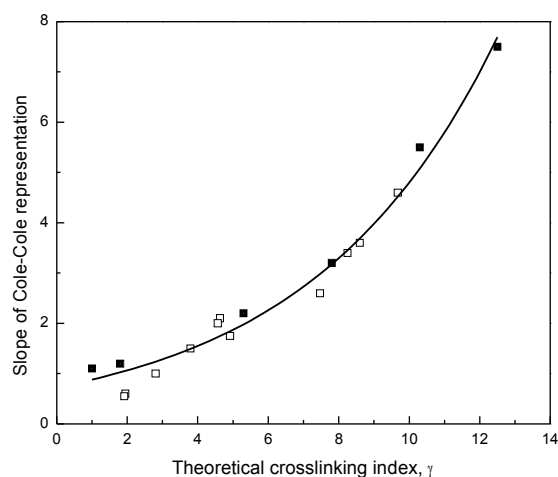


**Figure 34:** Slope of Cole-Cole representation as a function of theoretical crosslinking index  $\gamma$ . First series of copolymers prepared by conventional free radical polymerization and two copolymers by NMP (■). New series of NMP copolymers (□).

### 6.5.3 Analysis of the soluble part

#### 6.5.3.1 Densitometry

The solubility of a polymer depends on the length on its chains. A polymer dissolves when the segments of the chains are maintained distant from each other in the presence of solvent because the interactions polymer-solvent can break the weak van der Waals bonds but not the covalent bonds. However, the crosslinks that are created between the chains are covalent. Consequently, more the polymer is crosslinked, less the solvent is able to disperse the chains and the polymer swells only. The densitometry allows to follow the evolution of polymer insolubility. Instead of weighting the insoluble part, this technique determines the density of extracted solution. Its density must tend towards the density of the pure solvent used for extraction. The experimental device, described in the chapter 3.2.9, is a vibrating tube density meter that allows to find the resonance frequency of a tubes filled with the solution. This resonance frequency depends on the solution density:

$$\rho = A.T^2 + B$$

where with  $\rho$  is a density,  $T$  is a period and  $A$  and  $B$  are the constants determined by calibration. The

difference between the density of extract solution of cured polymer and the density of pure  $\text{CCl}_4$  is proportional to the soluble part of cured polymer. The results are given in Table 18 and plotted against theoretical crosslinking index in Figure 35.

**Table 18:** Thermally treated photoperoxidised BZS/S (100 mg) density of the  $\text{CCl}_4$  extracts (10 ml).

Crosslinked copolymer sample	Density [g/ml]
pure $\text{CCl}_4$	1.59405
PS	1.59007
BZS/S 0.5%	1.59008
BZS/S 1%	1.59013
BZS/S 2%	1.59249
BZS/S 4%	1.59334
BZS/S 8%	1.59289
BZS/S 13%	1.59371
BZS/S 4% BTXNOR	1.59336
BZS/S 4% StNO	1.59368

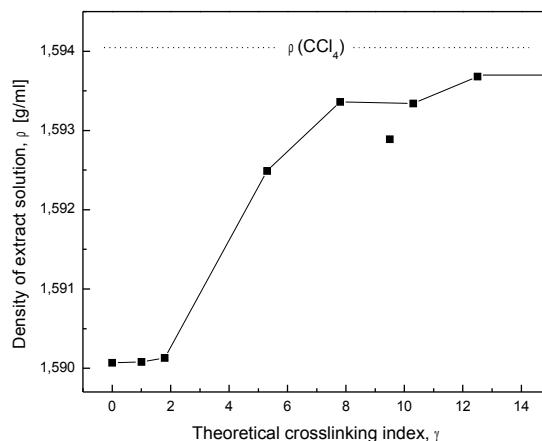


**Figure 35:** Density of  $\text{CCl}_4$  extract solutions (10 ml) of crosslinked polymer (100 mg) as a function of theoretical crosslinking index  $\gamma$ .

Solution of PS, that is 100 % soluble, has the lowest density. Density of extract solution of photoperoxidised and thermally treated BZS/S 0.5% and BZS/S 1% is very slightly higher than PS solution. Their molar masses are increased but no network is created. The amount of BZS in copolymer is not sufficient to reach the gel point. Crosslinked BZS/S 2% is 69 % insoluble and its  $\text{CCl}_4$  extract solution density is clearly higher. One can conclude that it is possible to reach the gel point for copolymers treated in this manner having theoretical crosslinking index  $\gamma = 2$  to 6. To determine the gel point exactly from densitometry, it is necessary to have more experimental points to find the onset of increasing  $\rho$ . Density is increasing rapidly to about  $\gamma = 10$ , then a plateau is reached; its value depends on PDI. BZS/S 8% is somewhat out of the curve because of lower molar masses.

### 6.5.3.2 Sol fraction

Knowing the distribution of initial polymer and sol fraction after crosslinking, we can calculate the crosslink density  $\nu_c$  using following equation<sup>80</sup>

$$M_c = \frac{\rho}{2\nu_c} = \frac{\epsilon S^\epsilon (I-S)}{I-S^\epsilon} M_w$$

where  $S$  is the sol fraction and  $\varepsilon$  is a dispersion parameter (defined as  $I - M_n/M_w$ ). All results are given in Table 19.

Dependence of gel fraction on crosslinking index is increasing steeply to a value about 0.7 for the most probable primary distribution ( $\varepsilon = 2$ ). Then, the increase is slow and reaches a plateau. Low polydispersity of crosslinkable copolymer leads to a lower sol fraction. Crosslinked BZS/S 4% StNO is 92 % insoluble. BZS/S 4% BTXNOR ( $PDI = 1.34$ ) has the same gel fraction as BZS/S 13% ( $PDI = 2.8$ ) although the BP content is  $2.6\times$  lower in BZS/S 4% BTXNOR than in BZS/S 13%.

Gel fraction is also depended on primary molecular weight. Crosslinked BZS/S 8% ( $M_w = 86200$  g/mol) contains larger amount of soluble part than BZS/S 4% ( $M_w = 156800$  g/mol).

For highly crosslinked samples, this method is inconvenient as it gives erroneous results. The result for BZS/S 13% is inaccurate because the plateau is reached. At the plateau region, small change in gel fraction percentage causes a big change in  $\gamma$ . Other results are on the limit of the method.

**Table 19:** Crosslink density  $\nu_c$  for a series of crosslinked copolymers BZS/S calculated from sol fraction.

Crosslinked copolymer sample	Gel fraction	Sol fraction	$\varepsilon$	$M_c$ [g/mol]	$\nu_c$ [mol/ml]	$\gamma$
BZS/S 2%	0.69	0.31	0.457	68600	$7.65\times 10^{-6}$	2.2
BZS/S 4%	0.85	0.15	0.487	42700	$1.23\times 10^{-5}$	3.7
BZS/S 8%	0.73	0.27	0.444	35400	$1.48\times 10^{-5}$	2.4
BZS/S 13%	0.86	0.14	0.643	141000	$3.71\times 10^{-6}$	4.6
BZS/S 4% BTXNOR	0.86	0.14	0.254	55500	$9.46\times 10^{-6}$	3.0
BZS/S 4% StNO	0.92	0.08	0.237	50500	$1.04\times 10^{-5}$	3.8

## 6.5.4 Analysis of the insoluble part

### 6.5.4.1 Swelling

Swelling measurement is a classic method for the characterisation of a crosslinked polymer. Equilibrium degree of swelling  $DS_E$  is defined as a ratio of volume of swollen gel and volume of dried gel. Typically,  $DS_E$  is calculated by weighting the swollen gel  $M_\infty$  and dried gel  $M_0$  knowing the density of polymer  $\rho_p$  and solvent  $\rho_s$ :

$$DS_E = \frac{V_\infty}{V_0} = I + \frac{\rho_p}{\rho_s} \left( \frac{M_\infty}{M_0} - I \right)$$

As the density of BZS/S copolymer was not determined, we have used the density of polystyrene ( $\rho_{PS} = 1.05$  g/ml). The density of  $CCl_4$  is 1.594 g/ml. Molecular weight between crosslinks  $M_c$  can be calculated as<sup>45</sup>

$$M_c = \frac{-V_m \rho_p \left( DS_E^{-1/3} - \frac{DS_E^{-1}}{2} \right)}{\ln(1 - DS_E^{-1}) + DS_E^{-1} + \chi DS_E^{-2}}$$

where  $V_m$  is molar volume of  $CCl_4$  (96.5 ml/mol) and  $\chi$  is an interaction parameter of PS/ $CCl_4$ . We can also express crosslink density  $\nu_c$  as  $\rho/2M_c$ . An interaction parameter  $\chi$  can be calculated as follows

$$\chi = \beta + \frac{V_m}{RT} (\delta_s - \delta_p)^2$$

where  $\beta$  is a lattice constant whose value is about 0.34,  $\delta_s$  and  $\delta_p$  represents the solubility parameter<sup>108</sup> of  $CCl_4$  (17.6 (MPa)<sup>1/2</sup>) and PS (18.6 (MPa)<sup>1/2</sup>).

A hypothetical perfect network may be defined as one having no free chain ends; that is, the primary molecular weight  $M$  for a perfect network would be infinite. Any real network must contain terminal chains bound at one end to a crosslinkage and terminated at the other by the end (free end) of a primary molecule. The factor  $(1 - 2M_c/M_n)$  expresses the correction for network imperfections resulting from chain ends<sup>45</sup>. For a perfect network ( $M = \infty$ ) it reduces to unity:

$$-\ln(1 - DS_E^{-1}) + DS_E^{-1} + \chi DS_E^{-2} = \frac{V_m \rho_p}{M_c} \left( 1 - \frac{2M_c}{M_n} \right) \left( DS_E^{-1/3} - \frac{DS_E^{-1}}{2} \right)$$

After separating of  $M_c$  we obtain the equation:

$$M_c = \left[ \frac{2}{M_n} \frac{\ln(1 - DS_E^{-1}) + DS_E^{-1} + \chi DS_E^{-2}}{V_m \rho_p \left( DS_E^{-1/3} - \frac{DS_E^{-1}}{2} \right)} \right]^{-1}$$

Swelling measurement results are given in Tables 20 and 21.  $DS_E$  in a good solvent decreases with increasing degree of crosslinking. It also decreases with increase in the primary molecular weight. A big difference can be seen between swelling measurement results made without and with a correction by the factor  $(1 - 2M_c/M_n)$  used for correction on imperfections caused by chain ends. The difference is important for low  $M_n$  mainly because for high  $M_n$  values, the factor  $(1 - 2M_c/M_n)$  tends to 1.

The results from classical swelling calculation (Table 20) shows that determined network density is depended on theoretical  $\gamma$ . This equation does not take into account primary molecular

weight. This method does not distinguish chemical and physical crosslinks. Including of correction factor  $(1 - 2M_c/M_n)$ , physical imperfections are partially suppressed. From Table 21 it can be concluded that network density and gel fraction of crosslinked polymer are increasing with BP content in the photoperoxidated copolymer. The correction on chain ends is then inevitable.

**Table 20:** Characterisation of the network of crosslinked BZS/S copolymers by swelling.

Crosslinked copolymer sample	$M_\infty$ [g]	$M_0$ [g]	$DS_E$	$M_c$ [g/mol]	$\nu_c$ [mol/ml]	$\gamma$
BZS/S 2%	2.11	0.069	20.5	105000	$0.50 \times 10^{-5}$	1.5
BZS/S 4%	1.69	0.085	13.5	48000	$1.10 \times 10^{-5}$	3.3
BZS/S 8%	1.73	0.073	15.9	66000	$0.80 \times 10^{-5}$	1.3
BZS/S 13%	0.65	0.086	5.3	6900	$7.60 \times 10^{-5}$	94
BZS/S 4% BTXNOR	2.02	0.086	15.8	65000	$0.81 \times 10^{-5}$	2.5
BZS/S 4% StNO	1.51	0.092	11.1	33000	$1.59 \times 10^{-5}$	5.8

**Table 21:** Characterisation of the network of crosslinked BZS/S copolymers by swelling regarding to network imperfections resulting from chain ends.

Crosslinked copolymer sample	$M_n$ [g/mol]	$DS_E$	$M_c$ [g/mol]	$\nu_c$ [mol/ml]	$\gamma$
BZS/S 2%	83500	20.5	29900	$1.76 \times 10^{-5}$	5.1
BZS/S 4%	80400	13.5	21800	$2.40 \times 10^{-5}$	7.2
BZS/S 8%	47800	15.9	17500	$2.99 \times 10^{-5}$	4.9
BZS/S 13%	230000	5.3	6500	$8.06 \times 10^{-5}$	100
BZS/S 4% BTXNOR	123100	15.8	31600	$1.66 \times 10^{-5}$	5.2
BZS/S 4% StNO	145000	11.1	22700	$2.31 \times 10^{-5}$	8.4

#### 6.5.4.2 Thermoporometry

Alternative method to the swelling measurement is a thermoporometry (described in chapter 5). Mesh size distribution of the final networks of the series of BZS/S copolymers swollen in  $\text{CCl}_4$  are shown in Figure 36. Average mesh sizes  $\zeta$  were calculated and are shown in Table 22. Mesh size  $\zeta$  of swollen crosslinked BZS/S 2% is on the limit of the method. This sample is just slightly crosslinked and its  $\zeta$  is quite large. In the thermogram, its peak of confined  $\text{CCl}_4$  can be partially overlapped by free  $\text{CCl}_4$  that was partially molten (temperature program described in chapter 3.2.7). No peak for a swollen network of BZS/S 13% was seen in the thermogram. Probably, this case is beyond the limits of the method. It can be explained by a very small apparent energy of thermal transition  $W_a$  in a very divided medium such as the network of BZS/S 13%.  $W_a$  is

exponentially dependent on a temperature:  $W_a = W_0 e^{0.04\Delta T}$ , where  $W_0$  is the energy of thermal transition of free solvent.

**Table 22:** Average mesh sizes  $\xi$  of the swollen polymer networks of crosslinked BZS/S samples.

Crosslinked copolymer sample	$\xi$ [nm]
BZS/S 2%	98
BZS/S 4%	34
BZS/S 8%	49
BZS/S 4% BTXNOR	51
BZS/S 4% StNO	24

Thermoporometry results are in agreement with the results obtained from swelling measurement. The densest network is that of BZS/S 4% StNO, followed by BZS/S 4%, then BZS/S 8% and BZS/S 4% BTXNOR are nearly equally dense and BZS/S 2% has the weakest network. Behaviour of BZS/S 8% can be explained by its lower molecular weight and BZS/S 4% BTXNOR by a lower content of BP after photoperoxidation step.

Average mesh size  $\xi$  is well correlating with  $DS_E$  (Figure 37). According to Canal and Peppas<sup>109</sup>,  $\xi \propto DS_E^{-1/2}$  (for  $10 < DS_E < 100$ ) and  $\xi \propto DS_E$  (for  $DS_E < 10$ ). In our case for the limited number of experimental points, the best correlation is for  $\xi$  vs.  $DS_E$  ( $R^2 = 0.956$ ).

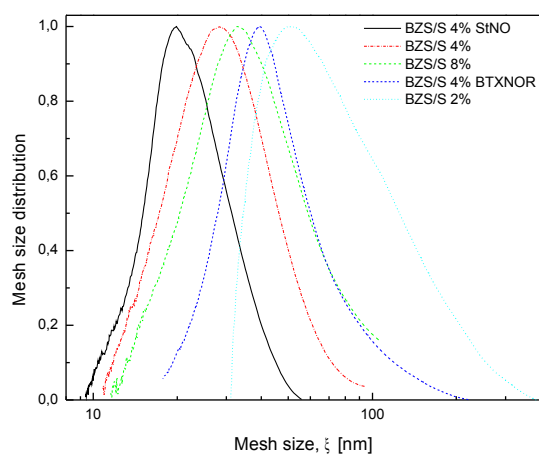


**Figure 36:** Mesh size distributions of the final networks of crosslinked BZS/S samples swollen in tetrachloromethane.

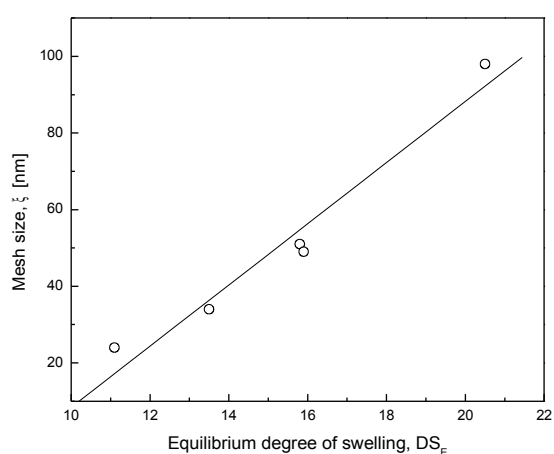


**Figure 37:** Correlation between the average mesh size  $\xi$  of the  $CCl_4$  swollen final network and the equilibrium degree of swelling  $DS_E$ .

## 6.6 Discussion

Plotting of final network properties as a function of BZS content (wt%) in copolymer is not correct because of variation of some parameters (molar mass, polydispersity, BZ photoconversion). This can be avoided by expressing of an average number of BP groups per polymer chain in photoperoxidised polymer from  $M_w$  that corresponds to the theoretical crosslinking index  $\gamma$ .

Figure 38 shows a collection of results from the rheology (Winter-Chambon criterion, Cole-Cole plot), densitometry, swelling and thermoporometry. First three techniques can be used in the pregel region ( $0 < \gamma < 4.8$ ). Winter-Chambon criterion, using slopes of low frequencies, is suitable for determining of the gel point (theoretical  $\gamma = 4.8$ ) and for characterising of the weak network. Denser network can be characterised by Cole-Cole representation. This method is very suitable to follow the evolution of molecular weight in the pregel regime. Another method applicable in the pregel region is a densitometry but the extract solution density in this region is not depended on  $\gamma$ . Then, a pronounced fall caused by the ability of reaching the gel point is observed. Hence, the onset of the fall can be used as an assessment of the gel formation. Contrary to the weighting of the sol or gel fraction, this method is experimentally more simple and is more precise. Also, it allows to characterise highly crosslinked materials moderately well.

Other methods are only applicable for the characterisation of the gel. Sol fraction determined by gravimetry can be used to calculate the crosslink density. This method is limited to the weak networks. In dense networks, a big change in crosslink density is accompanied by a small change in gel fraction and therefore the results are inaccurate. Melt rheology is a powerful tool. Besides evolution of  $M_w$  in pregel regime, determination of the gel point and characterisation of relative network density, the value of equilibrium shear modulus  $G_e$  allows to calculate the concentration of elastically effective network strands  $\nu$  and crosslink density  $\nu_c$  ( $\nu \neq 2\nu_c$ ). Swelling is a principal method for the study of network and should not be omitted. This technique is a simple and low-cost approach to measure of the swell ratio  $DS_E$  but it is difficult to obtain exact values when volatile solvents are used, since the solvent evaporates as the sample is being weighted. Additionally, it is difficult to determine when steady state is achieved. Thermoporometry is an alternative method to the swelling measurement and both methods are well correlating. In a very divided medium such as the network of BZS/S 13%, the apparent energy of thermal transition is too small and therefore it is not detectable in the thermogram.

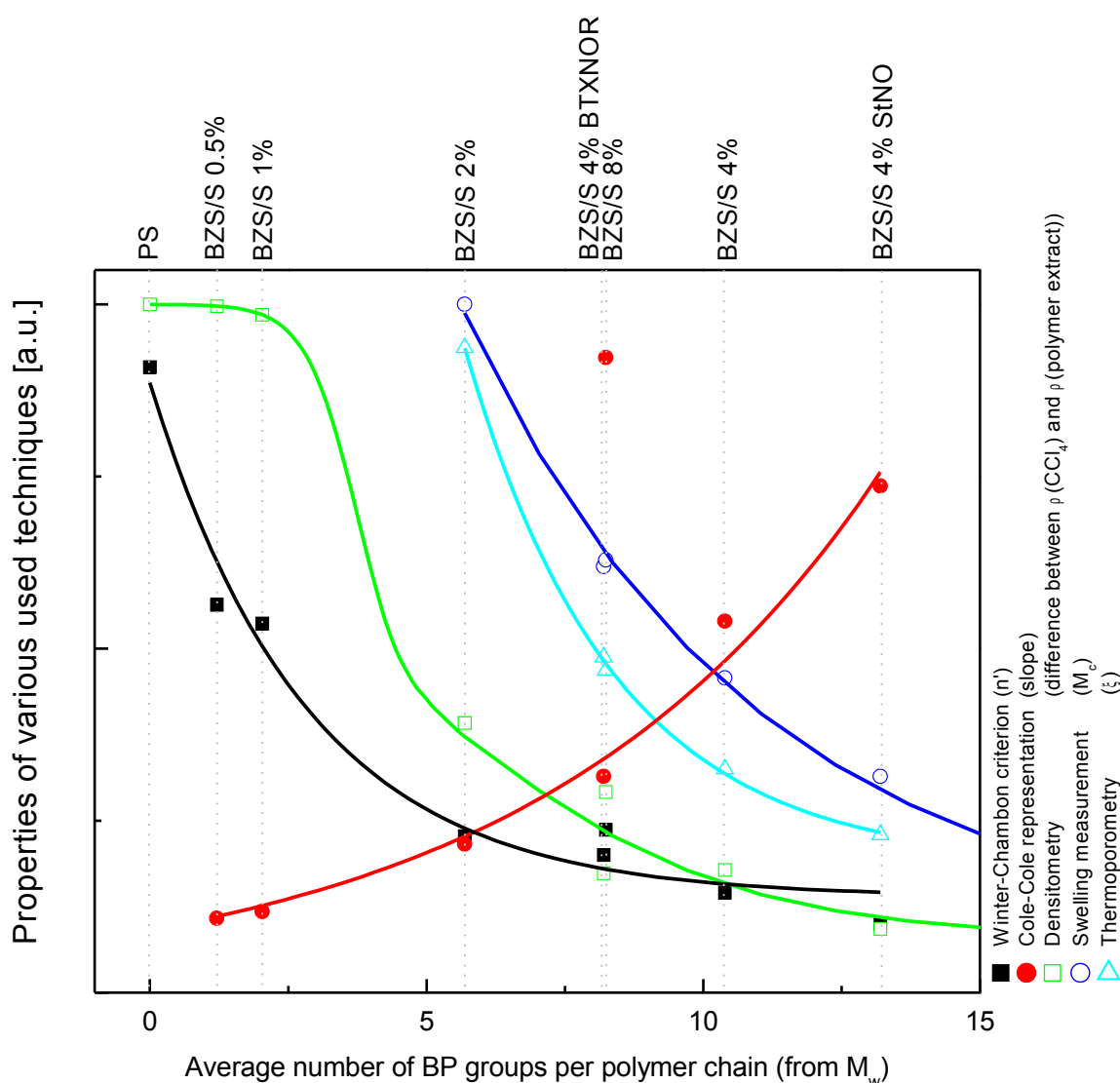


**Figure 38:** Correlations between Winter-Chambon criterion, Cole-Cole representation, densitometry, swelling measurement, thermoporometry as a function of an average number of BP groups per polymer chain of photoperoxidised polymer.

To obtain the efficiency of crosslinking, the crosslink densities  $\nu_c$  determined by various methods were compared with theoretical values  $\nu_c$  (Table 23). Theoretical  $\nu_c$  represents a molar concentration of BZ groups in copolymer multiplied by BZ conversion during photoperoxidation step (because only converted BZ to BP can take part in crosslinking) and divided by a factor of 2. This is due to 50 % probability that benzoyloxy macroradical will cause crosslinking because of the competition with low molecular benzoyloxy radical formed from BP (Scheme 10 and 11).

The classical theory of rubberlike elasticity specifies that equilibrium shear modulus  $G_e$  in infinitesimal deformations is given by  $G_e = \nu RT$ . That is a model of idealised network with fixed

crosslinks. Determined concentration of network strands is a function of theoretical crosslinking index  $\gamma$ . Therefore, it depends on primary molecular weight and concentration of crosslinker as well. This method does not distinguish chemical and physical crosslinks. Very similar results are obtained from swelling measurements. Swelling is also influenced by the entanglements because both chemical and physical crosslinks decreases the ability of solvent to swell the network.

Swelling measurements results were calculated without the impact of molar mass. As a consequence, the results are scattered. After the correction on imperfections resulting from chain ends, the results are in logical order. Increasing theoretical  $v_c$  leads to the higher network density. This correction suppresses only chain ends imperfections but the influence of the entanglements is still present in the results.

A rheological model that uses a criterion for entanglement trapping assuming that all four strands radiating from entanglement locus are terminated by chemical crosslinks, allow us to calculate the concentration of chemical crosslinks only. One can conclude that the efficiency of crosslinker is decreasing with increasing concentration of crosslinker. The same can be said for the swelling with correction. Almost equal  $M_n$  and  $M_w$  of BZS/S 2% and BZS/S 4% allow us to conclude that the efficiency of crosslinker (BP) is decreasing with increasing concentration. Initial BZS/S 4% has double concentration of BZ, resp. BP as BZS/S 2% but  $v_c$  in the network is increased by only 36 %, not 100 %. The same trend is observed for the results from calculations using sol fraction despite of differentness of results from both methods. Sol fraction is not affected by the concentration of entanglements. During crosslinking, the chain mobility is decreasing and prevents BP to crosslink. Also, larger oxygen concentration is necessary for the crosslinking at higher BP concentrations (Scheme 10). Therefore, decrease of efficiency of crosslinking with increasing BP structures concentration may be caused by insufficient concentration of oxygen.

**Table 23:** Comparison of theoretical values of crosslink densities  $\nu_c$  with crosslink densities  $\nu_c$  determined by various techniques and elastically effective strands  $\nu$  determined by rheology.

Crosslinked copolymer sample	Theoretical crosslink density $\nu_c$ [mol/ml]	Rheology for idealised network	Rheology with criterion for entanglement trapping		Sol fraction		Swelling		Swelling with correction on imperfection resulting from chain ends	
		$\nu$ [mol/ml]	$\nu_c$ [mol/ml]	Efficiency [%]	$\nu_c$ [mol/ml]	Efficiency [%]	$\nu_c$ [mol/ml]	Efficiency [%]	$\nu_c$ [mol/ml]	Efficiency [%]
BZS/S 2%	$1.82 \times 10^{-5}$	$0.52 \times 10^{-5}$	$1.47 \times 10^{-5}$	81	$0.77 \times 10^{-5}$	42	$0.50 \times 10^{-5}$	27	$1.76 \times 10^{-5}$	97
BZS/S 4% BTXNOR	$2.50 \times 10^{-5}$	$0.92 \times 10^{-5}$	$1.14 \times 10^{-5}$	46	$0.95 \times 10^{-5}$	38	$0.81 \times 10^{-5}$	32	$1.66 \times 10^{-5}$	66
BZS/S 4%	$3.48 \times 10^{-5}$	$1.48 \times 10^{-5}$	$1.83 \times 10^{-5}$	53	$1.23 \times 10^{-5}$	35	$1.10 \times 10^{-5}$	32	$2.40 \times 10^{-5}$	69
BZS/S 4% SNO	$3.48 \times 10^{-5}$	$1.67 \times 10^{-5}$	$1.17 \times 10^{-5}$	34	$1.04 \times 10^{-5}$	30	$1.59 \times 10^{-5}$	46	$2.31 \times 10^{-5}$	66
BZS/S 8%	$5.76 \times 10^{-5}$	$1.04 \times 10^{-5}$	$2.72 \times 10^{-5}$	47	$1.48 \times 10^{-5}$	26	$0.80 \times 10^{-5}$	14	$2.99 \times 10^{-5}$	52
BZS/S 13%	$8.17 \times 10^{-5}$	$4.44 \times 10^{-5}$	$1.42 \times 10^{-5}$	17	$0.37 \times 10^{-5}$	5	$7.60 \times 10^{-5}$	93	$8.06 \times 10^{-5}$	99

## 6.7 Conclusion

A series of crosslinkable styrene copolymers with different content of BZS monomer units was prepared by conventional free radical polymerization. Additionally, two copolymers were prepared by NMP despite of the presence of 1,2-dicarbonyls in monomer structures. The copolymers were photoperoxidised ( $\lambda > 370$  nm) and thermally treated (170 °C) to crosslink. From Winter-Chambon criterion, a minimal theoretical crosslinking index to reach the gel point was determined to be 4.8. It corresponds to the content of BZS between 1 and 2 wt% under given conditions. Consequently, photoperoxidised and thermally treated copolymers BZS/S 0.5% and BZS/S 1% did not reach the gel point. Densitometry can be also used for an assessment of the gel point. Final networks were studied by various techniques. The density of the final network is depended on BZS content, BZ conversion, molar mass and polydispersity of an initial copolymer. Efficiency of BP to crosslink decreases with increasing BP concentration and with increasing molar mass of initial copolymer. To build a dense network, we have to increase molar mass of primary crosslinkable polymer, increase the concentration of crosslinker and decrease the polydispersity.

## 7 STUDY OF PHOTOCHEMISTRY OF CAMPHORQUINONE-BEARING POLYMER

### 7.1 Introduction

Camphorquinone (CQ) is another industrially important representative of 1,2-dicarbonyl compounds. When compared with BZ, after irradiation it should produce two macroradicals, so its efficiency of crosslinking should be 2 times higher. Necessary condition for this assumption is the same photochemical behaviour as in the case of BZ. No diacyl peroxide formation was detected when CQ in polymer film was irradiated ( $\lambda > 370 \text{ nm}$ )<sup>43</sup> contrary to the BZ conversion to BP in polymer film<sup>12</sup>. Probably, formed low molecular peroxy anhydride of CQ is unstable and is immediately decomposed. It was also accompanied by a decrease of molecular weight of PS<sup>43</sup>.

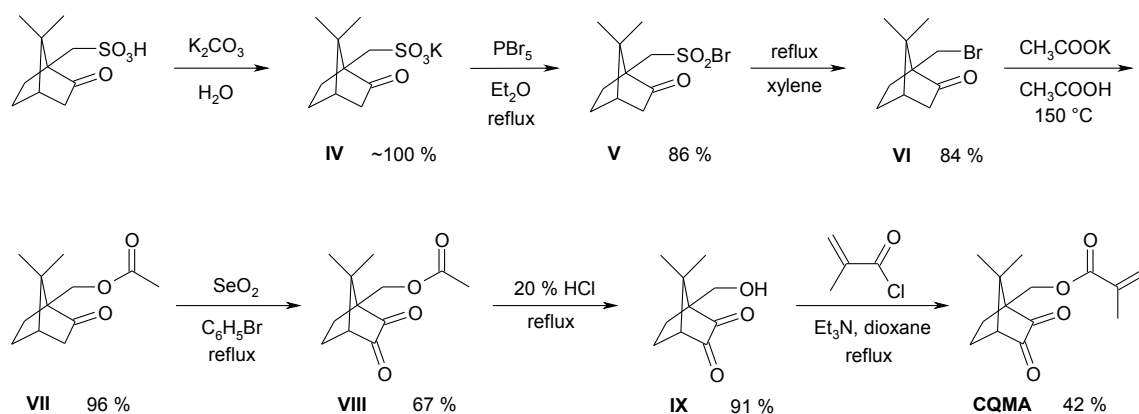
CQ-bearing monomer CQMA<sup>110</sup> was chosen to prepare a styrene copolymer CQMA/S. The goal is to find out whether stable peroxy anhydride of CQ would be formed upon irradiation or whether CQMA/S crosslinks upon irradiation that would indicate indirectly the photoperoxidation of CQ. Presuming the same mechanism as for BZS/S, higher network density can be expected because two macroradicals would be formed from one CQ group in comparison with BZS/S where only one macroradical and one low molecular radical is formed from one BZ group<sup>16-18</sup>.

### 7.2 Synthesis of CQMA

A monomer CQMA was synthesised in 7 steps from ( $\pm$ )-10-camphorsulphonic acid as a starting material (Scheme 17). Overall yield of the synthesis was 18 %. Total synthesis of (R)-10-methacryloyloxycamphorquinone from (R)-10-camphorsulphonic acid is known in the literature.

( $\pm$ )-10-Camphorsulphonic acid was neutralised with aqueous  $\text{K}_2\text{CO}_3$  solution and precisely dried to a constant weight. Formed potassium ( $\pm$ )-10-camphorsulphonate (**IV**) was used without further purification and in a reaction with  $\text{PBr}_5$  in dry refluxing ether gave ( $\pm$ )-10-camphorsulphonic acid bromide (**V**) in 86 % yield<sup>111,112</sup>. Unpurified product **V** was decomposed in dry refluxing xylene to ( $\pm$ )-10-bromocamphor (**VI**) in 84 % yield<sup>111</sup>. Although **V** was still visible on TLC, the prolongation of the reaction time did not increase the yield of the product. **VI** was purified by a

distillation followed by a crystallisation from methanol.



**Scheme 17:** Synthesis of the monomer CQMA.

**VI**, dried acetic acid and freshly molten potassium acetate were heated to 150 °C for 17 h and (±)-10-acetoxycamphor (**VII**) was obtained almost quantitatively<sup>112</sup>. The product **VII** was purified by a distillation under diminished pressure.

(±)-10-Acetoxycamphorquinone (**VIII**) was prepared by an oxidation of  $\alpha$ -methylene group adjacent to carbonyl group of **VII** with freshly resublimed  $\text{SeO}_2$  in refluxing bromobenzene<sup>113</sup>. Arose black selenium powder was filtrated and the product was purified by a column chromatography yielding 67 % of **VIII**.

**VIII** in refluxing 20 % aqueous HCl solution afforded (±)-10-hydroxycamphorquinone (**IX**) in 91 % yield which was purified by a column chromatography<sup>113</sup>. Its melting point was determined in a sealed capillary as it sublimes at higher temperatures. Its melting point is extremely large (~100-255 °C) and cannot be used to verify the purity.

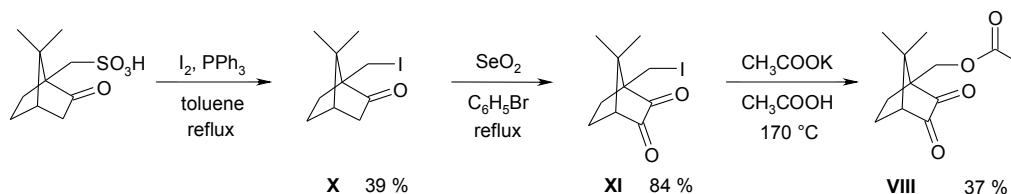
CQMA was prepared by an esterification of **IX** with methacryloyl chloride in the presence of triethylamine in refluxing dioxane solution<sup>110</sup>. An inhibitor (ionol) was added to avoid a partial polymerization of the product. CQMA was purified by a column chromatography followed by a crystallisation from ether at -20 °C. Solid CQMA was stored in a refrigerator.

The syntheses of **VIII**, **IX** and CQMA were performed in a dark room lighted by a lamp with a filter ORWO 113D ( $\lambda > 545 \text{ nm}$ ).

A big difference between the determined melting points of **VI**, **VIII**, **IX**, CQMA and those mentioned in the literature is caused by the configuration of these compounds. The compounds in this work are racemates but the corresponding compounds in the literature are pure (R)-enantiomers. The racemates can crystallise as a racemic mixture (lower mp), as a racemic compound (lower or higher mp) or rarely as a racemic solid solution (slightly lower or higher mp). The type of a crystallisation could be proven by a small addition of a pure enantiomer. It is a racemic mixture, if

the melting point increases. If the melting point decreases, it is a racemic compound. Unfortunately, we did not have the corresponding pure enantiomers.

Other ways of synthesis of the desired compound were undergone. ( $\pm$ )-10-Camphorsulphonic acid was transformed to ( $\pm$ )-10-camphorsulphonic acid chloride with  $\text{SOCl}_2$  in chloroform. Its thermal decomposition in dry refluxing xylene was not successful.



**Scheme 18:** Alternative synthesis of ( $\pm$ )-10-acetoxycamphorquinone (**VIII**).

Alternatively, the synthesis of **VIII** can be shortened to just 3 steps according to Scheme 18. This synthesis also avoids the use of expensive  $\text{PBr}_5$ . ( $\pm$ )-10-Iodocamphor (**X**) was prepared in one step from ( $\pm$ )-10-camphorsulphonic acid with iodine and  $\text{PPh}_3$  in refluxing toluene in 39 % yield<sup>114</sup>. The yield in the literature was higher (85 %). **X** was selectively oxidised with  $\text{SeO}_2$  in refluxing bromobenzene to ( $\pm$ )-10-iodocamphorquinone (**XI**) in 84 % yield. **XI**, dried  $\text{CH}_3\text{COOH}$  and freshly molten  $\text{CH}_3\text{COOK}$  were heated to 170 °C for 8 h and **VIII** was afforded in 37 % yield; some side products were obtained as well. Probably, **X** should be transformed to **VII** first and then to **VIII**.

All attempts to transform **XI** directly to CQMA were unsuccessful. **XI** was stirred at ambient temperature with different reagents: methacrylic acid/ $\text{Cs}_2\text{CO}_3$ /DMF, methacrylic acid/1,5-diazabicyclo[3.4.0]non-5-ene/benzene, methacrylic acid/ $\text{NaH}$ /*n*-hexane, methacrylic acid/ $\text{NaHCO}_3$ /DMF, potassium methacrylate/acetone, silver methacrylate/toluene.

### 7.2.1 Synthesis of Potassium ( $\pm$ )-10-Camphorsulphonate (**IV**)

( $\pm$ )-10-Camphorsulphonic acid (250 g, 1.08 mol) was dissolved in water (300 ml).  $\text{K}_2\text{CO}_3$  (79.3 g, 0.57 mol) was added to neutral reaction. Water was evaporated and acetone was added and salt was filtrated. The residue was evaporated and combined with filtered salt. Powdered salt was dried precisely to constant weight for several days in a vacuum desiccator over  $\text{P}_2\text{O}_5$ . The crude product potassium ( $\pm$ )-10-camphorsulphonate (**IV**) was used without further purification.

### 7.2.2 Synthesis of ( $\pm$ )-10-Camphorsulphonic Acid Bromide (V)

Stirred suspension of **IV** (62.0 g, 0.229 mol) in dry ether (300 ml) under argon was cooled to  $-60\text{ }^{\circ}\text{C}$ .  $\text{PBr}_5$  (100 g, 0.232 mol) was added at once. The cooling bath was removed and the mixture stirred for 1 h and then refluxed for 3 h. Reaction mixture was poured onto a mixture of ice (600 g) and water (600 ml). Ethereal layer and white solid were separated and the aqueous layer was extracted with ether ( $2 \times 100\text{ ml}$ ). The combined ethereal layers were washed with water (50 ml), dried over  $\text{Na}_2\text{SO}_4$  and evaporated to give a yellow solid ( $\pm$ )-10-camphorsulphonic acid bromide (**V**) (58.0 g, 86 %) which was used without further purification.

$R_f = 0.48$  (isohexane/ethyl acetate 3:1)

$^1\text{H NMR}$  ( $\text{CDCl}_3$ ):  $\delta$  (ppm) = 4.47 (d,  $^2J = 14.4\text{ Hz}$ , 1H, 10- $\text{H}_a$ ), 3.92 (d,  $^2J = 14.4\text{ Hz}$ , 1H, 10- $\text{H}_b$ ), 2.54-2.39 (m, 2H,  $\text{CH}_2$ ), 2.18-2.04 (m, 2H,  $\text{CH}_2$ ), 1.99 (d,  $J = 18.3\text{ Hz}$ , 1H,  $\text{CH}_2$ ), 1.84-1.74 (m, 1H,  $\text{CH}_2$ ), 1.49 (ddd,  $J = 12.3, 9.3, 3.6\text{ Hz}$ , 1H,  $\text{CH}_2$ ), 1.14 (s, 3H, 8-H), 0.93 (s, 3H, 9-H)

### 7.2.3 Synthesis of ( $\pm$ )-10-Bromocamphor (VI)

**V** (58.0 g, 0.196 mol) was dissolved in dry xylene. The solution was kept in dark with  $\text{CaCl}_2$  (10 g) overnight. The mixture was refluxed for 3 hours under argon. The solid part was filtrated and the mixture was concentrated. After distillation under diminished pressure followed by crystallisation from methanol, ( $\pm$ )-10-bromocamphor (**VI**) (38.3 g) was obtained in 84 % yield, mp  $77\text{-}78\text{ }^{\circ}\text{C}$  (lit.  $78\text{ }^{\circ}\text{C}$  for (R)-10-bromocamphor).

$R_f = 0.67$  (isohexane/ethyl acetate 3:1)

$^1\text{H NMR}$  ( $\text{CDCl}_3$ ):  $\delta$  (ppm) = 3.62 (d,  $^2J = 10.8\text{ Hz}$ , 1H, 10- $\text{H}_a$ ), 3.41 (d,  $^2J = 10.8\text{ Hz}$ , 1H, 10- $\text{H}_b$ ), 2.41 (ddd,  $J = 18.2, 4.9, 2.9\text{ Hz}$ , 1H, 3- $\text{H}_{\text{eq}}$ ), 2.17-2.09 (m, 2H, 4-H + 6-H), 2.08-1.97 (m, 1H, 5- $\text{H}_{\text{eq}}$ ), 1.91 (d,  $J = 18.2\text{ Hz}$ , 1H, 3- $\text{H}_{\text{ax}}$ ), 1.64-1.51 (m, 1H, 6-H), 1.41 (ddd,  $J = 12.3, 9.3, 3.4\text{ Hz}$ , 1H, 5- $\text{H}_{\text{ax}}$ ), 1.11 (s, 3H, 8-H), 0.95 (s, 3H, 9-H)

$^{13}\text{C NMR}$  ( $\text{CDCl}_3$ ):  $\delta$  (ppm) = 215.3 (C-2), 60.2 (C-1), 48.1 (C-7), 43.9 (C-4), 42.9 (C-3), 29.3 (C-10), 27.6 (C-6), 26.7 (C-5), 20.4 (C-8), 20.2 (C-9)

**FTIR** (KBr):  $1746\text{ cm}^{-1}$  (C=O)

### 7.2.4 Synthesis of (±)-10-Acetoxycamphor (VII)

**VI** (30.0 g, 130 mmol), dried acetic acid (60 g, 57 ml) and freshly molten potassium acetate (90.0 g, 917 mmol) were heated to 150 °C for 17 h. Cooled reaction mixture was dissolved in water (200 ml), neutralised with sodium carbonate and extracted with ether (3 × 100 ml). Combined ethereal layers were washed with water (50 ml), dried over Na<sub>2</sub>SO<sub>4</sub> and evaporated. (±)-10-Acetoxycamphor (**VII**) was obtained by a distillation under diminished pressure yielding 26.1 g (96 %).

**R<sub>f</sub>** = 0.49 (isohexane/ethyl acetate 3:1)

**<sup>1</sup>H NMR** (CDCl<sub>3</sub>): δ (ppm) = 4.28 (d, <sup>2</sup>J = 12.3 Hz, 1H, 10-H<sub>a</sub>), 4.23 (d, <sup>2</sup>J = 12.3 Hz, 1H, 10-H<sub>b</sub>), 2.43 (ddd, J = 18.2, 4.7, 2.3 Hz, 1H, 3-H<sub>eq</sub>), 2.10-1.93 (m, 3H, 4-H, 5-H<sub>eq</sub>, 6-H), 2.05 (s, 3H, CO-CH<sub>3</sub>), 1.87 (d, J = 18.5 Hz, 1H, 3-H<sub>ax</sub>), 1.48-1.34 (m, 2H, 5-H<sub>ax</sub> + 6-H), 1.06 (s, 3H, 8-H), 0.98 (s, 3H, 9-H)

**<sup>13</sup>C NMR** (CDCl<sub>3</sub>): δ (ppm) = 216.2 (C-2), 171.0 (C=O-CH<sub>3</sub>), 60.5 (C-10), 60.1 (C-1), 47.0 (C-7), 43.9 (C-4), 43.3 (C-3), 26.6 (C-6), 25.5 (C-5), 20.9 (CH<sub>3</sub>), 20.7 (CH<sub>3</sub>), 19.8 (CH<sub>3</sub>)

**FTIR** (neat): 1747 cm<sup>-1</sup> (C=O), 1744 cm<sup>-1</sup> (C=O)

### 7.2.5 Synthesis of (±)-10-Acetoxycamphorquinone (VIII)

**VII** (44.0 g, 209 mmol) and SeO<sub>2</sub> (29.5 g, 266 mmol) in bromobenzene were refluxed for 17 h. The solvent was evaporated. The reaction mixture was filtered through a short column of silica to remove selenium. Silica column was washed with ethyl acetate and the solution was concentrated. (±)-10-Acetoxycamphorquinone (**VIII**) was isolated by column chromatography on silica gel with ethyl acetate – isohexane 1:3 as an eluent to afford 31.3 g (67 %) of a yellow solid, mp 76-78 °C (lit. 88 °C for (R)-10-acetoxycamphorquinone).

**R<sub>f</sub>** = 0.32 (isohexane/ethyl acetate 3:1)

**<sup>1</sup>H NMR** (CDCl<sub>3</sub>): δ (ppm) = 4.40 (d, <sup>2</sup>J = 12.9 Hz, 1H, 10-H<sub>a</sub>), 4.36 (d, <sup>2</sup>J = 12.9 Hz, 1H, 10-H<sub>b</sub>), 2.64 (d, J = 5.3 Hz, 1H, 4-H), 2.30-2.10 (m, 2H), 2.08 (s, 3H, CO-CH<sub>3</sub>), 1.69 (d, J = 8.8 Hz, 2H), 1.17 (s, 3H, 8-H), 1.08 (s, 3H, 9-H)

**<sup>13</sup>C NMR** (CDCl<sub>3</sub>): δ (ppm) = 201.6 (C=O), 201.3 (C=O), 170.6 (C=O-CH<sub>3</sub>), 60.8 (C-1), 59.3 (C-10), 58.5 (C-4), 42.8 (C-7), 25.8 (CH<sub>2</sub>), 22.0 (CH<sub>3</sub>), 21.8 (CH<sub>2</sub>), 20.8 (CH<sub>3</sub>), 18.2 (CH<sub>3</sub>)

**FTIR** (KBr): 1771 cm<sup>-1</sup> (C=O), 1747 cm<sup>-1</sup> (C=O), 1736 cm<sup>-1</sup> (C=O)

### 7.2.6 Synthesis of ( $\pm$ )-10-Hydroxycamphorquinone (IX)

Solution of **VIII** (3.1g, 14 mmol) in 20 % HCl was refluxed for 2 h. Then, the solution was neutralised with Na<sub>2</sub>CO<sub>3</sub> and extracted with ethyl acetate (3 × 50 ml). The organic layer was dried with CaCl<sub>2</sub> and concentrated. ( $\pm$ )-10-Hydroxycamphorquinone (**IX**) was isolated by column chromatography on silica gel with ethyl acetate – isohexane 1:2 as an eluent to afford 2.3 g (91 %) of a yellow solid. It is a sublimating compound with a very wide mp ~100-255 °C determined in a sealed capillary (lit. 205 °C for (R)-10-hydroxycamphorquinone).

**R<sub>f</sub>** = 0.33 (isohexane/ethyl acetate 2:1)

**<sup>1</sup>H NMR** (CDCl<sub>3</sub>):  $\delta$  (ppm) = 4.00 (d, <sup>2</sup>*J* = 12.2 Hz, 1H, 10-H<sub>a</sub>), 3.87 (d, <sup>2</sup>*J* = 12.2 Hz, 1H, 10-H<sub>b</sub>), 2.63 (d, *J* = 4.9 Hz, 1H, 4-H), 2.26-2.19 (m, 1H, 5-H), 2.13-2.06 (m, 1H, 6-H), 1.79-1.66 (m, 2H, 5-H + 6-H), 1.15 (s, 3H, 8-H), 1.09 (s, 3H, 9-H)

**<sup>13</sup>C NMR** (CDCl<sub>3</sub>):  $\delta$  (ppm) = 205.0 (C-2), 202.2 (C-3), 62.9 (C-1), 59.2 (C-10), 58.7 (C-4), 42.5 (C-7), 25.9 (C-6), 22.3 (C-9), 21.9 (C-5), 17.8 (C-8)

**FTIR** (KBr): 3330 cm<sup>-1</sup> (O-H), 1769 cm<sup>-1</sup> (C=O), 1747 cm<sup>-1</sup> (C=O)

### 7.2.7 Synthesis of ( $\pm$ )-10-Methacryloyloxycamphorquinone (CQMA)

A solution of **IX** (6.76 g, 37.1 mmol) and ionol (100 mg) in dry dioxane (170 ml) under argon was cooled to 0 °C. Triethylamine (5.1 ml, 37 mmol), methacryloyl chloride (4 ml, 41 mmol) and dry dioxane (50 ml) were added through septum. The reaction mixture was refluxed for 2 h, then filtrated to remove triethylamine hydrochloride. Dioxane was distilled at ambient temperature. Crude product was isolated by a column chromatography on silica gel with ethyl acetate – isohexane 1:5 as an eluent. CQMA was crystallised from ether in a freezer to yield 3.9 g (42 %), mp 46-49 °C (lit. 91-92 °C for (R)-10-methacryloyloxycamphorquinone).

**R<sub>f</sub>** = 0.46 (isohexane/ethyl acetate 2:1)

**<sup>1</sup>H NMR** (CDCl<sub>3</sub>):  $\delta$  (ppm) = 6.08 (d, *J* = 1.8 Hz, 1H, vinyl-H<sub>a</sub>), 5.59 (d, *J* = 1.8 Hz, 1H, vinyl-H<sub>b</sub>), 4.48 (d, <sup>2</sup>*J* = 12.3 Hz, 1H, 10-H<sub>a</sub>), 4.42 (d, <sup>2</sup>*J* = 12.3 Hz, 1H, 10-H<sub>b</sub>), 2.64 (d, *J* = 5.3 Hz, 1H, 4-H), 2.28-2.16 (m, 2H, 5-H + 6-H), 1.94 (s, 3H, methacrylic CH<sub>3</sub>), 1.74-1.66 (m, 2H, 5-H + 6-H), 1.18 (s, 3H, 8-H), 1.09 (s, 3H, 9-H)

**<sup>13</sup>C NMR** (CDCl<sub>3</sub>):  $\delta$  (ppm) = 201.5 (C=O), 201.1 (C=O), 167.0 (O-CO), 135.8 (C=CH<sub>2</sub>), 126.2 (C=CH<sub>2</sub>), 61.1 (C-1), 59.5 (C-10), 58.6 (C-4), 42.8 (C-7), 25.9 (C-6), 22.1 (C-9), 21.8 (C-5), 18.3

(C-8), 18.3 (methacrylic CH<sub>3</sub>)

### 7.3 Synthesis of the copolymer CQMA/S

#### *Free-radical bulk polymerization (CQMA/S 1)*

An ampoule containing CQMA (0.199 g, 0.80 mmol), styrene (20 ml, 174 mmol) and AIBN (20 mg) was sealed under argon and polymerised at 59 °C for 4.5 h. The copolymer was precipitated twice from chloroform solution into 10× excess of methanol to yield 1.84 g (10 % conversion) of the desired copolymer.

#### *Living free-radical polymerization (CQMA/S 2)*

A solution of CQMA (0.202 g, 0.81 mmol), styrene (20 ml, 174 mmol) and StNO (38.5 mg) was deaerated with argon, sealed in an ampoule and polymerised at 125 °C for 6 h. After cooling, polymerization mixtures were diluted with chloroform and precipitated twice into 10× excess of methanol to yield 4.8 g (26 % conversion) of the desired copolymer.

The content of CQMA in CQMA/S copolymer was determined by UV/VIS and FTIR spectroscopy (Table 24). FTIR gives higher values than UV/VIS. Contrary to BZS that allows to prepare statistical copolymers, CQMA is more reactive than styrene in copolymerization. Copolymer CQMA/S 1 was prepared in lower conversion than CQMA/S 2, so CQMA/S 1 has higher CQMA content. Theoretical crosslinking index  $\gamma$  was calculated using equation  $\gamma = 2cM_w$  where c is the concentration of CQ groups in copolymer.

**Table 24:** Content of CQMA in monomer mixture and in copolymer CQMA/S determined by means of UV/VIS and FTIR spectroscopy and the theoretical crosslinking index  $\gamma$ .

<i>Copolymer sample</i>	<i>Determination method</i>	<i>CQMA in monomer mixture [wt%]</i>	<i>CQMA in copolymer [wt%]</i>	<i>CQMA in monomer mixture [mol%]</i>	<i>CQMA in copolymer [mol%]</i>	<i>Theoretical crosslinking index <math>\gamma</math></i>
CQMA/S 1	UV/VIS	1.09	1.47	0.45	0.62	35
CQMA/S 2		1.10	1.07	0.45	0.45	13
CQMA/S 1	FTIR	1.09	1.70	0.45	0.72	40
CQMA/S 2		1.10	1.41	0.45	0.59	18

## 7.4 Characterisation of molecular parameters of initial and irradiated CQMA/S

### 7.4.1 Rheological curves

The most sensitive region of the rheological curve to the molecular changes during a crosslinking process is the terminal zone. First,  $G'$  is always smaller than  $G''$ , as the initial polymer has more viscous behaviour. As crosslinking process proceeds,  $G'$  increases rapidly and becomes larger than  $G''$ , which is a characteristic feature of the crosslinked system that has a more elastic behaviour. At the gel point,  $G'$  and  $G''$  depend on frequency in an identical manner, corresponding to parallel lines in a frequency spectrum. The loss tangent  $\tan \delta$  becomes independent of frequency ( $\omega$ ).

The films were irradiated in SEPAP device described previously. Figures 39 and 40 show rheological curves of initial and irradiated copolymers. The curves of initial copolymer display typical rheological behaviour for melt polymers. The point of intersection divides the curve into terminal zone (low frequencies) and rubbery plateau region (high frequencies). From the curves of irradiated samples, a more elastic comportment can be seen. It means that a recombination of macroradicals occurred. These samples are uncrosslinked because  $G'$  is still lower than  $G''$ . The loss tangent  $\tan \delta$  confirms that the irradiated samples are in the vicinity of a gel point.

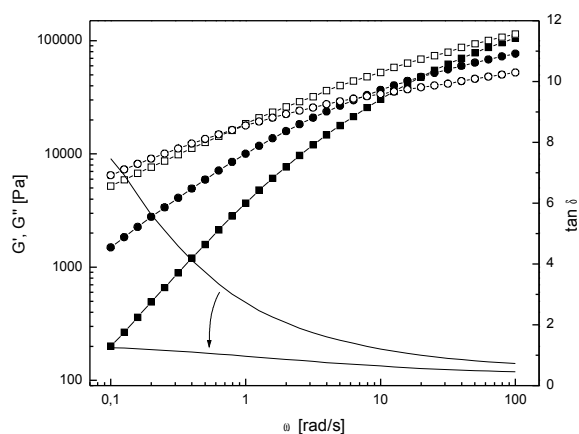


**Figure 39:** Storage ( $G'$ , ■, □) and loss ( $G''$ , ●, ○) moduli as a function of frequency pulsation  $\omega$  for initial (solid) and for irradiated CQMA/S 1 (hollow). The reference temperature was 170 °C.

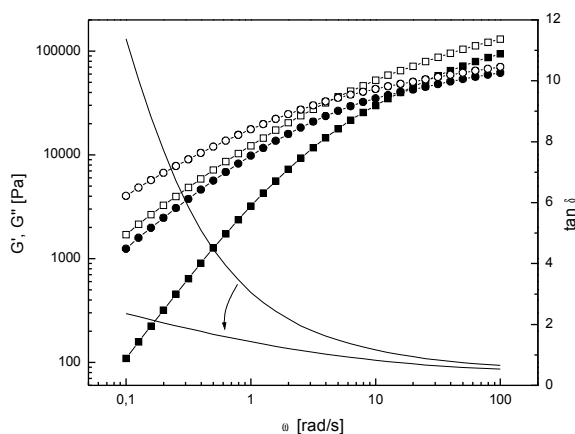


**Figure 40:** Storage ( $G'$ , ■, □) and loss ( $G''$ , ●, ○) moduli as a function of frequency pulsation  $\omega$  for initial (solid) and for irradiated CQMA/S 2 (hollow). The reference temperature was 170 °C.

### 7.4.2 Gel permeation chromatography and Cole-Cole representation

The films are still soluble in organic solvents after irradiation. PS equivalent molar masses were then determined by GPC for both copolymer before and after irradiation (Table 25). From rheology results, zero shear viscosity  $\eta_0$  and distribution parameter  $h$  were determined as well.

For both copolymers,  $M_w$  and polydispersities were increased. This is typical for crosslinking process. For the irradiated CQMA/S 1 copolymer, the extrapolation of Cole-Cole plot was not possible because the system is near the gel point. From GPC,  $M_w$  was doubled. For CQMA/S 2, the zero shear viscosity  $\eta_0$  that is proportional to  $M_w$  was increased by ( $\eta_0 \propto M_w^{3.4}$ ). From GPC,  $M_w$  was doubled. From power law ( $\eta_0 \propto M_w^{3.4}$ ),  $M_w$  was increased by 60 %.

**Table 25:** GPC and Cole-Cole results of initial and irradiated copolymers CQMA/S.

<i>Copolymer sample</i>	$M_w$ [g/mol]	$M_n$ [g/mol]	<i>PDI</i>	$\eta_0$ [Pa.s]	<i>h</i>
<i>Initial copolymer</i>					
CQMA/S 1	296400	178500	1.66	16600	0.43
CQMA/S 2	156400	100200	1.56	13700	0.36
<i>Irradiated and thermally treated copolymer</i>					
CQMA/S 1	598300	115300	5.19	-	-
CQMA/S 2	328600	116400	2.82	70500	0.45

## 7.5 Irradiation of CQMA/S

CQMA/S 1 film was irradiated in a SEPAP device described previously. The evolution during irradiation was monitored by FTIR (Figure 41, 42) and by UV/VIS spectroscopy (Figure 43).

The IR spectra of low molecular CQ doped in PS and copolymer CQMA/S during irradiation are not identical. Common bands that can be assigned are 1776, 1759  $\text{cm}^{-1}$  (dicarbonyl group of CQ) that are decreasing and 1815, 1770  $\text{cm}^{-1}$  (camphoric anhydride), 1701  $\text{cm}^{-1}$  (camphoric diacid) that are increasing. Except these bands, some new bands appeared increasing at 1805-1790, 1744, 1717  $\text{cm}^{-1}$  and a band decreasing at 1732  $\text{cm}^{-1}$ .

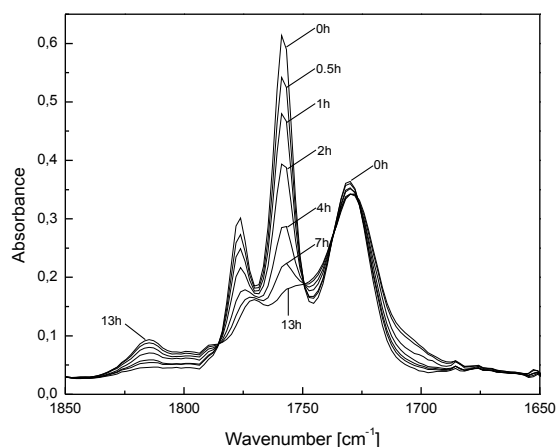


**Figure 41:** FTIR spectra of CQMA/S 1 film after irradiation in a SEPAP apparatus for the indicated periods. Spectrum of PS film was subtracted.

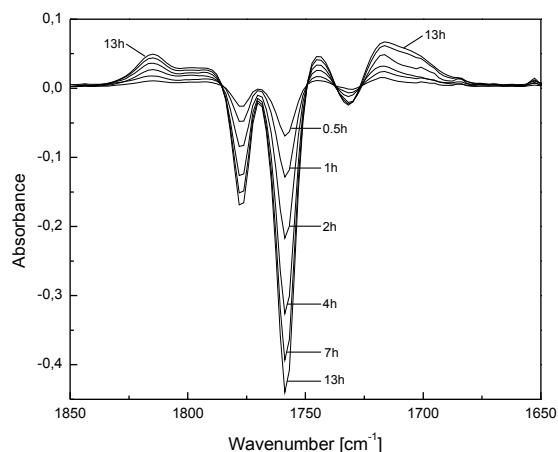


**Figure 42:** FTIR spectra of CQMA/S 1 film after irradiation in a SEPAP apparatus for the indicated periods. Spectrum of initial CQMA/S 1 film was subtracted.

After exposure of the irradiated film to temperature 90 °C during 2 h, no change was observed by IR spectroscopy. Thus, it signifies that no thermally unstable 8-member ring of camphordiacyl peroxide which IR vibration maxima would be expected to be in area about 1800  $\text{cm}^{-1}$  was present after irradiation.

From UV/VIS spectra, it is seen that 1,2-dicarbonyl group of CQ ( $n \rightarrow \pi^*$ ) is completely converted.

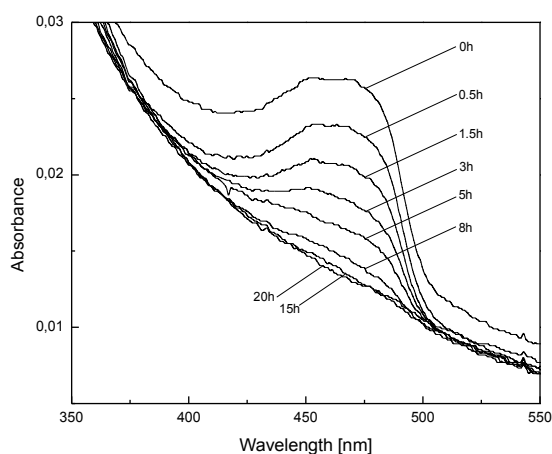


**Figure 43:** UV/VIS spectra of CQMA/S 1 film after irradiation in a SEPAP apparatus for the indicated periods.

As proven, no stable camphordiacyl peroxide were formed. It could be formed and immediately decomposed to camphoric diacid. It could be also converted into ester function linking

the macromolecular chain to each other and leading to increasing of molecular weight. A new band appearing at  $1744\text{ cm}^{-1}$  could be assigned to ester crosslinks. C=O band of CQMA (ester) at  $1730\text{ cm}^{-1}$  and the large band at  $1750\text{-}1800\text{ cm}^{-1}$  causes difficulties for a comparison. The mechanism is different in comparison to the photoperoxidation and crosslinking of BZ bearing polymers. Therefore, it can be assumed that the extent of decomposition of peroxy anhydride of CQ (if formed) is lower in comparison with BP pendant groups. Therefore, the extent of crosslinking is lower. Crosslinking induced primarily by an abstraction of hydrogen from camphor structure in triplet state, followed by recombination of radicals is also possible. Occurrence of crosslinking was confirmed by rheology and GPC.

BZS/S with a value of theoretical crosslinking index  $\gamma = 4$  is able to reach the gel point. CQMA/S 1 is the vicinity of gel point. Its theoretical crosslinking index  $\gamma$  was determined to be 35 from UV/VIS and 40 from FTIR. This means that CQ pendant groups are about 10 times less efficient for crosslinking than BZ.

## 7.6 Conclusion

Monomer CQMA was synthesised and its styrene copolymer CQMA/S was prepared too. Upon irradiation, no stable camphordiacyl peroxide was formed. Contrary to the observations for low molecular CQ doped in PS film, CQMA/S copolymer crosslinks upon irradiation and some different chemical species are formed. CQMA/S crosslinking is about one order less effective when compared to BZS/S. First results show that one of the decomposition product could be ester linkage formed by a decomposition of unstable camphordiacyl peroxide. This hypothesis is supported by increasing molecular weight.

## 8 CONCLUSION AND PERSPECTIVES

BZS, a new monomer bearing photoreactive benzil group, was synthesised in 4 steps from 2-phenoxyethyl acetate in overall 19 % yield. Its styrene copolymers BZS/S containing different amount of BZS were prepared by radical polymerization in bulk and in solution and by NMP in bulk. The contents of BZS in copolymer are practically the same as in the monomer mixtures and does not depend very much on conversion and BZS content in monomer mixture. It is a reflection of a very similar reactivity of both comonomers resulting in statistical copolymer with regular distribution of BZS in polymer chains. When irradiated at  $\lambda = 436$  nm in air, pendant BZ groups are transformed almost quantitatively to pendant BP groups. This step is accompanied by a partial crosslinking despite of using of the mildest irradiation conditions. Thermal treatment (91 °C) led to a significant crosslinking of the photoperoxidised BZS/S.

The pendant BP groups were converted into ester function crosslinks by irradiation or heating. This chemical evolution of crosslinking was monitored by FTIR and by swelling measurements. Thermoporometry, giving the mesh size of crosslinked polymer for different curing times, was used as an alternative method to follow these alterations. Carbon tetrachloride seems to be a suitable thermoporometry liquid probe to study the crosslinking of the styrene copolymers. All numerical relationships necessary to perform the calculations of the mesh size distributions from DSC thermograms were established. Densitometry, studying the soluble part of crosslinked material, represented a complementary method to the thermoporometry. First hour of the curing time (110 °C or  $\lambda > 300$  nm) leads to a pronounced crosslinking of the material, prolongation of the curing time leads only to a densification of the formed network.

A series of BZS/S copolymers bearing different content of BZS monomer units (0 – 13 wt%) was synthesised and characterised by GPC and rheology. Their final networks were studied using various methods. Global network was studied by rheological methods (Winter-Chambon criterion, Cole-Cole representation, model using rubberlike elasticity), insoluble part by thermoporometry and gravimetric swelling measurement, soluble part by densitometry. The pregel regime can be characterised by decreasing slopes of rheological curves at low frequencies and by Cole-Cole plot giving the weight average molecular weight. Gel point could not be determined by densitometry because of lack of experimental points. Using Winter-Chambon criterion, the gel point was

determined to be reachable for copolymers with a theoretical crosslinking index equal to 4.8 (number of photo-converted BZ groups per polymer chain calculated from  $M_w$ ), that corresponds to 1 – 2 wt% content of BZS units in copolymer depending on molecular weight.

Different methods of characterisation of network give different results. Rheological model using rubberlike elasticity with a criterion on entrapment of entanglements gives the density of chemical crosslinks only. The results from calculations using sol fraction gave the same trend. Basic rheological equation from theory of rubberlike elasticity for idealised network and swelling measurement take into account both chemical and physical crosslinks. Swelling results were improved by a correction on imperfection resulting from chain ends. Mesh sizes of swollen polymer network determined by thermoporometry correlate well with equilibrium degree of swelling. A good correlation between the results of the mentioned various techniques and an average number of BP groups per polymer chain of a photoperoxidised polymer was established. The efficiency of crosslinker (BP) is decreasing with increasing BP content and increasing molecular weight of initial polymer. It can be explained by lower probability of forming junction points in densely crosslinked material. The optimising of crosslinking conditions remains for the perspective. The factors supporting the construction of a dense network are high molar mass and low polydispersity of initial polymer and high concentration of crosslinker. From this point of view, the use of copolymers with narrow molecular weights distribution prepared by NMP is advantageous.

Methacrylate monomer CQMA bearing CQ group was synthesised 7 steps from ( $\pm$ )-10-camphorsulphonic acid as a starting material in 18 % overall yield. Its styrene copolymers were prepared and irradiated. No stable camphordiacyl peroxide was formed. Some additional species were created in comparison to the irradiation of CQ doped in PS. A band in IR spectra corresponding to esters and increasing molecular weight during irradiation could support the formation of unstable camphordiacyl peroxide and its decomposition into ester crosslinks. CQMA/S copolymer crosslinks about one order less efficiently than BZS/S copolymer.

The mechanism of BZ photoperoxidation was not proved yet. Preparing of soluble photoperoxidised polymer can open new possibilities of application. For this, experimental conditions that could minimise the extent of side products during photoperoxidation should be found.

The mechanism of crosslinking seems to be clear. Therefore, the influence of oxygen and different conditions should be investigated. Photo-crosslinking and thermo-crosslinking should be compared using different light and various temperatures. Promising can be also simultaneous photoperoxidation and crosslinking in one step at lower wavelength.

Applicability of BZS/S copolymer should be studied for modification of solid surfaces and for preparation of architecturally defined nanoparticles via intramolecular chain collapse.

## REFERENCES

- 1 Pappas, S.P. *Comprehensive Polymer Science*, Pergamon Press **1989**, *6*, 135.
- 2 Krongauz, V.V.; Trifunac, A.D. *Process in Photoreactive Polymers*, Chapman & Hall, New York **1995**, 405.
- 3 Harth, E.; Van Horn, B.; Lee, V.Y.; Germack, D.S.; Gonzales, C.P.; Miller, R.D.; Hawker, C.J. *J. Am. Chem. Soc.* **2002**, *124*, 8653-8660.
- 4 Ryu, D.Y.; Shin, K.; Drockenmuller, E.; Hawker, C.J.; Russell, T.P. *Science* **2005**, *308*, 236-239.
- 5 Schinner, R.; Wolff, T.; Kuckling, D. *Ber. Bunsenges Phys. Chem.* **1998**, *102*, 1710-1714.
- 6 Gupta, I.; Gupta, S.N.; Neckers, D.C. *J. Polym. Sci.: Polym. Chem. Ed.* **1982**, *20*, 147-157.
- 7 Allen, N.S.; Catalina, F.; Green, P.N.; Green, W.A. *Eur. Polym. J.* **1986**, *22*, 49.
- 8 JP 03028852, OKI Electric Industry Co. Ltd., invs: Sakata, Y.; Ito, T. *Chem. Abstr.* **1989**, *112*, 28141b.
- 9 JP 01046745, Canon K. K., invs.: Okuma, N.; Takenochi, M.; Mizagawa, M. *Chem. Abstr.* **1991**, *115*, 18635p.
- 10 Klinger, H. *Chem. Ber.* **1886**, *19*, 1862.
- 11 Kósa, C.; Lukáč, I. *Chem. Listy* **1996**, *90*, 287-294.
- 12 Lukáč, I.; Kósa, C. *Macromol. Rapid. Commun.* **1994**, *15*, 929-934.
- 13 Simbürger, H.; Kern, W.; Hummel, K.; Hagg, C. *Polymer* **2000**, *41*, 7883-7897.
- 14 Catalina, F.; Peinado, C.; Blanco, M.; Allen, N.S.; Corrales, T.; Lukáč, I. *Polymer* **1998**, *39*, 4399-4408.
- 15 Catalina, F.; Peinado, C.; Blanco, M.; Alonso, A.; Allen, N.S. *J. Photochem. Photobiol. A: Chem* **2000**, *131*, 141-146.
- 16 Kósa, C.; Lukáč, I.; Weiss, R.G. *Macromolecules* **2000**, *33*, 4015-4022.
- 17 Mosnáček, J.; Weiss, R.G.; Lukáč, I. *Macromolecules* **2002**, *35*, 3870-3875.
- 18 Mosnáček, J.; Weiss, R.G.; Lukáč, I. *Macromolecules* **2004**, *37*, 1304-1311.
- 19 Mosnáček, J.; Lukáč, I.; Chromik, Š.; Kostič, I.; Hrdlovič, P. *J. Pol. Sci.: Part A: Pol. Chem.* **2004**, *42*, 765-771.
- 20 Greenley, R. Z. *Polymer Handbook*, 4th ed.; Brandrup, J.; Immergut, E. H.; Grulke, E. A.; Eds.; Wiley-Interscience: New York **1999**, p.181.
- 21 Murayama, K.; Ono, K.; Osugy, J. *Bull. Chem. Soc. Jpn.* **1972**, *45*, 847-851.
- 22 Bunbury, D. L.; Wang, C. T. *Can. J. Chem.* **1968**, *46*, 1473-1479.

- 23 Bunbury, D. L.; Chuang, T. T. *Can. J. Chem.* **1969**, *47*, 2045-2055.
- 24 Cáceres, T.; Encinas, M.V.; Lissi, E. *J. Photochem.* **1984**, *27*, 109-114.
- 25 McDowell, C.A.; Sharples, L.K. *Can. J. Chem.* **1958**, *36*, 251.
- 26 Park, J.W.; Kim, E.K.; Park, K.K. *Bull. Korean Chem. Soc.* **2002**, *23*, 1229-1234.
- 27 Mehrotra, K.N.; Pandey, G.P. *Bull. Chem. Soc. Jpn.* **1980**, *53*, 1081-1084.
- 28 Gream, G.E.; Paice, J.S.; Uszinski, B.S. *J. Chem. Soc. D* **1970**, *15*, 895.
- 29 Inoue, H.; Takido, S.; Somemiya, T.; Momura, Y. *Tetrahedron Lett.* **1973**, *14*, 2755-2758.
- 30 Buckland, S.J.; Davidson, R.S. *J. Photochem.* **1987**, *36*, 39-49.
- 31 Sawaki, Y. *Tetrahedron* **1985**, *41*, 2199-2205.
- 32 Cosa, G.; Scaiano, J.C. *J. Am. Chem. Soc.* **2004**, *126*, 8636-8637.
- 33 Sawaki, Y.; Foote, C.S. *J. Org. Chem.* **1983**, *48*, 4934-4940.
- 34 Lukáč, I.; Hrdlovič, P.; Schnabel, W. *Macromol. Chem. Phys.* **1994**, *195*, 2233-2245.
- 35 Kósa, C.; Lukáč, I.; Weiss, R.G. *Macromol. Chem. Phys.* **1999**, *200*, 1080-1085.
- 36 Hrdlovič, P.; Lukáč, I. in *Developments in Polymer Degradation*, Grassie, N., Ed.; Applied Science: London **1982**, *4*, 101-141.
- 37 Rabek, J. F. *Mechanisms of Photophysical Processes and Photochemical Reactions in Polymers*; Wiley: New York **1987**, p.520.
- 38 Andrzejewska, E.; Linden, L.Å.; Rabek, J.F. *Macromol. Chem. Commun.* **1998**, *119*, 441-449.
- 39 Rubin, M.B.; Gutman, A.L. *J. Org. Chem.* **1986**, *51*, 2511-2515
- 40 Rubin, M.B.; Ben-Bassat, J.M. *Tetrahedron* **1970**, *26*, 3579-3589.
- 41 Rubin, M.B.; Labarge, R.G. *J. Org. Chem.* **1966**, *31*, 3283-3289.
- 42 Meinwald, J.; Klingele, H.O. *J. Am. Chem. Soc.* **1966**, *88*, 2071-2073.
- 43 Mosnáček, J.; Lukáč, I. *J. Photochem. Photobiol. A: Chem.* **2002**, *151*, 95-104.
- 44 Flory, P.J. *J. Chem. Phys.* **1950**, *18*, 108.
- 45 Flory, P.J. *Principles of polymer chemistry*, Ithaca: Cornell University Press **1953**.
- 46 Ding, Z.Y.; Aklonis, J.J.; Salovey, R. *J. Pol. Sci. Part B* **1991**, *29*, 1035-1038.
- 47 Aithal, U.S.; Aminabhavi T.M. *J. Chem. Ed.* **1990**, *67*, 82-85.
- 48 Freger, V.; Bottino, A.; Capannelli, G.; Perry, M.; Gitis, V.; Belfer, S. *J. Membr. Sci.* **2005**, *256*, 134-142.
- 49 Baba, M.; Nedelec, J.-M.; Lacoste, J. *J. Phys. Chem. B* **2003**, *107*, 12884-12890.
- 50 Eliassi, A.; Modarress, H. *Eur. Polym. J.* **2001**, *37*, 1487-1492.
- 51 Cecopieri-Gómez, M.L.; Palacios-Alquisira, J. *J. Braz. Chem. Soc.* **2005**, *16*, 426-433.
- 52 Elbs, H.; Krausch, G. *Polymer* **2004**, *45*, 7935-7942.
- 53 Mantovani, F.; Grassi, M.; Colombo, I.; Lapasin, R. *Fluid Phase Equilib.* **2000**, *167*, 63-81.

- 54 Landry, M.R. *Thermochim. Acta* **2005**, *433*, 27-50.
- 55 León y León, C.A. *Adv. Colloid Interface Sci.* **1998**, *76-77*, 341-372.
- 56 Reinoso, F.R. *Characterization of Porous Solids*, Elsevier Science Publishers B.V.: Amsterdam **1991**, *2*, 543-551.
- 57 Thomson, W. *Phil. Mag.* **1871**, *42*, 448.
- 58 Tammann, G. *Chem. Abstr.* **1920**, *14*, 3553.
- 59 Meissner, F. *Chem. Abstr.* **1920**, *14*, 3553.
- 60 Kubelka, P. *Chem. Abstr.* **1932**, *26*, 5241.
- 61 Reiss, H.; Wilson, I.B. *J. Colloid. Sci.* **1948**, *3*, 551-561.
- 62 Still, R.C.; Skapski, A.S. *J. Chem. Phys.* **1956**, *24*, 644-651.
- 63 Skapski, A.S. *J. Chem. Phys.* **1959**, *31*, 573.
- 64 Kuhn, W.; Majer, H. *Z. Phys. Chem.* **1955**, *3*, 330-340.
- 65 Kuhn, W.; Peterli, E.; Majer, H. *J. Pol. Sci.* **1955**, *16*, 539-548.
- 66 Brun, M.; Lallemand, A.; Quinson, J.-F.; Eyraud, C. *Thermochim. Acta*, **1977**, *21*, 59-88.
- 67 Scherer, G.W. *Cem. Concr. Res.* **1999**, *29*, 1347-1358.
- 68 Deruelle, O.; Spalla, O.; Barboux, P.; Lambard, J. *J. Non-Cryst. Sol.* **2000**, *261*, 237-251.
- 69 Ehrburger-Dolle, F.; Dallamano, J.; Elaloui, E.; Pajonk, G.M. *J. Non-Cryst. Sol.* **1995**, *186*, 9-17.
- 70 Escribano, S.; Aldebert, P.; Pineri, M. *Electrochim. Acta* **1998**, *43*, 2195-2202.
- 71 Quinson, J.-F.; Tchikam, N.; Dumas, J.; Bovier, C.; Serughetti, J.; Guizard, C.; Larbot, A.; Cot, L. *J. Non-Cryst. Sol.* **1988**, *99*, 151-159.
- 72 Ishikiriyama, K.; Sakamoto, A.; Todoki, M.; Tayama, T.; Tanaka, K.; Kobayashi, T. *Thermochim. Acta* **1995**, *267*, 169-180.
- 73 Hay, J.N.; Laity, P.R. *Polymer* **2000**, *41*, 6171-6180.
- 74 Sliwinska-Bartkowiak, M.; Gras, J.; Sikorski, R.; Radhakrishnan, R.; Gelb, L.; Gubbins, K.E. *Langmuir* **1999**, *15*, 6060-6069.
- 75 Wulff, M. *Thermochim. Acta* **2004**, *419*, 291-294.
- 76 Baba, M.; Nedelec, J.-M.; Lacoste, J.; Gardette, J.-L.; Morel, M. *Polym. Degrad. Stab.* **2003**, *80*, 305-313.
- 77 Baba, M.; Nedelec, J.-M.; Lacoste, J.; Gardette, J.-L. *J. Non-Cryst. Sol.* **2003**, *315*, 228-238.
- 78 Billamboz, N.; Baba, M.; Grivet, M.; Nedelec, J.-M. *J. Phys. Chem. B* **2004**, *108*, 12032-12037.
- 79 Nedelec, J.-M.; Grolier, J.-P. E.; Baba, M. *J. Sol-Gel Sci. Techn.* **2006**, *40*, 191-200.
- 80 Meissner, B.; Zilvar, V. *Fyzika polymerů*, SNTL, Praha **1987**.
- 81 Baba, M.; Lacoste, J.; Gardette, J.-L. *Polym. Degrad. Stab.* **1999**, *65*, 421-424.

## REFERENCES

---

- 82 Bussière, P.-O.; Gardette, J.-L.; Lacoste, J.; Baba, M. *Polym. Degrad. Stab.* **2005**, *88*, 182-188.
- 83 Reiner, M. *Deformation, Strain and Flow. An Elementary Introduction to Rheology*, H. K. Lewis & Co. Ltd. **1969**.
- 84 Bingham, E.C.; Spooner, L.W. *Ind. Eng. Chem.* **1931**, *23*, 785-786.
- 85 Commereuc, S. *J. Chem. Ed.* **1999**, *76*, 1528-1532.
- 86 Commereuc, S.; Bonhomme, S.; Verney, V.; Lacoste, J. *Polymer* **2000**, *41*, 917-923.
- 87 Winter, H.H. *Encyclopedia of polymer science and engineering*. New York: Wiley **1989**, p.343.
- 88 Chambon, F.; Winter, H.H. *Polym. Bull.* **1985**, *13*, 499-503.
- 89 Winter, H.H.; Chambon, F. *J. Rheol.* **1986**, *30*, 367.
- 90 Chambon, F.; Winter, H.H. *J. Rheol.* **1987**, *31*, 683.
- 91 Kjoniksen, A.; Nyström, B. *Macromolecules* **1996**, *29*, 5215-5222.
- 92 Eloundou, J.P.; Feve, M.; Gerard, J.F.; Harran, D.; Pascault, J.P. *Macromolecules* **1996**, *29*, 6907-6916.
- 93 Chiou, B.; English, R.J.; Khan, S.K. *Macromolecules* **1996**, *29*, 5368-5374.
- 94 Raghavan, S.R.; Chen, L.A.; McDowell, C.; Khan S.A. *Polymer* **1996**, *37*, 5869-5875.
- 95 Bernard, D.A.; Noolandi, J. *Macromolecules* **1982**, *15*, 1553-1559.
- 96 Vega, J.F.; Munoz-Escalona, A.; Santamaria, A.; Munoz, M.E.; Lafuente, P. *Macromolecules* **1996**, *29*, 960.
- 97 Montfort, J.P.; Marin, G.; Monge, P. *Macromolecules* **1984**, *17*, 1551.
- 98 Verney, V.; Koërper, E.; Michel, A. *Makromol. Chem., Macromol. Symp.* **1989**, *25*, 187-198.
- 99 Ferry, J.D. *Viscoelastic properties of polymers*, 2<sup>nd</sup> Ed., J.Wiley & Sons, New York **1970**.
- 100 Mancke, R.G.; Dickie, R.A.; Ferry, J.D. *J. Pol. Sci.: Part A-2* **1968**, *6*, 1783-1789.
- 101 Flory, P.J. *Chem. Rev.* **1944**, *35*, 51.
- 102 Lukáč, I.; Kačuráková, M.; Malík, Ľ. *Collect. Czech. Chem. Commun.* **1987**, *52*, 756-760.
- 103 Lukáč, I.; Zvara, I.; Kulíčková, M.; Hrdlovič, P. *Collect. Czech. Chem. Commun.* **1980**, *45*, 1826-1830.
- 104 Lukáč, I.; Zvara, I.; Hrdlovič, P. *Eur. Polym. J.* **1982**, *18*, 427-433.
- 105 Husár, B.; Lukáč, I. *J. Photochem. Photobiol. A: Chem.* **2007**, doi:10.1016/j.jphotochem.2007.10.001
- 106 Takei, T.; Onoda, Y.; Fuji, M.; Watanabe, T.; Chikazawa, M. *Thermochim. Acta* **2000**, *352-353*, 199-204.
- 107 Husár, B.; Commereuc, S.; Lukáč, I.; Chmela, Š.; Nedelec, J.M.; Baba, M. *J. Phys. Chem. B* **2006**, *110*, 5315-5320.
- 108 Grulke, E. A. In *Polymer Handbook*, 4th ed.; Brandrup, J.; Immergut, E. H.; Grulke, E. A.; Eds.;

---

Wiley-Interscience: New York **1999**, p. VII/675.

109 Canal, T.; Peppas, N.A. *J. Biomed. Mater. Res.* **1989**, *23*, 1183-1193.

110 Angiolini, L.; Caretti, D.; Salatelli, E. *Macromol. Chem. Phys.* **2000**, *201*, 2646-2653.

111 Dallacker, F.; Alroggen, I.; Krings, H.; Laurs, B.; Lipp, M. *Justus Liebigs Ann. Chem.* **1961**, *647*, 23-36.

112 Dallacker, F.; Ulrichs, K.; Lipp, M. *Justus Liebigs Ann. Chem.* **1963**, *667*, 50-55.

113 Połośki, T.; Dauter, Z. *J. Chem. Soc. Perkin Trans. I* **1986**, 1781-1788.

114 Sell, T.; Laschat, S.; Dix, I.; Jones, P.G. *Eur. J. Org. Chem.* **2000**, 4119-4124.

## RESUME

Les groupes pendants benzile (BZ) du copolymère de styrène sont convertis pratiquement quantitativement en fonctions peroxyde de dibenzoyl (BP) par irradiation à l'état solide des films polymères à  $\lambda > 400$  nm. La décomposition par voie thermique ou photochimique des BP est une voie efficace d'obtention d'un réseau tridimensionnel de réticulation. Les réseaux finals obtenus par photo-réticulation et thermo-réticulation sont similaires. Les réseaux finals ont été caractérisés par rhéologie (Winter-Chambon, Cole-Cole, modèle théorique), gonflement, thermoporosimétrie et densimétrie. Une corrélation a été établie entre les résultats des différentes techniques et le nombre de groupes BP par chaîne. Les facteurs favorisant une construction du réseau dense sont : des masses molaire élevées et une faible polydispersité du copolymère initial et une concentration élevée du BP. L'efficacité de la réticulation du copolymère portant un groupe pendant camphrequinone est nettement inférieure.

**Mots clés :** benzile, polystyrène, copolymérisation, photochimie, réseau, rhéologie, thermoporosimétrie

## ABSTRACT

Benzil (BZ) pendant groups of styrene copolymers were converted almost quantitatively into benzoyl peroxide (BP) by irradiation of solid polymer films at  $\lambda > 400$  nm. Thermal or photochemical decomposition of BP is an efficient way to obtain a 3D network of crosslinking. Final networks from photo-crosslinking and thermo-crosslinking are similar. Final networks were characterized by rheology (Winter-Chambon, Cole-Cole, theoretical model), swelling, thermoporometry and densitometry. A correlation between results of various methods and number of BP groups per chain was established. The factors supporting a the construction of a dense network are: high molar masses and low polydispersities of original copolymer and high concentration of BP. The efficiency of crosslinking of a copolymer bearing camphorquinone pendant group is significantly lower.

**Keywords:** benzil, polystyrene, copolymerization, photochemistry, network, rheology, thermoporometry